The Cu_A Center of Cytochrome Oxidase: Electronic Structure Calculations and Electron-Tunneling Pathways

Thesis by

Benjamin E. Ramirez

In Partial Fulfillment of the Requirements
for the Degree
Doctor of Philosophy

California Institute of Technology
Defended September 29, 1997

ABSTRACT

The Cu_A center is a mixed valence, dithoilate-bridged, binuclear copper center that is found in cytochrome oxidase. It serves as the initial acceptor of electrons from cytochrome c. The Cu_A center has distinct UV/Vis and EPR spectroscopic features. It is likely that this site has an extremely low inner-sphere reorganization energy because it very efficiently transfer electrons st low reaction driving forces over long distances (~15-20 Å) in less than a millisecond. We undertook DFT calculations on a Cu_A model complex to examine the structure, spectroscopic assignments and reorganization energy of the center. The optimized structure of the Cu_A model complex closely resembles the structure determined from x-ray diffraction studies. The rms overlap of the optimized structure with the structure derived from EXAFS data is 0.16 Å. Based on the calculated MO diagram, we assign the bands in the UV/Vis absorption spectrum to transitions originating from lower lying doubly-filled orbitals into a σ_{Cu}* singly-occupied HOMO that is primarily Cu d_{x2-y2}/S p_x in character. We find that the character of the HOMO as well as the transition energies and intensities are extremely sensitive to the Cu-S-Cu angle. We also calculated the optimized structure of the reduced center to examine the role of the protein in reducing the inner-sphere reorganization energy. The following picture emerges from the calculations of the coordination geometry: the protein framework imposes a structure, with a low dielectric cavity in which the trigonal geometry of the oxidized form is optimal. In addition, this framework prevents the reduced structure from distorting to its optimal (linear, two-coordinate) structure. This so-called rack effect of the folded protein enables Cu_A and blue copper centers to function as very efficient electron-transfer agents.

Table of Contents

List of Figures and Tables

Chapter 4. Electron-Tunneling Pathways in Cytochrome Oxidase

Chapter 1.

Introduction to Copper Electron-Transfer Centers in Proteins

Life would not be the same without copper. Copper centers in proteins participate in electron transfer (ET) reactions that occur in the two foremost biological redox processes: photosynthesis and respiration (Figure 1). These processes are responsible for the majority of oxygen produced and consumed, respectively, on this planet. The main components of the photosynthetic machinery are three redox membrane proteins: photosytem I and II, and cytochrome b_6f. The copper protein plastocyanin serves to transfer electrons from cytochrome b_6f to photosystem I. The main components of the respiratory redox chain are found in the membrane of mitochondria: NADH dehydrogenase, cytochrome bc_1, and cytochrome. Cytochrome oxidase contains a copper center that mediates the long-range (> 10 Å) transfer of electrons from cytochrome c to cytochrome a. Although various components comprise the machinery of these systems, copper proteins are critical components in the chain of ET centers. In addition to ET, copper is also found in the heme a_3-Cu_B site of cytochrome oxidase, the catalytic center where oxygen reduction occurs.

Plastocyanin belongs to the family blue copper proteins. Blue copper proteins participate in numerous biological electron transfer processes. Other examples of blue copper proteins include azurin, stellacyanin, cucumber basic protein and amicyanin. These proteins cycle between two redox states, blue Cu(II), which has an unusually intense absorption at $\lambda_{max} \sim 600$ nm ($\varepsilon \sim 4500\ M^{-1}cm^{-1}$), and colorless Cu(I). In the active site, a single copper ion is bound in a distorted tetrahedral, nearly trigonal, geometry by one cysteine and two histidines (Figure 2). The axial coordination of the conserved Met is variable; the S_γ(Met)-Cu distance ranges from 2.5 to 3.1 Å. These sites have reduction potentials ~ 300 mV (the actual range is 184 to 680 mV) and fairly low

Figure 1. Schematic picture of the electron transfer chains involved in (a) photosynthesis and (b) respiration. In photosynthesis, the electrons derived from the oxidation of water flow from photosystem II to the cytochrome b_6f complex via plastoquinol (PQ). Electrons are transferred to photosystem I from cytochrome b_6f via the blue copper protein plastocyanin. In respiration, the electrons originating from NADH are transferred to ubiquinone by the NADH dehydrogenase complex. Ubiquinol donates electrons to the cytochrome bc_1 complex. Cytochrome c transfers electrons from the bc_1 complex to the binuclear, mixed valence Cu_A center in cytochrome oxidase.

a)

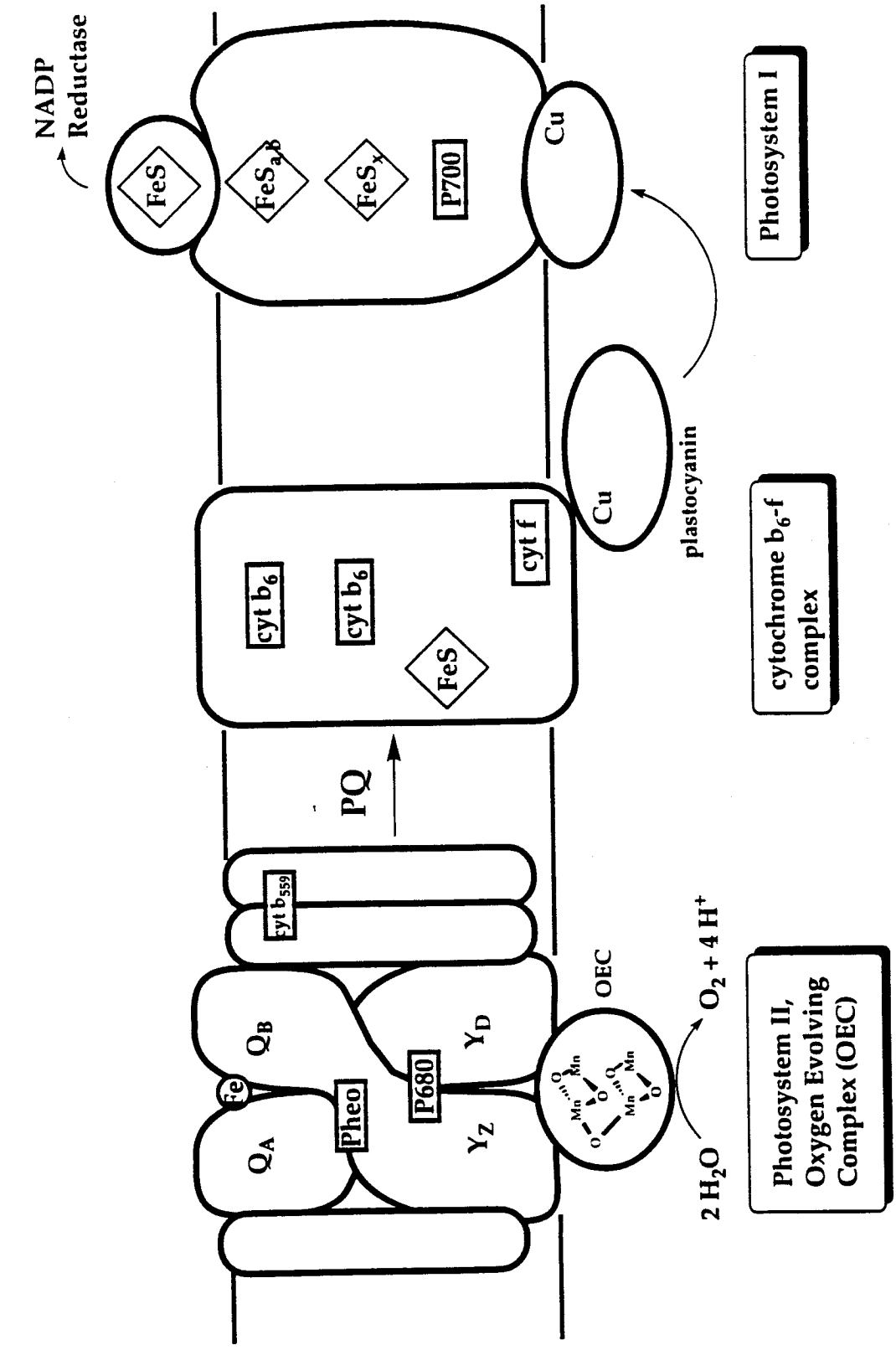
NADP
Reductase
FeS
$FeS_{a,B}$
FeS_x
P700
Cu
Photosystem I
cyt b_6
cyt b_6
FeS
cyt f
Cu
plastocyanin
cytochrome b_6-f complex
PQ
cyt b_{559}
Q_B
Fe
Q_A
Pheo
P680
Y_D
Y_Z
OEC
$O_2 + 4\ H^+$
$2\ H_2O$
Photosystem II, Oxygen Evolving Complex (OEC)

b)

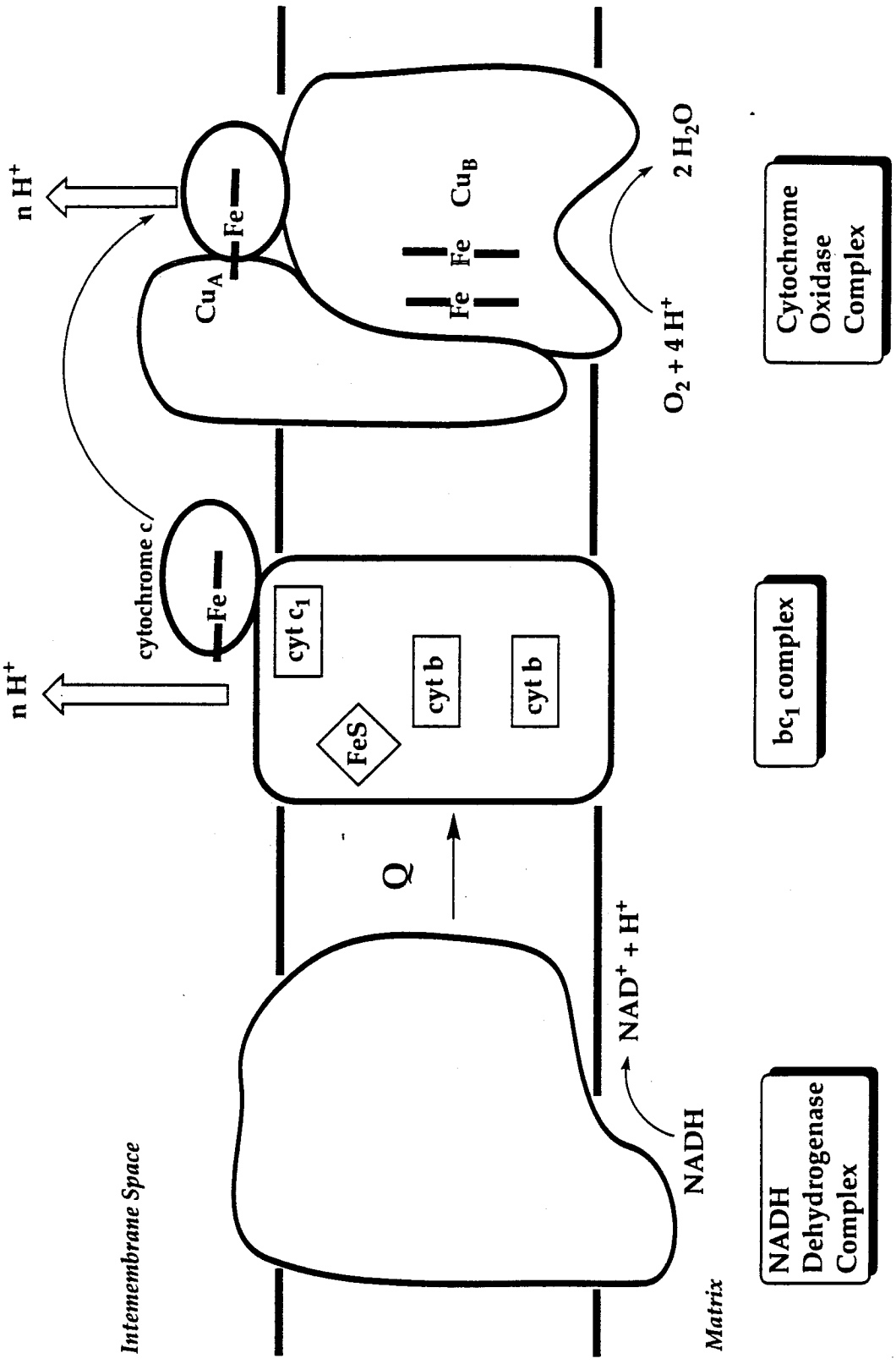
n H+
n H+
cytochrome c
Fe
Cu_A
Fe
Cu_B
Fe
Fe
cyt c1
cyt b
cyt b
FeS
Q
NAD+ + H+
NADH
2 H2O
O2 + 4 H+
Cytochrome Oxidase Complex
bc1 complex
NADH Dehydrogenase Complex
Intemembrane Space
Matrix

reorganization energies, measured to be ~ 0.3 eV in ruthenium-modified derivatives of azurin.

For a long time it was believed that the copper center that mediates electron transfer between cytochrome c and cytochrome a of cytochrome oxidase, the Cu_A center, was very similar to the blue copper sites. In fact, the only difference between the sequences of the copper binding region of the two proteins is a slightly longer loop and an additional cysteine residue in the Cu_A domain, the membrane-attached subunit II domain of cytochrome oxidase. This difference allows the copper stoichiometry to go from one to two, giving rise to a dithiolate bridged binuclear copper center (Figure 2) with distinct spectroscopic features. The EPR spectrum of Cu_A shows a seven-line hyperfine splitting pattern best described by the existence of a mixed-valence Cu(1.5)/Cu(1.5) center. The electron is distributed equally over each copper ion. The ET reactions that involve the Cu_A center have low driving forces, hence, it is believed that the Cu_A center has an extremely low reorganization energy ~ 0.1 eV. Why, apparently, a binuclear cofactor evolved from a blue copper center in subunit II of cytochrome oxidase is a major focus of this thesis.

The thesis is organized as follows: Chapter 2 contains background on the Cu_A center, including a brief historical account of research on the Cu_A center and survey spectroscopic data from EPR, UV/Vis, Resonance Raman and EXAFS studies of the center. Also included is a discussion of the structure of Cu_A and cytochrome oxidase and a comparison of Cu_A and blue copper proteins. Chapter 3 describes the results of Density Functional Theory (DFT) electronic structure calculations on the Cu_A center. Results are reported on the calculation of the optimized geometry and molecular orbital (MO)

Figure 2. Schematic representation of the (a) blue copper and (b) Cu_A centers.

a)

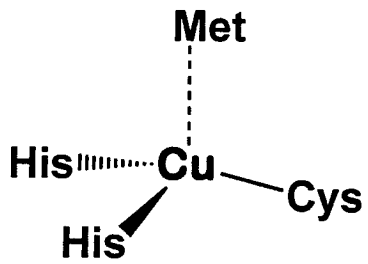

Blue Copper center

b)

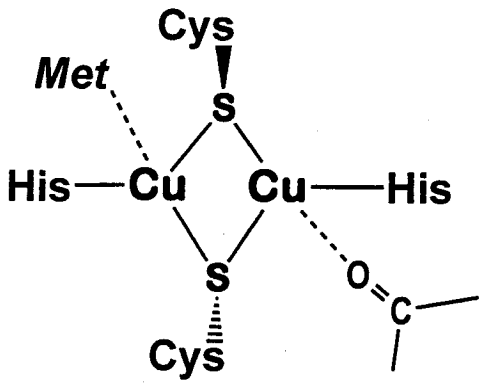

Cu_A center

diagram of a Cu_A model complex. Based on the calculated MO diagram, assignments of the experimentally observed absorbance transitions are proposed. In addition, the affect of the structure of the Cu_A center on the nature of the orbitals and transition energies and intensities is reported. Last, results are presented on optimized structure of the reduced blue copper and Cu_A center. This includes a discussion of the Cu_A and blue copper inner-sphere reorganization energy and the role of the protein framework or rack in imparting unusual feature to these centers. The last chapter, Chapter 4, describes ET pathways in cytochrome oxidase. After a brief review of the pathway model, the ET pathways between the various redox cofactors in cytochrome oxidase are discussed.

Chapter 2.

The Cu_A Center in Cytochrome Oxidase:

History and Background

INTRODUCTION

The Cu_A center of cytochrome oxidase serves as the initial acceptor of electrons from cytochrome c. Electrons from Cu_A are transferred, via heme a, to the binuclear heme a_3-Cu_B unit where oxygen reduction occurs[1] (Figures 1). Now it is known that the Cu_A center is a dithiolate bridged binuclear copper center (Figure 2) that acts as a single electron acceptor with two oxidation states: Cu(I)/Cu(I) and the mixed valence Cu(I)/Cu(II) species. These conclusions were reached only after considerable experimental efforts over the past forty years that culminated in the determination of the crystal structure of cytochrome oxidase.[2,3] To appreciate our current understanding of the Cu_A center a brief history of research on this center is appropriate.

HISTORY

The pioneering cytochrome oxidase researchers O. Warburg and D. Keilin initially had differing views on the copper contents of cytochrome oxidase. From his studies on the photochemical dissociation of CO from cytochrome oxidase, Warburg claimed that the enzyme was a heme-containing protein.[4] On the other hand, Keilin believed that cytochrome oxidase was a copper protein.[5] Almost ten years after Warburg's studies, Keilin discovered cytochrome a_3 and observed that it behaved as Warburg had claimed.[6] Hence, the view of cytochrome oxidase as a heme protein was firmly established. Just as the hemes dominate the absorption spectrum, early studies focused primarily on these centers. A functional role for copper was all but forgotten until H. Beinert investigated the EPR properties of the Cu_A center.

Figure 1. Diagram showing the redox centers and ET pathways in cytochrome oxidase based on the bovine enzyme x-ray structure. The oval at the top represents the Cu_A domain of subunit II, which is anchored to the membrane by a transmembrane helix (not shown). The Cu_A domain lies atop subunit I with the Cu_A center (the purple oval) poised directly above heme a (represented as a square). Efficient electron transfer pathways between the Cu_A and heme a and heme a and heme a_3-Cu_B are indicated by thick shaded lines.

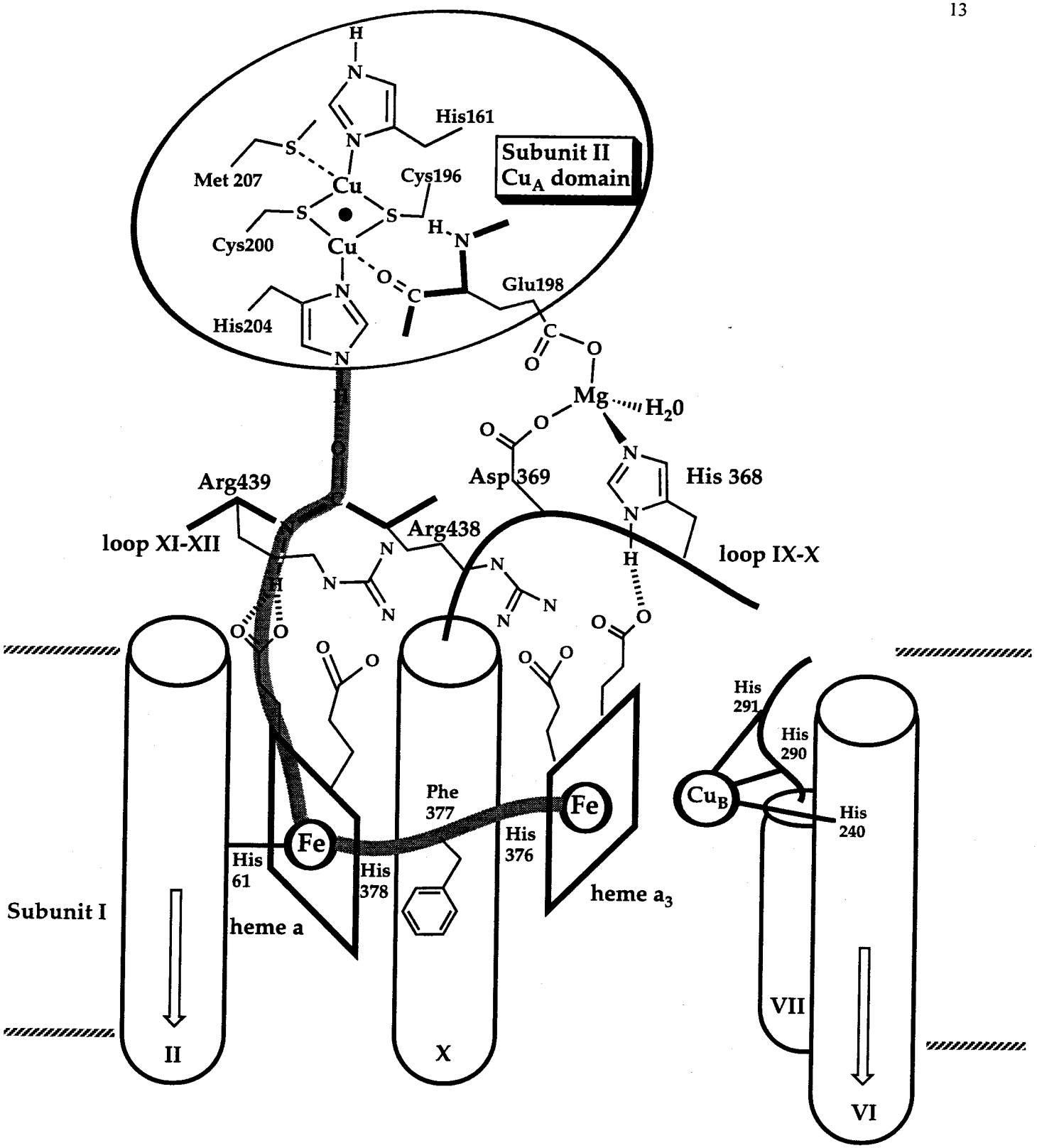
His161
Subunit II
Cu$_A$ domain
Met 207
Cys196
Cys200
Glu198
His204
Mg
H$_2$0
Asp 369
His 368
Arg439
Arg438
loop XI-XII
loop IX-X
His
291
His
290
Cu$_B$
His
240
Phe
377
Fe
Fe
His
61
His
378
His
376
heme a
heme a$_3$
Subunit I
II
X
VII
VI

Figure 2. Structure of the Cu_A center in cytochrome oxidase based on the bovine enzyme x-ray structure. The Cu_A center is a dithiolate bridged binuclear copper center. It has terminal histidine ligands that complete the nearly trigonal coordination. In addition, a Met thioether and a Glu backbone carbonyl act as weak axial ligands.

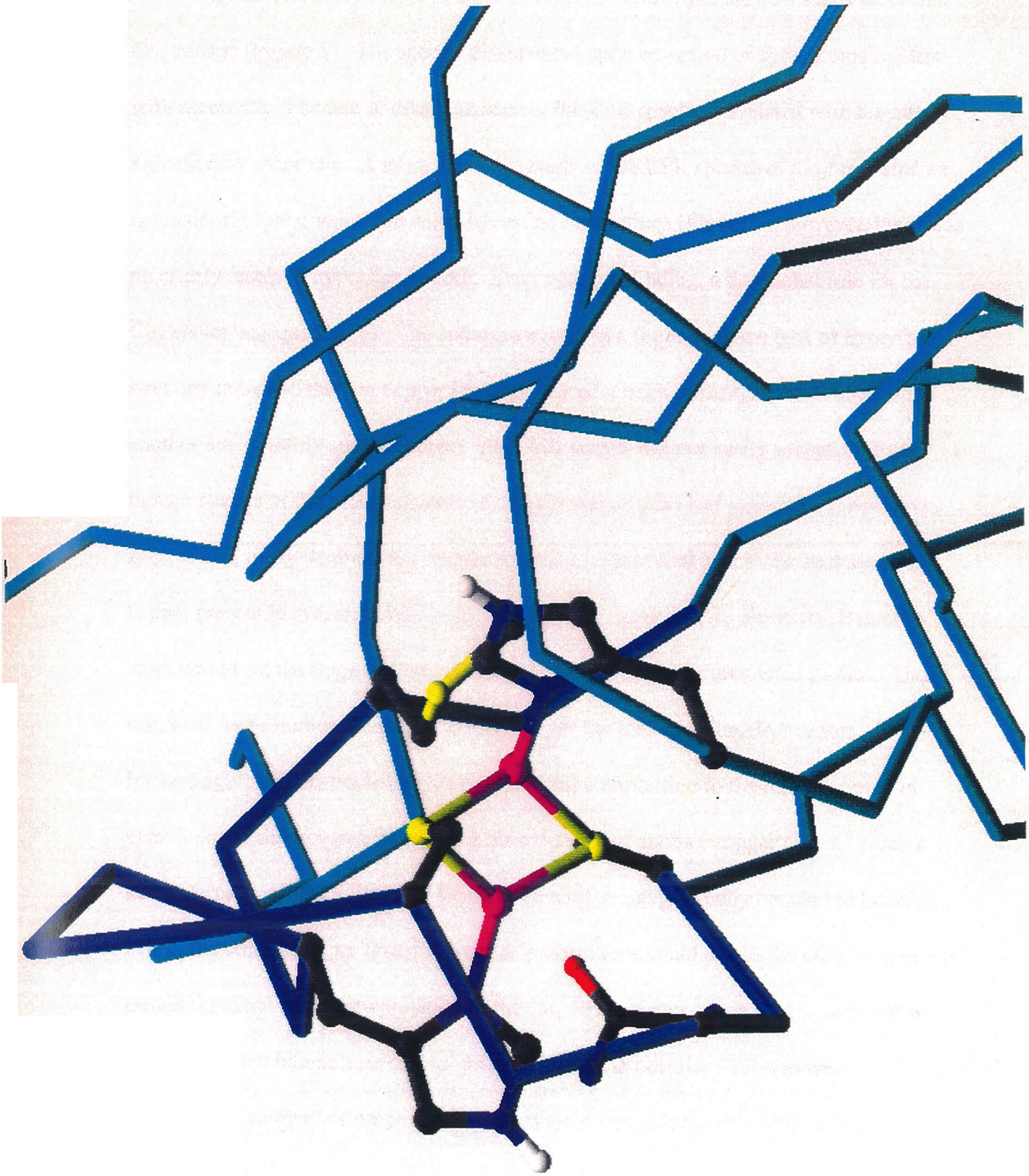

In 1959, H. Beinert reported the EPR spectrum of what we now know to be the Cu_A center[7] (Figure 3). The spectra disappeared upon reduction of cytochrome oxidase with ascorbate. The rate of disappearance of the EPR spectra correlated with the rate of reduction by ascorbate. A more extensive study of the EPR spectra of Cu_A[8] revealed an anomalously low g-value and small hyperfine interactions (Figure 3), however, there was no clearly resolved hyperfine pattern. Even with this finding, a functional role for the Cu_A center was questioned. The authors asserted in a footnote that a lack of hyperfine structure indicated that the copper ion experienced a large exchange interactions with another ion, possibly another copper ion. This notion was not easily accepted. Even though studies of the metal contents of cytochrome oxidase had reported a copper:iron ratio of one, many doubted that copper served any functional role in the enzyme. Any copper present in preparations was more than likely an impurity. However, Beinert's work would set the stage for over thirty years of extensive spectroscopic studies. The results of these studies would ultimately support the idea of a binuclear center. Interestingly, Beinert made another fundamental contribution to the role of copper in cytochrome oxidase when he reported the existence of another copper center,[9] what is now referred to as Cu_B. Cu_B was found to be antiferromagnetically coupled to heme a_3, hence, the second copper found in oxidase preparations could not be the other copper ion Beinert invoked in his interpretation of the Cu_A EPR spectra. Researchers were left to search for other interactions that might give rise to the peculiar EPR spectra. Nonetheless, Beinert's finding established cytochrome oxidase as a heme-copper oxidase.

Figure 3. Cu_A EPR spectra from Beinert's (a) 1959 paper and (b) 1962 paper. Note the original figure legends are included.

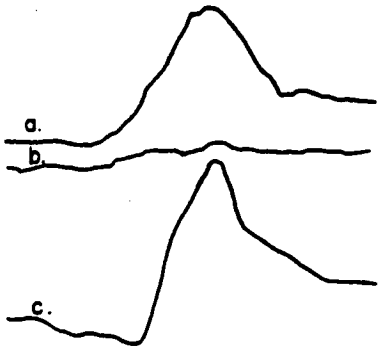

Figure 1. EPR signals (g=2.05 (1); peak to peak width for (a) 160 gauss) of 42 mg of cytochrome oxidase (10 μmoles of Cu per g of protein) in 0.3 ml of 0.1 M phosphate (pH 7.5) aerobically at -100°: (a) untreated; (b) 5 minutes after addition of 25 μl of 1 M ascorbate (pH 6.5); (c) as (a) in the presence of 0.003 M cyanide.

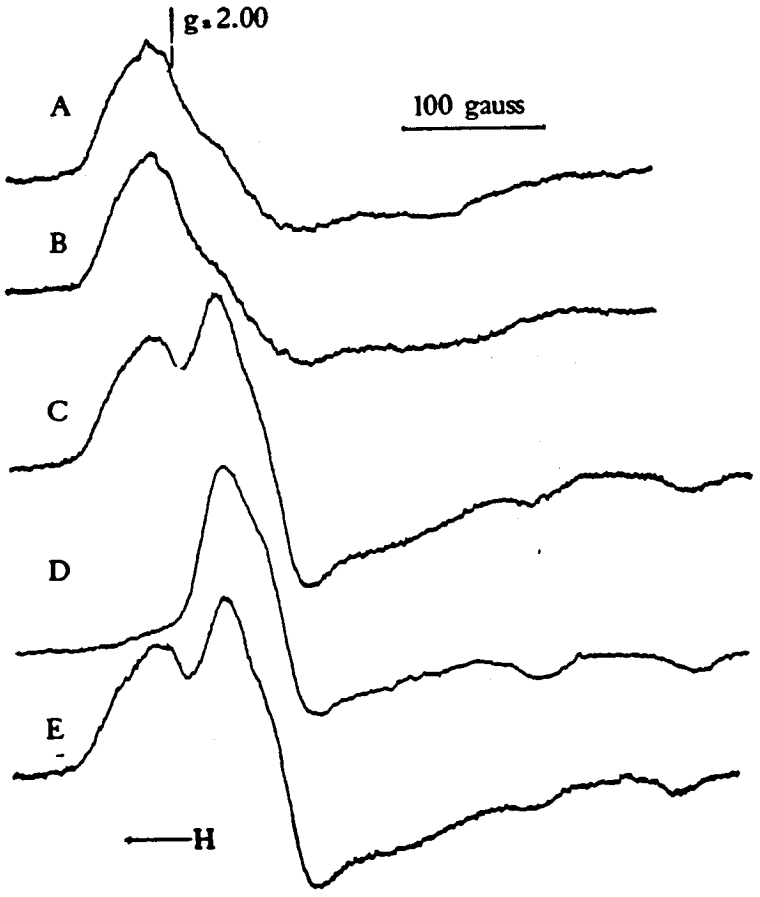

FIG. 8. EPR spectra of cytochrome oxidase (3.0 mg dissolved in 0.10 ml of sucrose) in the presence of added Cu^{2+} and EDTA. *A*, Untreated; *B*, after addition of 0.3 μmole of EDTA, pH 7.4; *C*, sample *B* after addition of 30 mμmoles of $CuSO_4$; *D*, sample *C*, reduced with 1.2 μmoles of ascorbate and 4 mμmoles of cytochrome *c*; *E*, sample *D*, reoxidized by aeration.

BACKGROUND

Pre-modern Era of Cu_A Research

The findings of Beinert set the stage for what may be referred to as the pre-modern era of research on Cu_A. During this period, techniques from the areas of protein chemistry and spectroscopy would be brought to bear on the study of the Cu_A center. Early on, paramagnetic resonance studies dominated the field. Vanngard constructed a plot of g-values and hyperfine splittings for various copper compounds, the blue copper proteins and the Cu_A center.[10] He found that the various blue copper proteins fell in one region of the plot, but that the CuA was in a region all alone. Attempts were made to explain the anomalously low g-values and small hyperfine coupling constants of the Cu_A center. The application of multifrequency EPR was indispensable in resolving the hyperfine splitting pattern of the Cu_A center. In 1979, resolved hyperfine interactions were observed in the 2-4 GHz EPR spectrum of Cu_A[11] (Figure 4). The authors proposed that the splitting may be due to another paramagnetic center, possibly the heme of cytochrome a. They made this assertion largely because there was no compelling evidence to invoke a binuclear copper model for Cu_A since most studies of the metal contents of cytochrome oxidase had not conclusively found a copper:iron ratio greater than one. Although their work did not revive the notion of a binuclear copper center, it clearly demonstrated that the magnitude of the hyperfine interaction was too large to be due to ^{15}N or ^{1}H. This conclusion was confirmed by ENDOR results published soon thereafter.

Figure 4. The first observation of a seven line hyperfine splitting pattern in the low frequency Cu_A EPR spectra reported in 1979. The features of the seven line hyperfine splitting pattern are marked with roman numerals (I-VII).

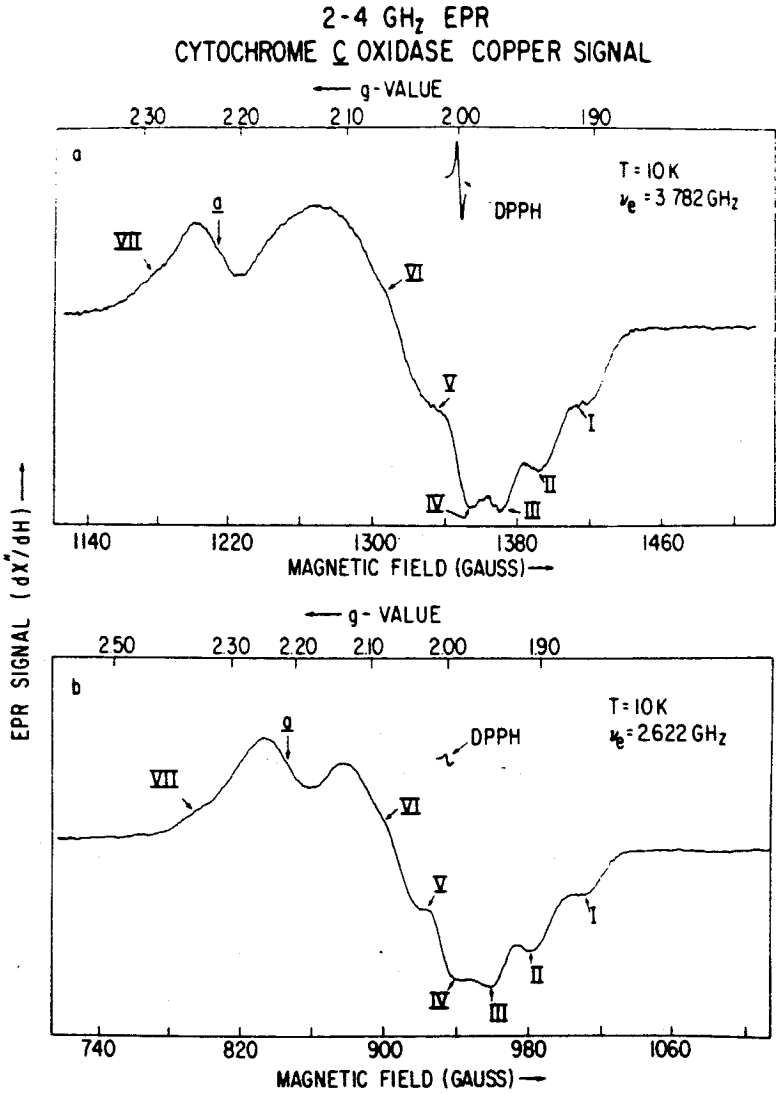

FIG. 2. EPR spectra of the EPR-detectable copper signal from cytochrome *c* oxidase taken at EPR frequencies of 3.78 GHz (*a*) and 2.62 GHz (*b*). The features labeled I, II, III, IV, V, VI, and VII are the newly resolved features. The feature labeled *a* occurs at the g_y value associated with cytochrome *a*. Conditions are as in Fig. 1. *g* values are indicated at the *top* of each spectrum and magnetic field strengths at the *bottom*. A speck of α,α'-diphenyl-β-picryl-hydrazyl (DPPH) was introduced on a thin wand along the side of the sample to provide a precise *g* value calibration. The magnetic field was swept over the range shown in *a* in a time of 8 min with an instrumental time constant of 1 s and over the range shown in *b* in a time of 16 min with an experimental time constant of 3 s.

During this period, the efforts of Sunney Chan and coworkers helped to identify the ligands of the Cu_A center. They undertook EPR and ENDOR studies of isotopically enriched samples of cytochrome oxidase,[12,13] namely [1,3-^{15}N]-His, [β,β-^{2}H]-Cys and [^{13}C]-Cys labeled protein. Their results strongly suggested that two Cys and two His residues were ligands of the Cu_A center. The notion of two Cys residues was notable at the time. It demonstrated that the Cu_A center was indeed distinct compared to the blue copper proteins. It helped to explain the unusual spectroscopic properties, namely the low g-values. Jumping ahead, we know that the extra Cys is the only difference between the blue copper and Cu_A sites and that the two Cys residues are largely responsible for the unique properties and spectroscopic features of the site. Based on the data available at the time, Chan and coworkers proposed a model for the Cu_A center where a single copper ion is ligated by two His and two Cys residues in a tetrahedral manner (Figure 5). In this model, extensive delocalization of the electron onto the two Cys sulfur atoms accounted for the anomalous EPR values. This model served as the basis for a proton pumping scheme involving the Cu_A center. This model, although controversial, did find acceptance and can be found in a number of biochemistry textbooks. Unfortunately, time would prove the Chan model of Cu_A incorrect. But it should be remembered that Sunney Chan's work was crucial in identifying the two Cys ligands of Cu_A and provided researchers in the field a set of ligands from which they could construct their own structural models of Cu_A.

The pre-modern era of research on Cu_A did not end quietly. Instead, it ended with a revived interested in the binuclear Cu_A model. Kroneck, Zumft and coworkers undertook extensive spectroscopic studies[14,15] on an enzyme involved in bacterial

Figure 5. Models of the Cu_A center: (a) the Chan model. (b) The terminal binuclear model; it gained support from the notion of a Cu-Cu bond. (c) The bridging binuclear model; the structure that is observed.

a)

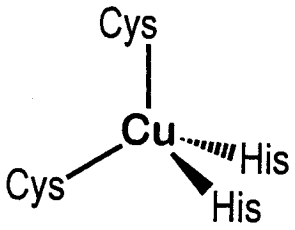

b)

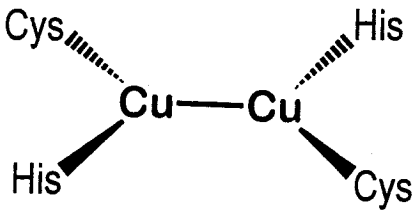

c)

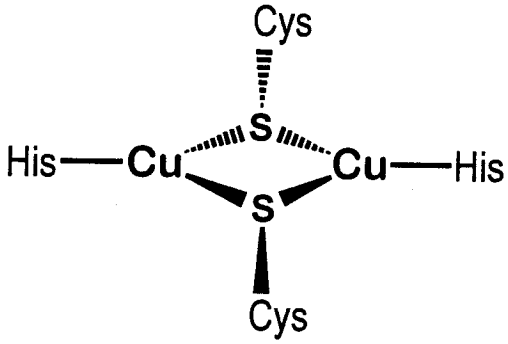

denitrification N_2O reductase (N_2OR). The EPR spectrum of N_2OR was similar to that of Cu_A except that hyperfine structure was present that could not be explained in terms of a mononuclear model. They used a binuclear model of the copper A site in N_2OR to interpret their EPR data. They reasoned that since the EPR spectrum of N_2OR looked similar to that of cytochrome oxidase that the two sites must be must be related, i.e. the Cu_A site of cytochrome oxidase must also be binuclear. This interpretation was immediately challenged.[16] The binuclear model was not accepted initially because studies of the metal contents of cytochrome oxidase could not unequivocally demonstrate a copper:iron ratio of 3:2. In addition the Chan model was attractive since it included a mechanism for the linkage of redox reactions with proton pumping. The modern era of research on Cu_A would bring to bear results in accord with the binuclear Cu_A model.

The modern era of Cu_A research

The beginning of the modern era of research on Cu_A is marked by the production of soluble Cu_A domains. This was achieved by recombinant expression of the soluble portion of cytochrome oxidase subunit II. Soluble Cu_A domains from *Bacillus Subtillus,*[17]. *Paracoccus denitrificans,*[18] and *Thermus thermophlus*[19] have been produced. These fragments have virtually identical spectroscopic features as compared to the Cu_A site in cytochrome oxidase and are even able to accept electrons from cytochrome c. Hence the results obtained from studies on the soluble Cu_A domains can confidently be applied to interpret the properties of the intact site in cytochrome oxidase. The identity of the His and Cys residues proposed to be ligands of the Cu_A center was verified by mutagenesis studies on the *P. den.* Cu_A soluble domain.[17] The production of soluble Cu_A

domains enabled the undertaking of extensive spectroscopic studies by numerous techniques including UV/Vis absoprtion, CD, MCD, EPR, EXAFS and Resonance Raman. Not all the domains produced were studied to the same extent by these various methods. Hence in what follows the data for the fragment that was studied most extensively will be presented. Explicit mention will be made of cases where data have been reported that indicate significant differences in the spectroscopic features between domains from different species. Curiously enough no x-ray structure data has been reported for any of the soluble Cu_A domains. Even though the structure of the intact cytochrome oxidase has been solved, x-ray diffraction data on the soluble Cu_A domains is of interest because they may lead to a higher resolution structure. The structure of an engineered fragment, the purple cyoA fragment, where a Cu_A center has been engineered into the soluble subunit domain of ubiquinol oxidase has been reported.[20] However, this site exhibits perturbed absorption properties and hence one should proceed cautiously in interpreting the relevance of spectroscopic and structural studies on this fragment in regards to the native Cu_A site. In the same vein, the studies of Cu_A sites engineered into blue copper proteins will not be discussed.[21,22] The pertinence of results obtained from these studies in regards to the properties of the native site is questionable since it is not clear that the spectroscopic features, which for the most part are perturbed relative to the native, are the result of a design that is not optimal or some other factor. Also, since this is a review on Cu_A from cytochrome oxidase, studies of the copper A site of N_2OR will not be discussed in great detail. While it is clear that the two sites are similar it is not certain that they are identical. For one thing, the copper A site of N_2OR is not part of a redox-linked proton pump.

Cu_A SPECTROSCOPIC DATA

EPR

It is appropriate to start with EPR studies of the soluble Cu_A domains, since it was the EPR spectrum of Cu_A that first attracted interest to this site. Multifrequency studies at Q, S, and X frequencies (~35, ~9, and ~4 GHz, respectively) of ^{65}Cu and ^{63}Cu substituted *Thermus thermophilus* fragment have been reported[23] (Figure 6). As noted previously, the resolution of the hyperfine interactions are best resolved at lower frequencies. The EPR data support a model for the Cu_A center where one electron is distributed equally between the two copper ions. The numerical values used to simulate the experimental spectrum are: $g_x = 1.996$, $g_y = 2.11$, and $g_z = 2.187$; $A_x = 15$ G, $A_y = 29$ G, and $A_z = 28.5$ G . The related blue copper proteins have g-values of ~2.25 and ~2.04 and hyperfine coupling constants in the range of 35 – 80 G.

Figure 6. Low frequency EPR spectra of the Cu_A center in the *Thermus thermophilus* soluble domain. The spectra labeled a and b are the observed ^{63}Cu and ^{65}Cu spectra. The spectra labeled c and d are the simulated ^{63}Cu and ^{65}Cu spectra.

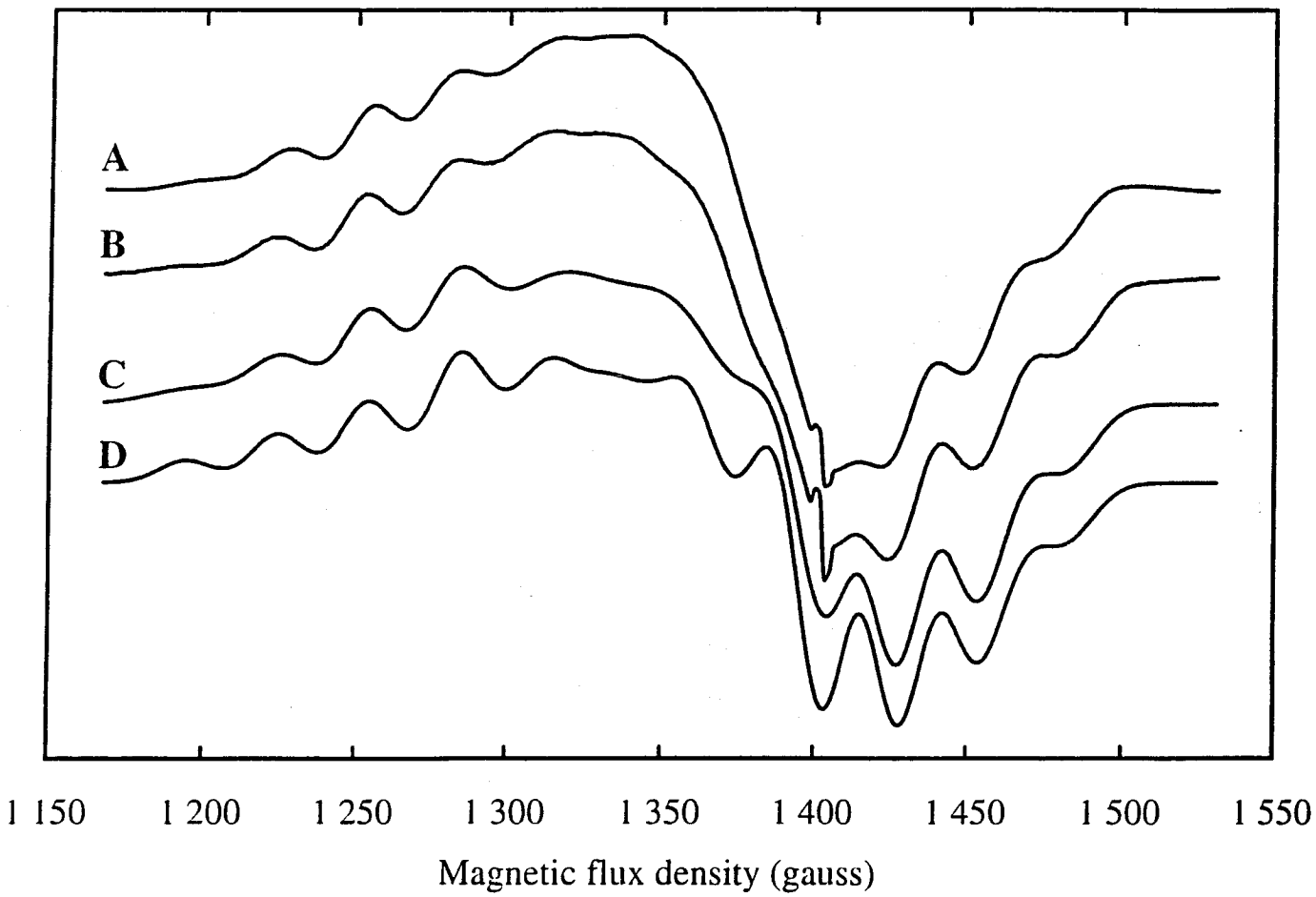
A
B
C
D
1 150
1 200
1 250
1 300
1 350
1 400
1 450
1 500
1 550
Magnetic flux density (gauss)

Optical Spectra

Absorption and CD data recorded for the *Thermus thermophilus* soluble Cu_A domain are shown in Figure 7. The absorption spectrum shows three major features: two absorption bands of nearly equal intensity at 480 nm (ε = ~2500 $M^{-1}cm^{-1}$) and 530 nm (ε = ~2500 $M^{-1}cm^{-1}$) and a less intense and broader absorption feature centered at 830 nm (ε = ~15000 $M^{-1}cm^{-1}$). There is also an absorption peak at 360 nm (ε = ~1900 $M^{-1}cm^{-1}$). The CD spectrum shows that the bands at 480 and 530 nm are oppositely polarized. The assignment of these bands will be discussed in more detail below. For comparison, the blue copper absorption spectrum is dominated by a single absorption band with a maximum absorption wavelength ~ 600 nm (ε = ~2500 $M^{-1}cm^{-1}$).

Figure 7. (a) UV/Vis and CD spectra (solid lines) of the Cu_A center in the *Thermus thermophilus* soluble domain compared to the same spectra (dashed lines) of azurin. (b) Polarized absorption spectra of a single crystal of the *Thermus thermophilus* soluble domain (recorded by William B. Connick).

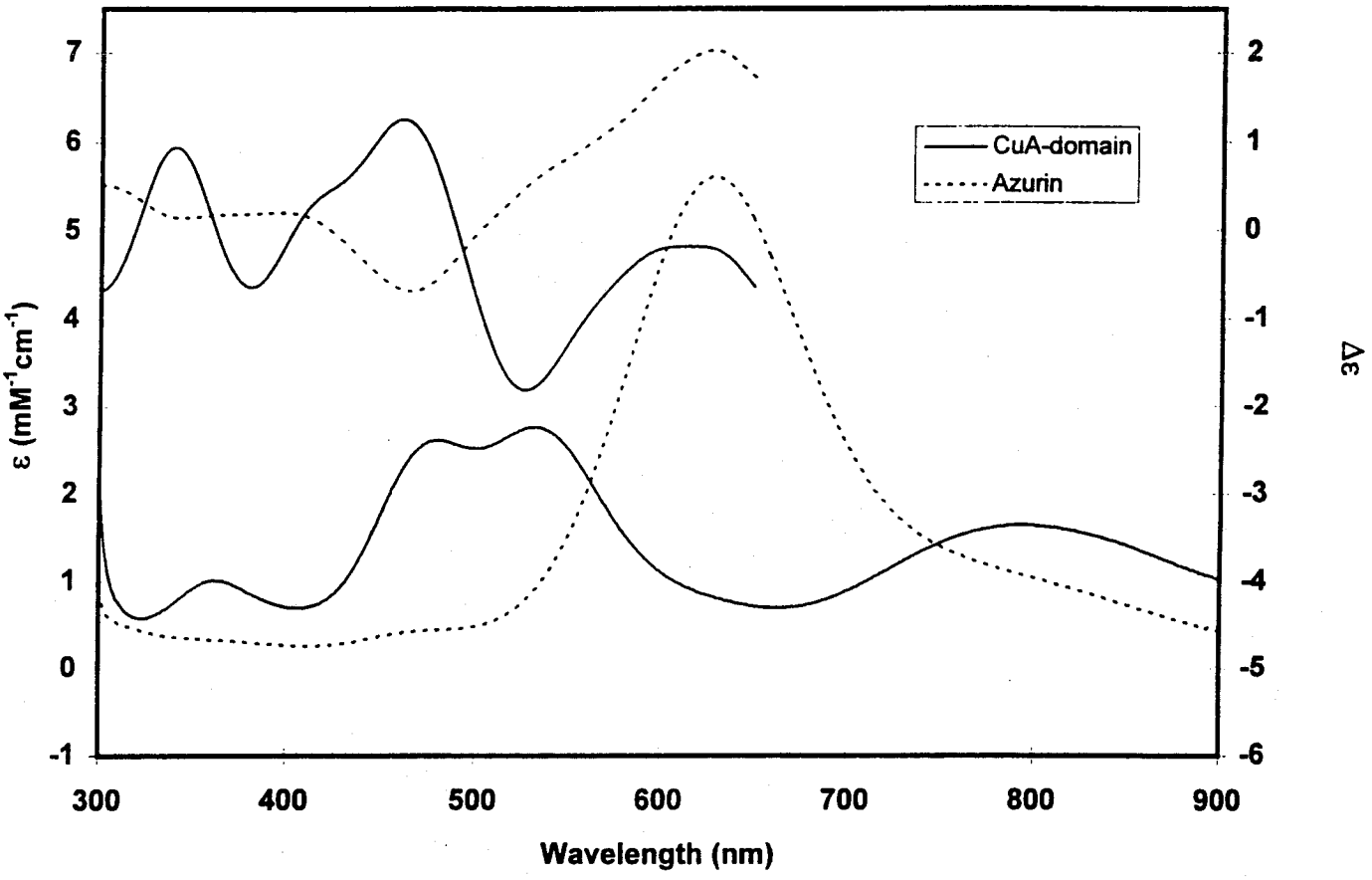
CuA-domain
Azurin
ε (mM-1cm-1)
Δε
Wavelength (nm)
7
6
5
4
3
2
1
0
-1
2
1
0
-1
-2
-3
-4
-5
-6
300
400
500
600
700
800
900

b

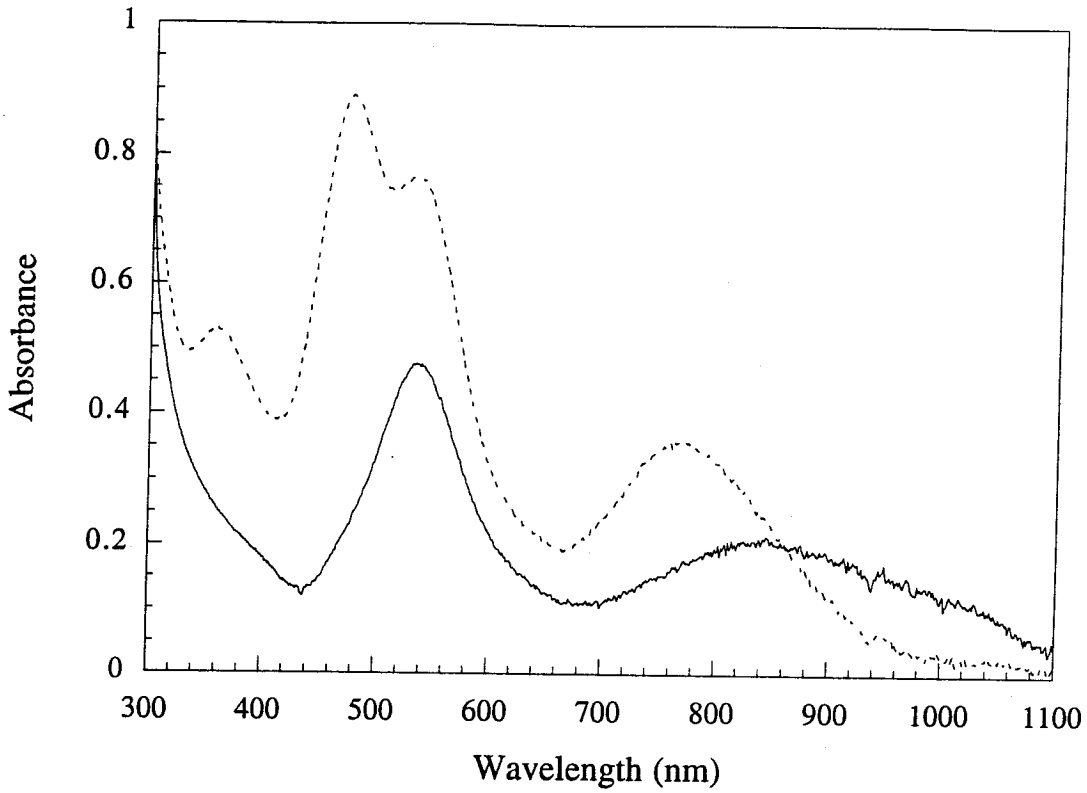
Absorbance
1
0.8
0.6
0.4
0.2
0
300
400
500
600
700
800
900
1000
1100
Wavelength (nm)

Resonance Raman

Resonance Raman (RR) is perhaps the technique that has benefited the most from the production of soluble Cu_A domains. As mentioned before, the optical spectrum of cytochrome oxidase is dominated by the heme groups. This severely hindered RR studies of the Cu_A site since the absorption features of this site are considerably less intense than the heme absorption features. The fact that all the soluble Cu_A domains produced thus far have been studied by RR[24],[25] is testimony to how much the production of these fragments has facilitated these type of studies. The RR spectrum is dominated by three vibrational modes at 339, 260 and 139 cm^{-1}. Normal coordinate analysis found these three bands to be A_g stretching modes.[26] All three bands showed considerable ^{34}S isotope shifts. The ^{65}Cu isotope shifts are smaller in comparison to the ^{34}S isotope shifts (Figure 9). Most of these studies were performed using blue excitation at either 488 or 514 nm. A separate study by another group reported considerably larger ^{65}Cu isotope shifts using a red excitation source (800-850 nm).[27] This supported the notion that a Cu-Cu bond was present in the Cu_A center because the observed ^{65}Cu isotope shifts were close to the values calculated using a harmonic oscillator approximation for a diatomic molecule. The existence of a metal-metal bond in the Cu_A center will be discussed in more detail below. None of the modes showed any significant ^{15}N isotope shifts. This is in stark contrast to the ^{15}N isotope shits observed in the RR spectra of blue copper proteins.

Figure 8. Resonance Raman spectra of the *Paracoccus denitrificans* and *Bacillus subtillus* soluble Cu_A domains. The top panel shows the blue excitation spectra (488 and 514 nm) showing the ^{34}S, ^{65}Cu, and ^{15}N isotope shifts. The bottom panel shows the red excitation spectra (800 and 850 nm). Incorporation of ^{65}Cu primarily affects the feature at ~130 cm^{-1}.

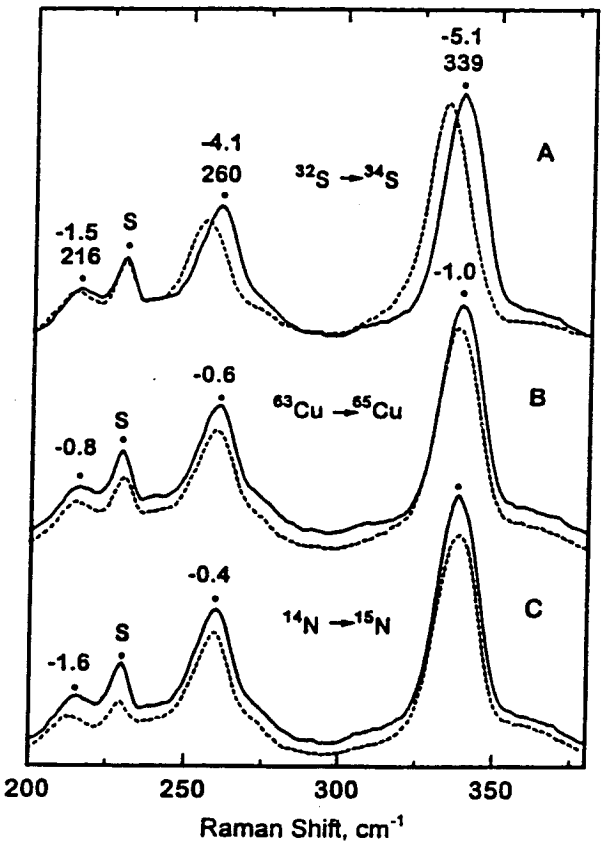
-5.1
339
-4.1
260
$^{32}S \rightarrow ^{34}S$
A
-1.5
216
S
-1.0
-0.6
$^{63}Cu \rightarrow ^{65}Cu$
B
-0.8
S
-0.4
$^{14}N \rightarrow ^{15}N$
C
-1.6
S
200
250
300
350
Raman Shift, cm^{-1}

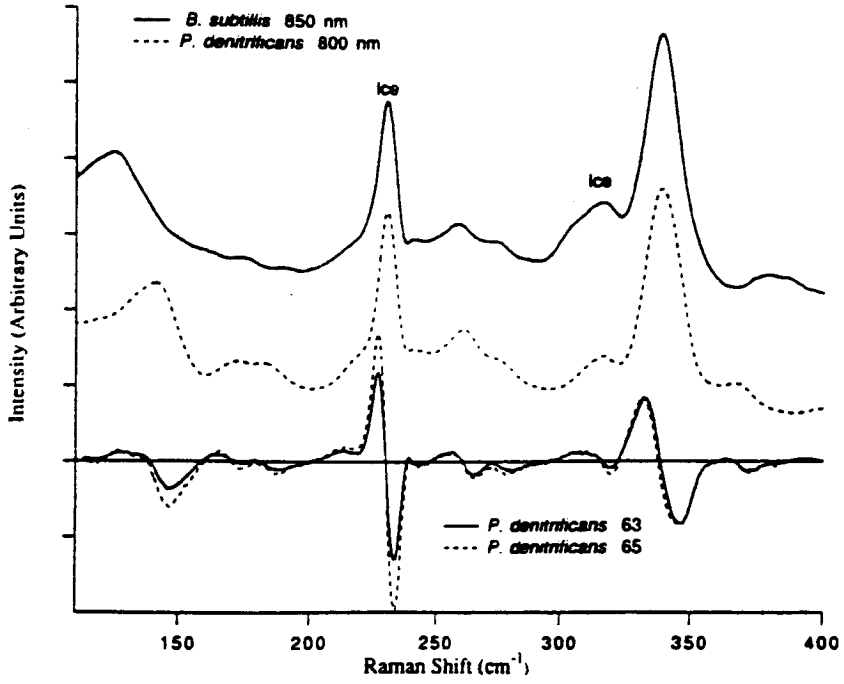
B. subtilis 850 nm
P. denitrificans 800 nm
Ice
Ice
Intensity (Arbitrary Units)
P. denitrificans 63
P. denitrificans 65
150
200
250
300
350
400
Raman Shift (cm^{-1})

EXAFS

It is appropriate to end this section with a summary of EXAFS results obtained on the Cu_A center because these studies provide the highest resolution structural data available for the Cu_A center. EXAFS data have been reported for the *Thermus thermophilus* domain in both the oxidized (mixed valence) and reduced forms[28] (Figure 10). Data for both proteins indicate the presence of a short Cu-Cu distance of 2.43 Å. It should be noted that this is significantly shorter that the 2.6 and 2.7 Å distances found in the *Paracoccus denitirficans* and bovine cytochrome oxidase x-ray structures. The Cu-S and Cu-N distances determined by EXAFS are 2.3 and 1.96 Å, respectively. The error reported for these values is ±0.02 Å. Using the values of the Cu-S and Cu-Cu distances determined by EXAFS, one calculates a Cu-S-Cu angle of 65°. The Cu-S EXAFS component displays very little temperature dependence, implying that the Cu-S distance does not vary a great deal. On the other hand, the Cu-Cu component displays a marked temperature dependence. These findings support the results obtained form RR studies that suggest in the lowest energy vibrational mode there is a symmetrical displacement of the Cu and S atoms with little to no change in the Cu-S distance.

Figure 9. (a) The original EXAFS spectrum of the Cu_A center in the *Bacillus subtillus* soluble domain that provided the first evidence for a Cu-Cu bond. (b) EXAFS data on the oxidized and reduced *Thermus thermophilus* soluble Cu_A domains. The Cu-Cu distance in the oxidized state deduced from this data is 2.43 Å.

a

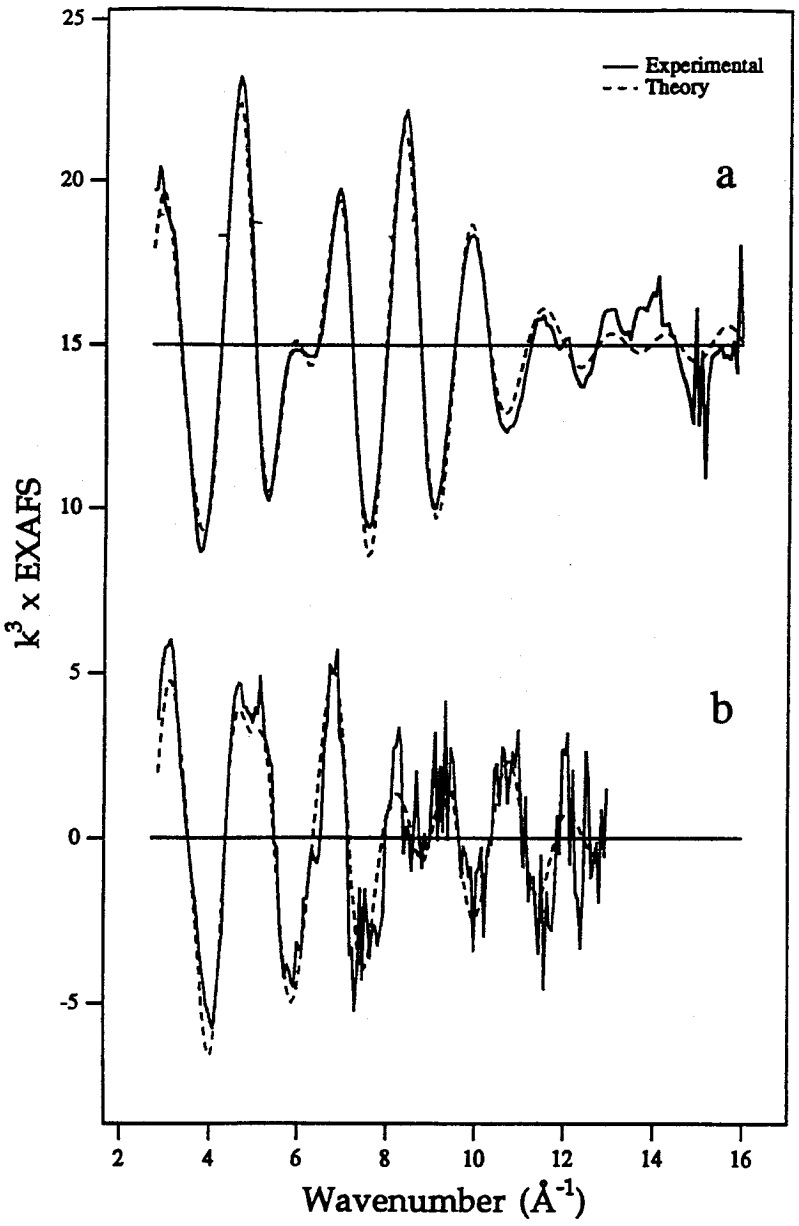
Experimental
Theory
a
b
25
20
15
10
5
0
-5
2
4
6
8
10
12
14
16
k3 x EXAFS
Wavenumber (Å-1)

b

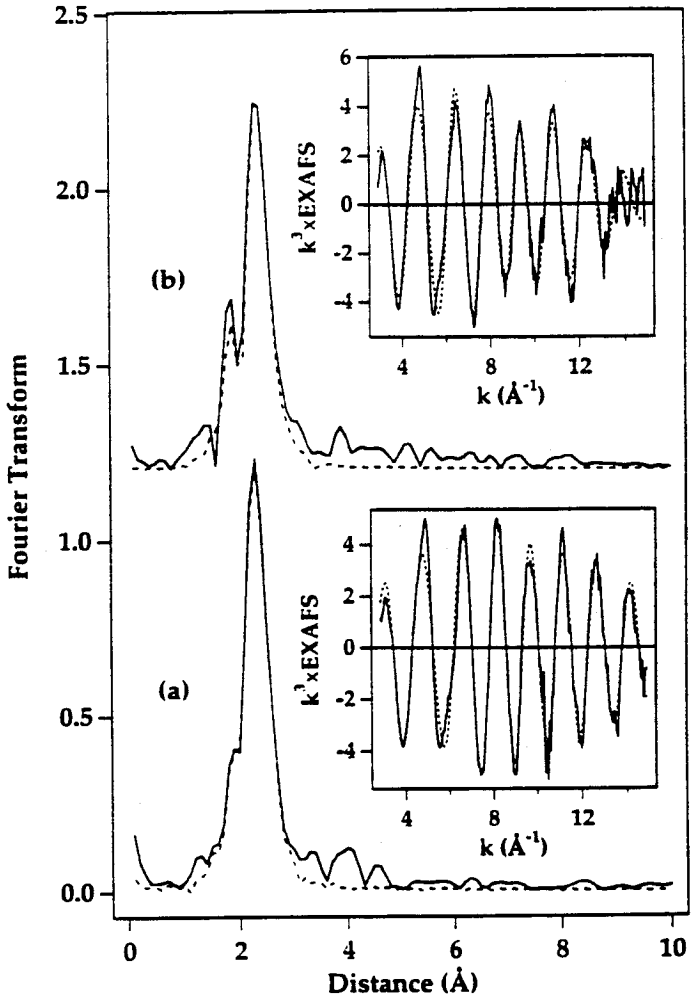

Figure 4. EXAFS of *T. thermophilus* Cu_A: (a) simulated versus experimental Fourier transforms and EXAFS (inset) of mixed-valence protein and (b) simulated versus experimental Fourier transforms and EXAFS (inset) of fully reduced protein.

STRUCTURE OF CYTOCHROME OXIDASE

The solution of the x-ray structures of cytochrome oxidase provided conclusive evidence for the binuclear nature of the Cu_A center. It also affords a view of the Cu_A center in relation to the other redox centers in the enzyme. However, it should be kept in mind that the resolution of the x-ray structures is less than desired. Determining the location of the atoms of the Cu_A site was not unambiguous. With that in mind, the structural parameters of the Cu_A center determined by EXAFS agree with those determined by x-ray crystallography within the resolution of the x-ray structures. In discussing the structure of cytochrome oxidase, the data obtained for the bovine enzyme will be cited, since this system is the most complete, i.e., the structure was solved with the non-redox active centers intact as well. The structure of the Cu_A center consists of two copper ions symmetrically bridged by two Cys thiolates, forming a planar Cu_2S_2 rhomb. Each copper has a terminal histidine ligand; one copper ion has a backbone carbonyl of a Glu residue and the other copper ion a thioether sulfur of a Met side chain that act as weak axial ligands. The Cu-Cu axis is nearly perpendicular to the membrane (i.e., colinear with the membrane normal). The Cu_A center is nearly equidistant from the other two redox centers in cytochrome oxidase. The metal-metal distance from Cu_A to heme a is ~19 Å; from Cu_A to the iron atom of heme a_3 the distance is ~22 Å. This might lead one to believe that electron transfer is equally efficient between Cu_A and either heme a or heme a_3. However, as will be discussed in greater detail in a Chapter 4, a very efficient ET pathway exists between the Cu_A center and heme a of subunit I. This greatly favors the reduction of heme a, compared to heme a_3, by Cu_A.

[1] Brezezinki, P. *Biochemistry* **1996**, *35*, 5611-5615.

[2] Tsukihara, T.; et al. *Science* **1996**, *269*, 1069-1074.

[3] Iwata, S.; Ostermeier, C; Ludwig, B.; Michel, B. *Nature* **1996**, *376*, 660-669.

[4] Warburg, O.; Negelein, E. *Biochem Z.* **1929**, *214*, 64-100.

[5] Keilin, D.; Hartree, E.F. *Nature* **1938**, *141*, 870-871.

[6] Keilin, D.; Hartree, E.F. *Proc. Roy. Soc. London* **1939**, *B127*, 169-191.

[7] Sands, R.H.; Beinert, H. *Biochem. Biophys. Res. Comm.* **1959**, *1*, 175-179.

[8]; Beinert, H.; Griffiths,D.E.; Wharton, D.; Sands, R.H. *J. Biol. Chem.* **1962**, *237*, 2337-2346.

[9] Beinert, H. in *The Biochemistry of Copper* Academic Press: **1966**, 213-234.

[10] Vanngard, T. in *Copper Proteins* John Wiley & Sons: **1972**, 411-447.

[11] Froncisz, W.; et al. *J. Biol. Chem.* **1979**, *254*, 7482-7484.

[12] Stevens, T.H.; Martin, C.T.; Wang, H.; Brudvig, G.W.; Scholes, C.P.; Chan, S.I. *J. Biol. Chem.* **1982**, *257*, 12106-12113.

[13] Martin, C.T.; Scholes, C.P.; Chan, S.I. *J. Biol. Chem.* **1988**, *263*, 8420-8429.

[14] Kroneck, P.M.H.; Antholine, W.E.; Riester, J.; Zumft, W.G. *FEBS Lett.* **1988**, *242*, 70-74.

[15] Antholine, W.E.; Kastrau, D.H.W.; Steffens, G.C., Buse, G.; Zumft, W.G.; Kroneck, P.M.H.; *Eur. J. Bioch.* **1992**, *209*, 875-881.

[16] Li, P.M.; Malmstrom, B.G.; Chan, S.I. *FEBS Lett.* **1989**, *248*, 210-211.

[17] von Wachenfeldt, C.; de Vries, S.; van der Oost, J. *FEBS Lett.* **1994**, *340*, 109-113.

[18] Saraste

[19]Slutter, C.E.; Sanders, D.; Wittung, P.; Malmstrom, B.G.; Aasa, R.; Richards, J.H.; Gray, H.B.; Fee, J.A. *Biochemistry*, **1996**, *35*, 3387-3395.

[20] Wilmanns, M.; Lappalainen, P.; Kelly, M.; Sauer-Eriksson, E.; Saraste, M. *Proc. Nat. Acad. Sci.* **1995**, *92*, 11955-11959.

[21] Dennison, C.; Vijgenboom, E.; de Vries, S.; van der Oost, J.; Canters, G.W. *FEBS Lett.* **1995**, *365*, 92-94.

[22] Hay, M.; Richards, J.H.; Lu, Y. *Proc. Nat. Acad. Sci.* **1996**, *93*, 461-465.

[23] Karpefors, M.; Slutter, C.E.; Fee, J.A.; Aasa, R.; Kallebring, B.; Larsson, S.; Vanngard, T. *Biophys. J.* **1996**, *71*, 2823-2829.

[24] Andrew, C.R. et al. J. Am. Chem. Soc. 1994, 116, 10759-10760.

[25] Andrew, C.R.; Sander-Loehr, J. *Acc. Chem. Res.* **1996**, *29*, 365-372.

[26] Andrew, C.R.; et al. *J. Am. Chem. Soc.* **1996**, *118*, 10436-10445.

[27] Wallace-Williams, S.E.; et al. *J. Am. Chem. Soc.* **1996**, *118*, 3986-3987.

[28] Blackburn N.J.; et al. *J. Am. Chem. Soc.* **1997**, *119*, 6135-6143.

Chapter 3.

Density Functional Theory Electronic Structure Calculations on the Cu_A Center in Cytochrome Oxidase

OVERVIEW

This chapter describes the results of ab initio electronic structure calculations undertaken on a model of the Cu_A center in cytochrome oxidase. The method used in these calculations is Becke3-LYP DFT[1] implemented in the pseudospectral electronic structure calculation program PS-GVB.[2] After brief introduction and background sections, results are reported for the calculated optimized geometry, HOMO, and transition energies and intensities of a model of the blue copper site. These results indicate that Becke3-LYP DFT accurately describes the geometry and the optical absorption spectrum of blue copper sites. The next section describes the results of the optimized geometry and molecular orbital diagram calculated for the Cu_A center. The optimized structure agrees very well with the structure derived from the most recent EXAFS data on soluble Cu_A fragments. The HOMO calculated by DFT agrees with the HOMO character calculated by different approaches. However, the agreement between the calculated transition energies and intensities and experimental data is not as satisfactory. But the polarization of the optical transitions appears to be correctly described. The next section presents results that indicate that the electronic structure of Cu_A is *extremely* sensitive to the value of the Cu-S-Cu angle. The last section describes calculations of the optimized structures of the reduced forms of the blue copper and Cu_A model complexes. In both cases our results indicate that the coordination environment of the protein favors the oxidized form of the copper center.

INTRODUCTION

Although the unusual spectroscopic features of the Cu_A center have attracted the interest of experimentalists for many years, only recently have theorists undertaken calculations on this site. This has largely been due to the lack of conclusive information on the structure, copper stoichiometry, and absorption spectrum of the Cu_A center. This did not prevent some researchers from pursuing calculations. But it should come as no surprise that the two papers on the electronic structure of Cu_A published prior to the report of the crystal structures of cytochrome oxidase are based on incorrect structures. The first paper derived a molecular orbital diagram of the Cu_A center based on the mononuclear Chan model.[3] The second paper utilized semiempirical methods to calculate orbital energy levels for the terminal model of the Cu_A center.[4] In this structure, each copper has a Cys and His ligand; the third coordinating group is the other copper, implying the existence of metal-metal bond. Now that it has been determined conclusively that the Cu_A center is dithiolate bridged binuclear copper complex, theoreticians are in a much better position to propose an interpretation of the spectroscopic features of this center.

Because they have been computationally intractable, first principle (ab initio) calculations of the electronic structure of metal complexes have not been widely reported. The development of basis sets suitable for first row transition metals[5] and methods to efficiently calculate wavefunctions[6] along with the ever growing size and speed of computational resources have greatly facilitated such calculations. Using an effective core potential for the two copper ions, the number of basis functions for the minimal model of the Cu_A center used in the calculations reported herein is ~280. A few years

ago, calculations of this magnitude would have required the use of devoted resources. Nowadays, calculations of this size can be run on workstations in a reasonable amount of time.

The main focus of the theoretical calculations on the Cu_A center is the calculation of the molecular orbital energy diagram that will serve as a basis for assigning the observed spectroscopic features of the Cu_A center. The wealth of spectroscopic data on the Cu_A center is both a blessing and a curse. On the one hand, it provides detailed information that is invaluable in judging the quality of the calculations. On the other hand, it makes big demands from theory. The undertaking of electronic structure calculations should provide some insight into the origin of the spectroscopic features, how they contribute to the function of the Cu_A center, and what role the protein serves in reducing the reorganization energy of the center. Before proceeding with the presentation of the results of the calculations, a brief overview of the methods used in these calculations is presented.

BACKGROUND

Comparison of DFT calculations on blue copper sites with previous calculations

Geometry optimization

In order to assess the suitability of our approach as well as compare the results of our calculations with results obtained by different methods we chose to undertake calculations on a complex, $[Cu(SCH_2CH_3)(Im)_2]^+$, that serves as a model for the copper site in blue copper proteins. Initially, for the geometry optimization we used two starting structures with C_s symmetry (Figure 1): in one the imidazole rings were coplanar, perpendicular to the symmetry plane. In the other, the rings were perpendicular to the ligand atom (SN_2) plane, the plane formed by the sulfur and nitrogen atoms. In the optimized C_s symmetry structure the imidazole rings are tilted slightly out of the SN_2 plane. This structure does not agree well with the blue copper site in azurin, which has C_1 symmetry. In azurin, the imidazole rings are tilted slightly out of the plane but the ring planes are nearly parallel. A structure with C_1 symmetry similar to the azurin site was obtained by manually rotating the imidazole rings of the C_s optimized structure. The optimized C_1 structure is nearly superposable on the azurin active site (Figure 2). The calculated Cu-S and Cu-N bond lengths are 2.19 and 2.037 Å. The calculated bond length and angle are compared to experimental values in Table I. The C_1 optimized Cu(II) structure is ~0.05 eV lower in energy than the C_s optimized Cu(II) structure. The geometry optimization statistics of the C_1 structure are listed in Table II.

Figure 1. The two initial C_s symmetry structures used in the geometry optimization of the blue copper model complex $[Cu(SCH_2CH_3)(Im)_2]$. In the structure on the top the imidazole rings are perpendicular to the trigonal ligand atom plane. In the structure on the bottom the rings are perpendicular to the symmetry plane.

Blue Copper Model Complexes

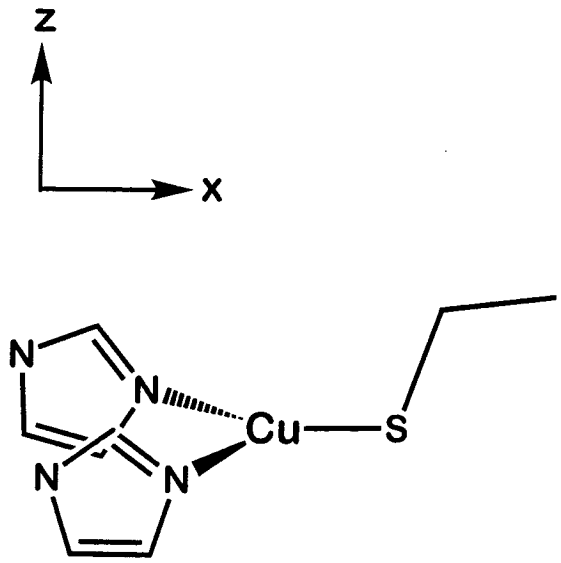

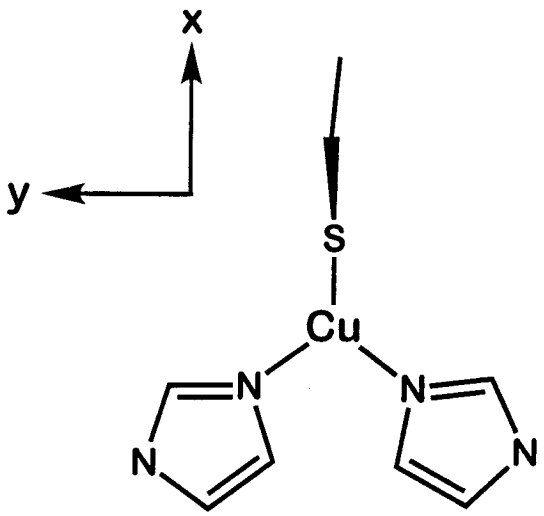

Figure 2. Comparison of the optimized C_1 symmetry Cu(II) structure of the blue copper model complex with the copper site of azurin.

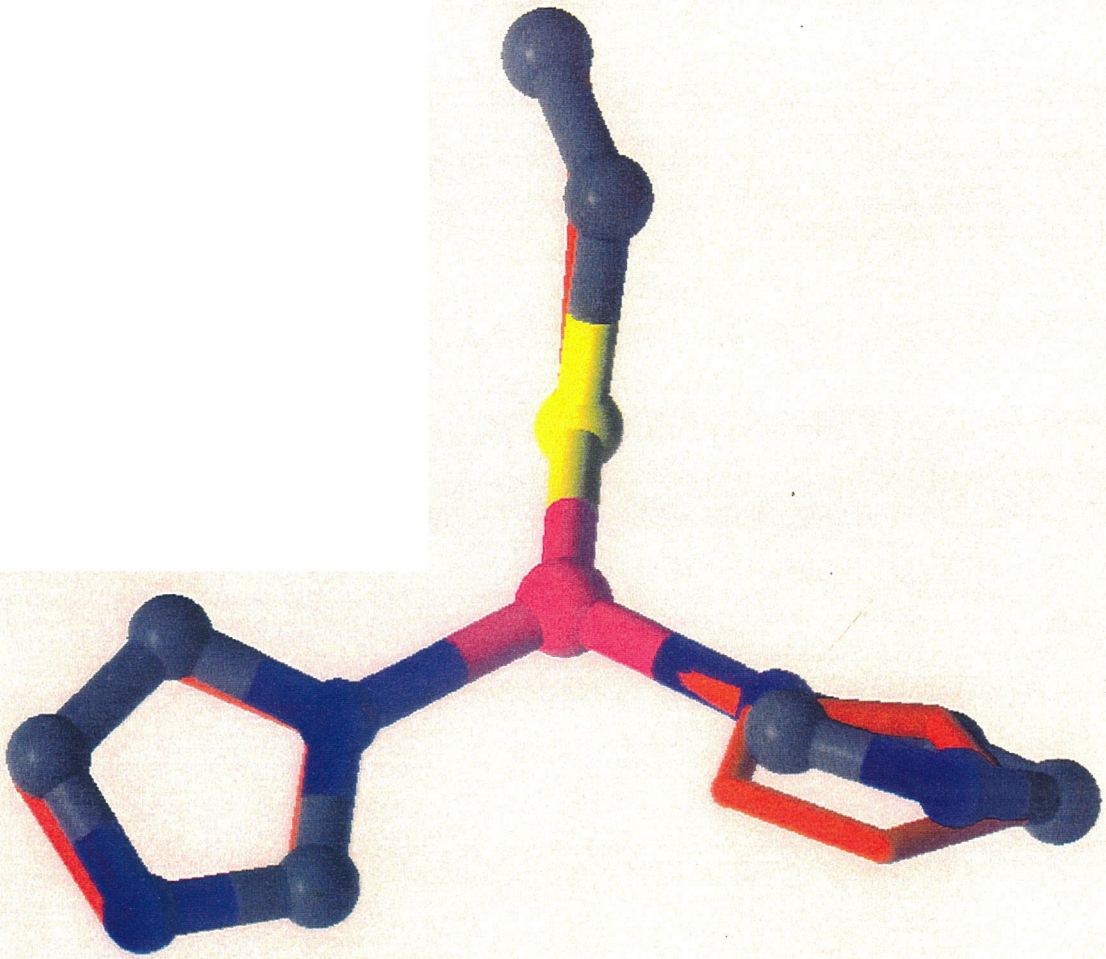

Table I. Comparison of Oxidized Blue Copper Structures

		optimized Cu(II) structure		*experiment*
	symmetry	C_s	C_i	
distance(Å)				
Cu-S		2.216	2.19	2.12
Cu-N		2.039	2.037	2.06
angle(°)				
S-Cu-N		122.66	127	120
N-Cu-N		114	106	103
dihedral(°)				
S-Cu-N-C_γ		±28.76	140	
			137	

Table II. Geometry Optimization Statistics of Cu(II) C_1 Blue Copper Structure

	Actual values	*Default values*
criteria		
Gradient maximum	3.77×10^{-4}	4.5×10^{-4}
Gradient rms	1.08×10^{-4}	3.0×10^{-4}
Displacement maximum	1.31×10^{-3}	1.8×10^{-3}
Displacement rms	2.68×10^{-4}	1.2×10^{-3}

Quantities are in atomic units (hartrees, bohr, etc.).

Character of the HOMO

The HOMO calculated by DFT for the C_1 structure is π antibonding, primarily Cu d_{xy} and S p_y in character (Figure 3). This is essentially identical with the HOMO calculated by Solomon using SCF-Xα-SW methods(Figure 4). Using the C_1 optimized geometry, we calculate only a single optical transition with reasonable intensity from a lower lying filled (doubly-occupied) orbital into the singly-occupied HOMO (Figure 5). The transition is polarized in the x-direction and has an energy of ~15,960 cm^{-1} (experimental value ~16,000 cm^{-1}). It originates from a π bonding Cu d_{xy}/S p_y orbital. Thus, this transition is assigned as a ligand-to-metal charge-transfer (LMCT) transition. Any d-d transitions that may occur in the blue copper centers are predicted to be higher in energy than (lie to the blue of) the LMCT transition.

These results indicate that the Becke3-LYP DFT method accurately describes the geometry of the oxidized blue copper site. The agreement with the experimental transition energy of the characteristic absorption feature is exceptionally good. However, the calculated energies of the d-d transitions are much higher than the values extracted from experiment.

Figure 3. The blue copper HOMO calculated by Becke3-LYP DFT.

Blue Copper HOMO

S p_y-Cu d_{xy} π^*

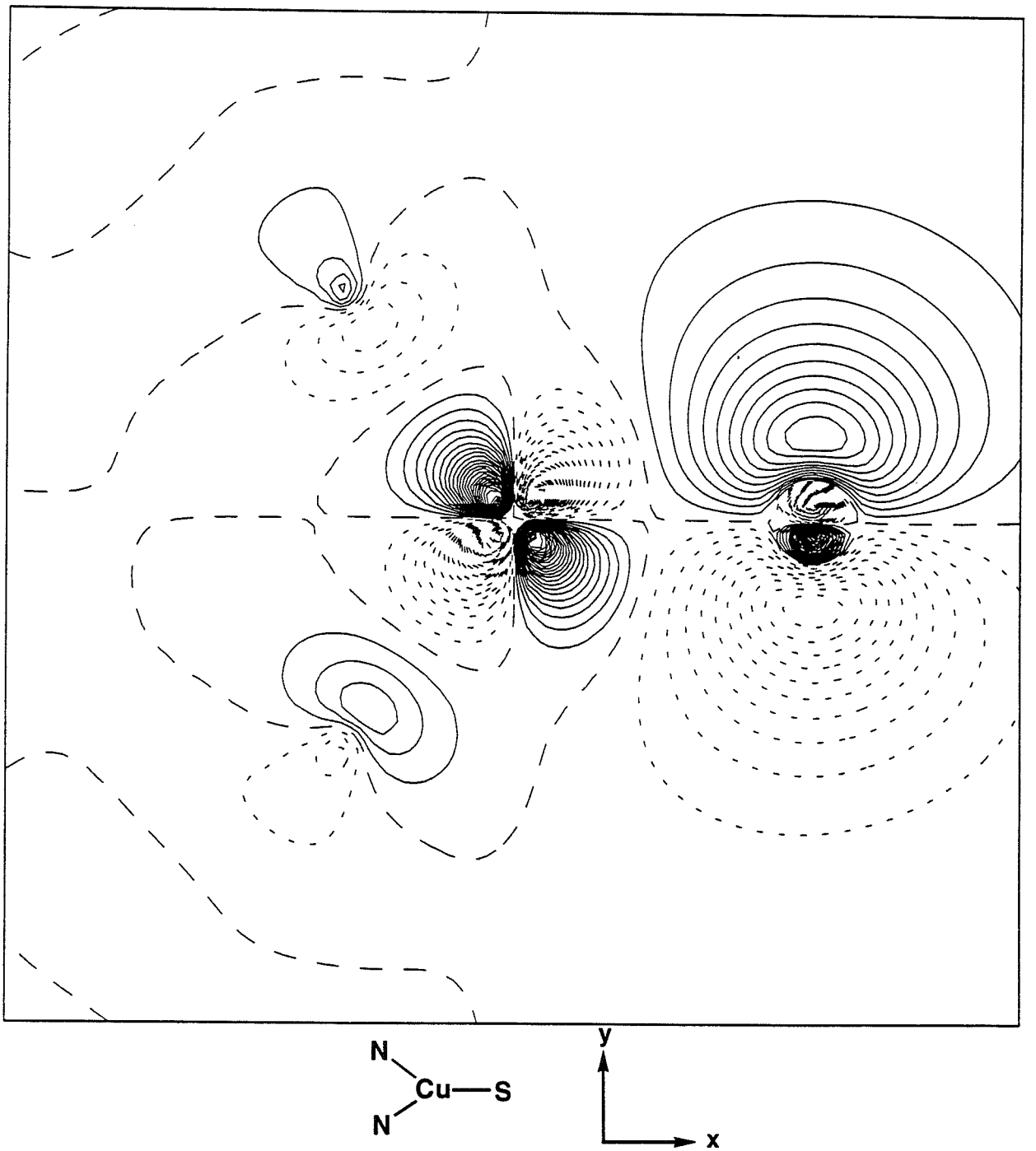

Figure 4. The blue copper HOMO calculated by the Xα-SW method.

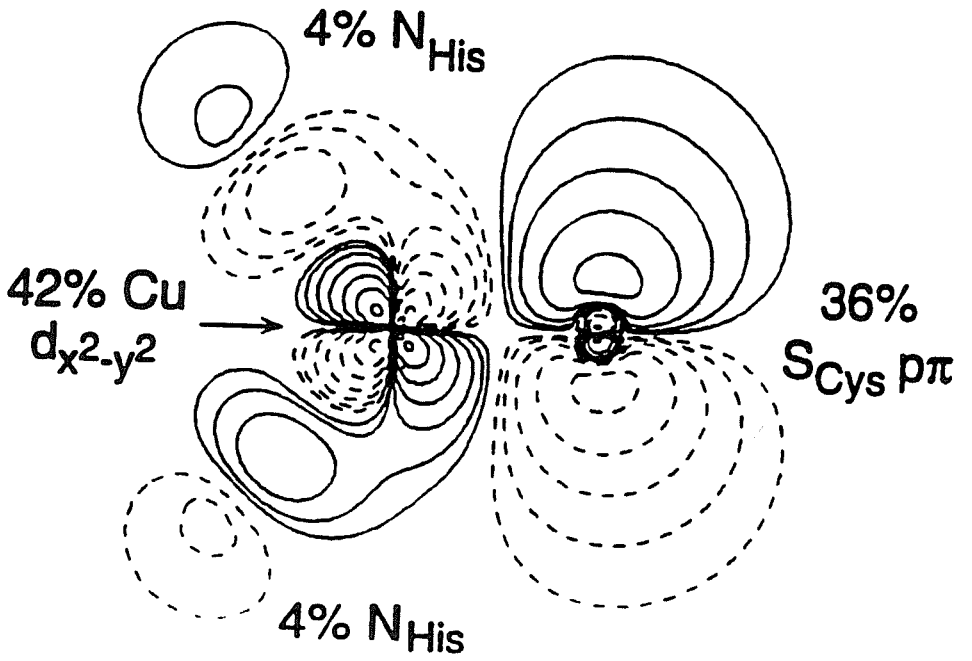
4% N$_{His}$
42% Cu
$d_{x^2-y^2}$
36%
S$_{Cys}$ pπ
4% N$_{His}$

Figure 5. Calculated spectrum of the optimized Cu(II) C_1 blue copper model complex. A single optical transition with reasonable intensity at 15,690 cm^{-1} and polarized in the x-direction is predicted. The characteristic experimental transition of the blue copper proteins occurs at ~16,000 cm^{-1}. The vertical lines with y-coordinates 0.5 and 1.0 along the x-axis indicate the relative energy spacing of the highest-lying molecular orbitals.

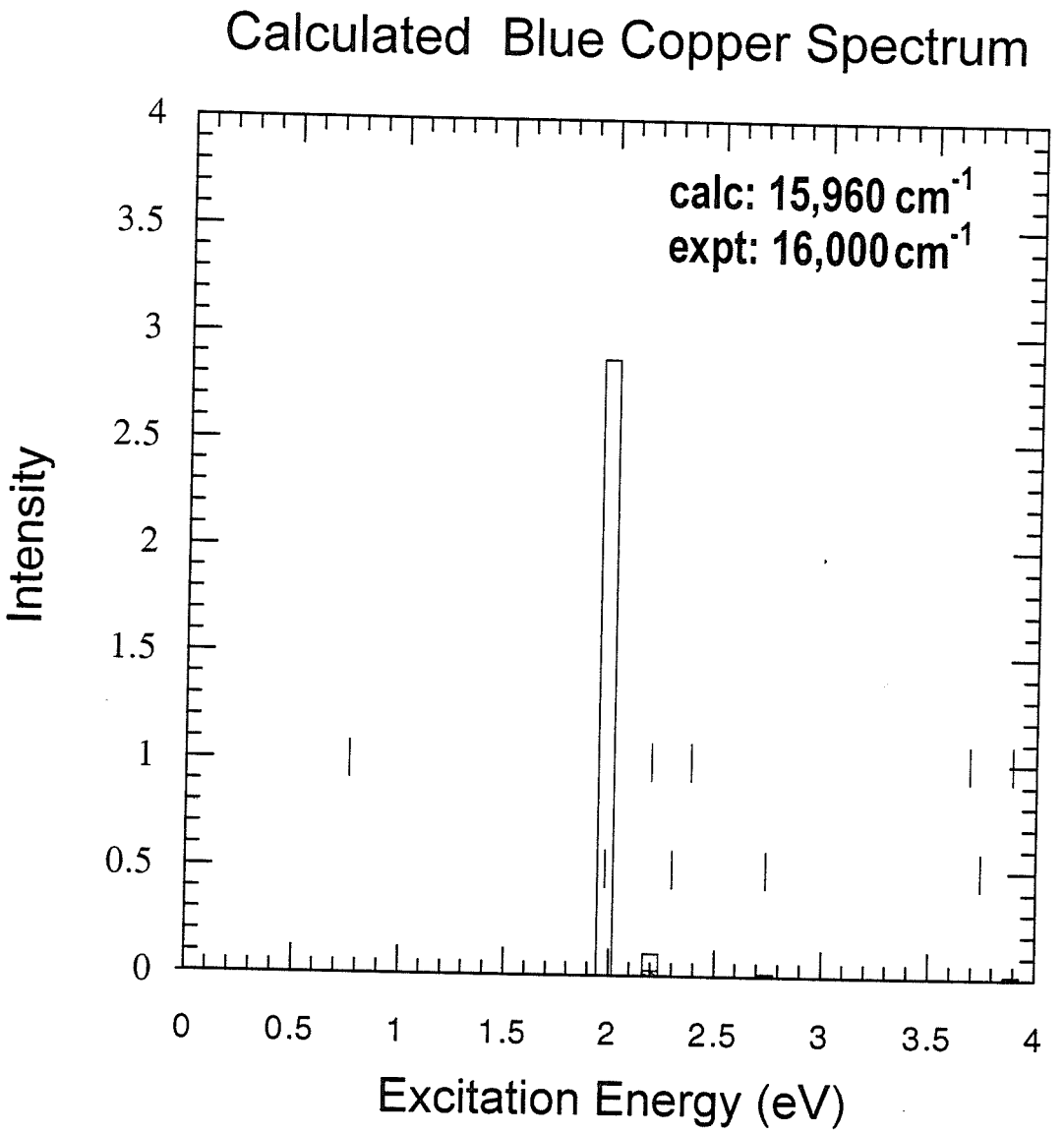
Calculated Blue Copper Spectrum
calc: 15,960 cm-1
expt: 16,000 cm-1
Intensity
Excitation Energy (eV)
0
0.5
1
1.5
2
2.5
3
3.5
4

RESULTS

Geometry Optimization

General description of calculations

Initially, we utilized a simplified model of the Cu_A center where the Cys side chains are represented by methanethiol groups and the His side chains by ammonia groups. The coordinates of the initial structure were based on the accepted idealized values for bond lengths, angles, etc. We started by calculating the HF wavefunction of this complex for the mixed valence Cu(I)/Cu(II) state. The SCF calculation converged satisfactorily. We then decided to pursue geometry optimization of the Cu_A model complex. For the geometry optimization, imidazole groups were used in place of ammonia groups because they are a better approximation for histidine and one might observe significant differences in bond lengths, orbital energies and transition intensities. In the crystal structure, a thioether sulfur of a Met residue and a backbone carbonyl are located within 3 Å of the two copper ions (one per each copper). These interactions may serve to prevent water from occupying the site, thereby keeping the redox potential high and the reorganization energy low while at the same time preventing collapse of the site to a tetrahedral form. In either case, the axial ligands are at too far a distance to bond strongly to the copper ions and are not expected to alter the molecular orbital diagram significantly. For that reason, they were excluded from the calculations.

The starting structure for the optimization used the same initial coordinates derived from accepted values and had overall C_i symmetry (Figure 6). Optimization of the geometry for the complex in the Cu(I)/Cu(II) state was slow and not smooth. Initially the SCF portion of the calculation would not converge. Convergence in the SCF segment

Figure 6. The Cu_A model complex $[Cu_2(SCH_3)_2(Im)_2]$. The SCH_3 groups represent the Cys side chains and the imidazole (Im) groups represent the histidine side chains. The structure has C_i symmetry overall.

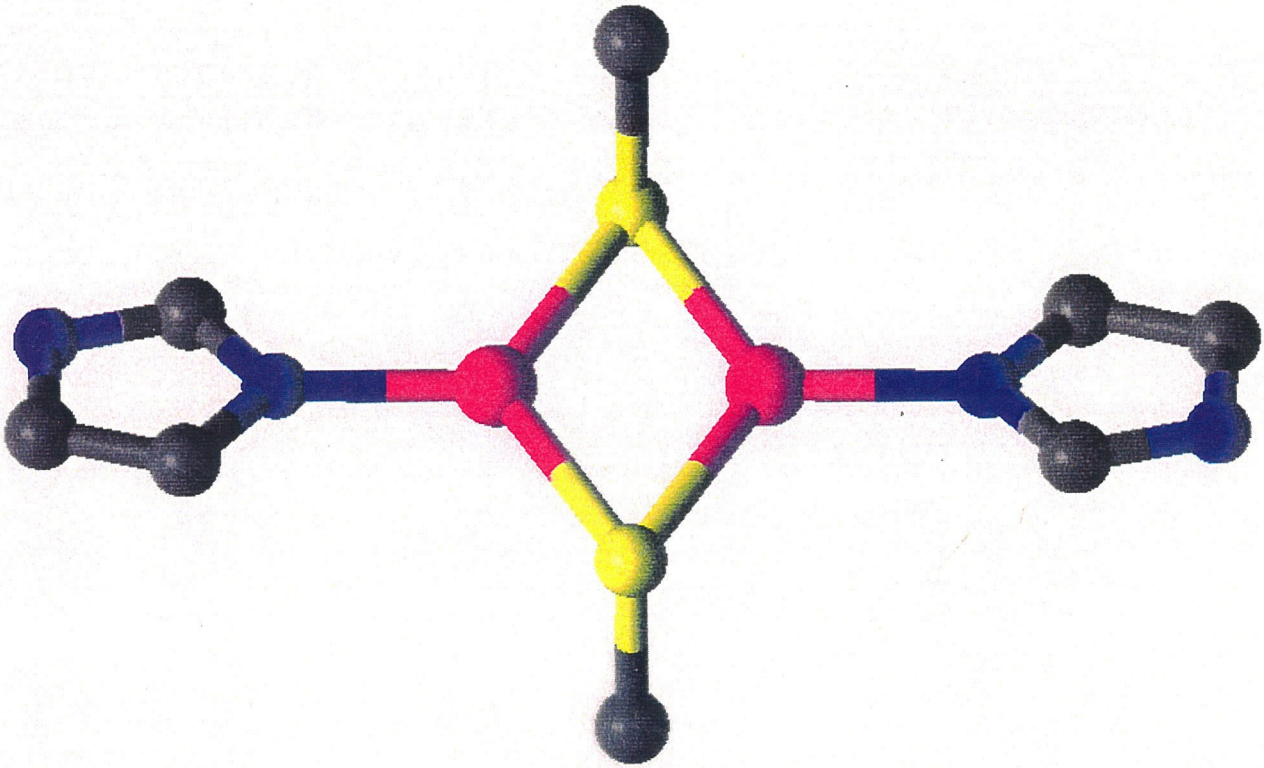

was improved by shifting the energy levels of the virtual orbitals. Although we were able to improve convergence in the SCF calculation, convergence of the geometry optimized structure was slow and difficult. The criteria used to judge the quality of the optimization are the nuclear displacement, the size of the gradients and the total energy change. The default values for these parameters in the PS-GVB program were used in the optimization calculation. Initially, the geometry optimization failed to converge in fifty iteration steps. The energy fluctuated during the calculation, hinting of the existence of a low-lying state. At this point, it was necessary to implement Culot-Fletcher trust radius adjustment during the geometry optimization. Convergence of an optimized structure was finally achieved but the statistics did not behave ideally. It was necessary to employ two other options in the PS-GVB before satisfactory convergence was finally achieved. First, finer grids were implemented for the DFT part of the gradient. Second, instead of using the standard Cholesky decomposition for inverting the RwR matrix, a singular value decomposition method was used. Implementation of these options resulted in a fairly smooth optimization with good statistics (Table III).

Table III. Geometry Optimization Statistics of Cu(I)/Cu(II) Cu_A Structure

criteria	*Actual values*	*Default values*
Gradient maximum	2.35×10^{-4}	4.5×10^{-4}
Gradient rms	7.50×10^{-5}	3.0×10^{-4}
Displacement maximum	1.33×10^{-3}	1.8×10^{-3}
Displacement rms	3.85×10^{-4}	1.2×10^{-3}

Quantities are in atomic units (hartrees, bohr, etc.).

Evaluation of optimized structure

In general, the geometry optimized structure agrees well with the experimental data available for the Cu_A center (Table IV and Figure 7). Over the course of time, experimental data from different sources have produced three distinct structures of the Cu_A center. Before the two x-ray structures of cytochrome oxidase were published, the accepted structure of the dithiolate bridged binuclear Cu_A center, model I, was based on indirect data from various Cu_A spectroscopic studies.[7] The structure of the Cu_A center obtained from the 2.8 Å x-ray structure of bovine cytochrome oxidase,[8] is referred to as model II. The last model, model III, is based on data from the most recent EXAFS study of the Cu_A center.[9] For completeness, we compared the geometry optimized structures with all three experimental structures. The geometry optimized structure agrees very well with data obtained from the most recent EXAFS study of the Cu_A center. The rms difference for the superposition of the heavy atoms of the optimized structure with those of models I, II, and III are: 0.22 Å, 0.19 Å, and 0.16 Å (Figure 7), respectively. (Optimization of the Cu_A model with another DFT method resulted in a very similar structure.) The various experimental structures have different values for two features that define the structure of the Cu_2S_2 core and have a tremendous influence on the nature of the electronic structure: the Cu-Cu distance and the Cu-S-Cu angle. Experimental support and the importance of differences in the values of the Cu-Cu distance and the Cu-S-Cu angle, as well as other features that differ among the various structures are discussed below.

Figure 7. Comparison of the optimized oxidized Cu_A model complex with the Cu_A structure deduced from EXAFS studies. The overall rms overlap of the heavy atoms is 0.16 Å.

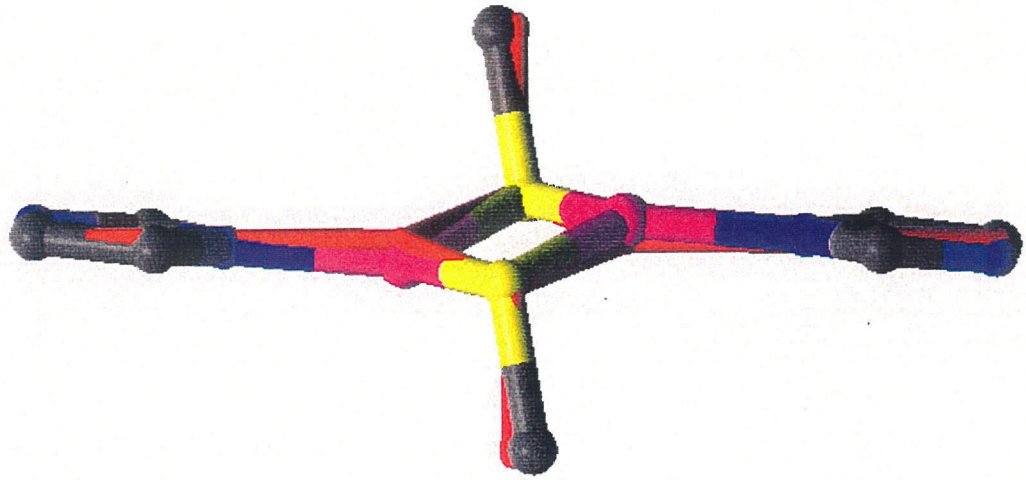

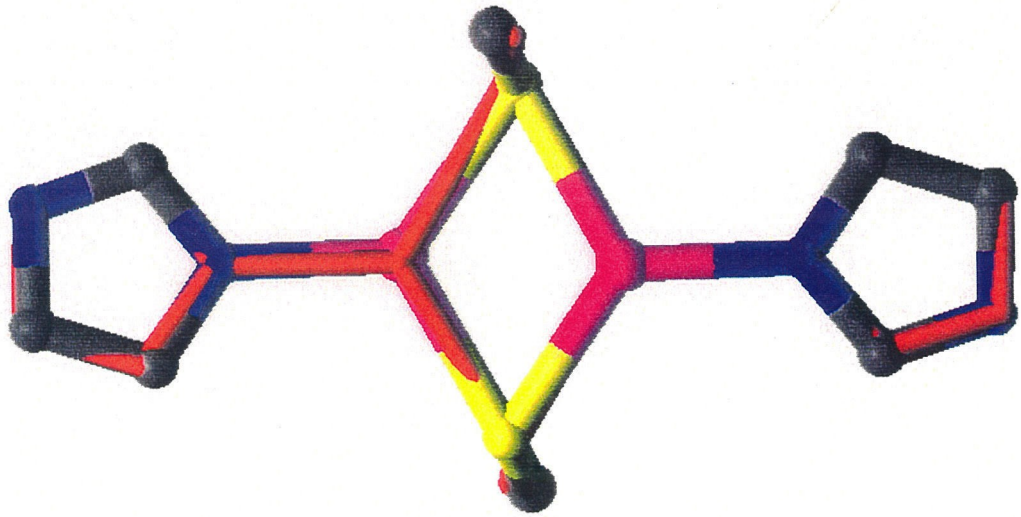

Table IV: Cu_A Structural Data

	theory	***experiment***		
	DFT	EXAFS model III	x-ray model II	accepted model I
distance(Å)				
Cu-Cu	2.46	2.43	2.6 – 2.7	2.5
Cu-S	2.35	2.3	2.1 – 2.3	2.2
Cu-N	1.98	1.96	1.8 – 1.9	1.9
angle(°)				
Cu-S-Cu	63	65	70	70
C-S–S	107	--	110 – 120	120
N-Cu–Cu	180	--	140 – 160	160
Rms overlap		0.168	0.199	0.201

Structural differences between optimized and accepted structural features

1. Cu-Cu distances and structure of Cu_2S_2 core

Perhaps the most difficult issue to address by either theoretical or experimental studies is whether or not a Cu-Cu bond is present in the Cu_A center. To date, distance has been the main criterion for judging the existence of a Cu-Cu bond. We calculate a Cu-Cu distance of 2.45 Å. In model I, the previously accepted Cu_A structure, the Cu-Cu distance is ~2.5 Å. The bovine cytochrome oxidase x-ray structure (model II) indicates a Cu-Cu distance of 2.7 Å. X-ray structure data are not of high enough (atomic) resolution to address this issue. In model III, the structure based on data obtained from the most recent EXAFS study of the Cu_A center, the Cu-Cu distance is 2.43 Å. The other feature that characterizes the structure of the Cu_2S_2 core is the value of the Cu-S-Cu angle. We calculate a Cu-S-Cu angle of 63°. The value of the Cu-S-Cu angle in models I and II is ~ 70°; in model III the angle is ~ 65°. The calculated values agree extremely well with the EXAFS data. The calculated structure and the EXAFS data support the view of a Cu-Cu bond in Cu_A.

If we exclude for the moment the most recent EXAFS results and compare our results to data obtained from the x-ray structure of bovine cytochrome oxidase, our calculated values do not agree as well as with the experimental data. We calculate a Cu-Cu distance of 2.46 Å and a Cu-S-Cu angle of 63°. In the x-ray structure, the Cu-Cu distance is 2.7 Å and the Cu-S-Cu angle is 70°. It is reasonable to ascribe the observed differences to constraints imposed by the protein framework. This led us to investigate how the calculated HOMO and transition energies and intensities vary as a function of the Cu-S-Cu angle. The results of these calculations, which are discussed below, indicate

that the electronic structure of Cu_A is *extremely* sensitive to the value of the Cu-S-Cu angle.

2. Angle of the C-S bond

Another feature that differs significantly between the optimized structure and the idealized experimental structure is the angle that the methyl group (in terms of the protein, the C_β of the Cys side chain) makes with respect to the Cu_2S_2 plane. In the optimized structure this angle is 107°; the value determined from the x-ray structures is ~110° - 120°. However, as expressed in one of the x-ray structure research papers, the electron density due to the sulfur atoms could not be determined unambiguously. Thus, the distance between the two sulfur atoms determined from the x-ray structure has a sizeable degree of uncertainty. The value of 107° that we obtained for the optimized structure can easily be accommodated within the published x-ray structures. If we consider the location of the C_β atoms to be fairly certain and hold their positions fixed, by reducing the x-ray Cu-Cu distance by 0.2 Å, which brings the value more in line with the previously accepted value, as well as the value obtained from the most recent EXAFS work and our calculated value, the S-S distance increases and hence the angle that the C_β makes with the Cu_2S_2 plane decreases. As will be presented below, changing the value of the C-S-Cu angle to 120° in our optimized structure has very little effect on transition energies and intensities.

We attempted to investigate what effect a C-S-Cu_2S_2 plane angle of 120° would have on the geometry and electronic structure. The value of this angle is expected to have a significant effect on the character of sulfur p orbitals involved in bonding to the copper ions and, hence, on the electronic structure of the site. If we consider the two

extreme cases of 90° and 180°, the nature of the sulfur bonding to the copper ions is potentially very different. In the 90° case, the S p_z orbital would be involved in bonding with the methyl group (or C_β), leaving the S p_x and p_y orbitals to interact with the copper ions. If the value were instead 180°, the S p_y orbital would be involved in bonding to the methyl group, leaving the sulfur p_x and p_z orbitals to interact with the copper ions. In this latter case, one would expect the sulfur to form a sigma bond to the copper via the S p_x orbital and a pi bond to the copper via the S p_z and Cu d_{z2} (or possibly Cu d_{xz} or Cu d_{yz}). In the former case, one would expect the only sigma bonding to occur between sulfur and copper via the S p_x and p_y and the Cu d_{x2-y2} and d_{xy} orbitals. We attempted to do a constrained geometry optimization where the value of the C-S-Cu was held fixed at 120°. Unfortunately, we were never able to satisfactorily converge a structure.

3. Tilt of imidazole rings

The other feature that differs significantly between the optimized structure is the tilt of the imidazole rings with respect to the Cu_2S_2 plane. In both of the cytochrome oxidase x-ray structures, the values of this angle are ~160° and ~140°. From an inspection of the structure, one might expect there to be some deviation from planarity at the copper site due to the presence of the weakly interacting axial ligands. Further indirect experimental support for the tilting of the imidazole rings comes from resonance Raman (RR) studies.[10] Two models of the Cu_A center were used to fit RR data: one had a planar core with the copper sulfur and nitrogen atoms all in one plane and in the other the nitrogen atoms were tilted slightly out of the plane. Using normal coordinate analysis, a model of the Cu_A center where the imidazole rings are tilted 20° – 40° with respect to the Cu_2S_2 plane gives the best fit to the RR data. As with the case of the C-S-Cu_2S_2 plane

angle, we were unable to pursue geometry optimization with this angle fixed at 160°. As discussed below, altering the tilt of the imidazole rings in the optimized structure has little effect on the transition energies and intensities.

The Cu_A Molecular Orbital Diagram

Overall description and nature of the HOMO

We need only consider the sixteen highest lying molecular orbitals (MOs) to discuss the nature of the HOMO and the assignments of the Cu_A optical spectroscopic transitions. These sixteen MOs are derived from 10 copper 3d orbitals, the $3d_{x2-y2}$, $3d_{xy}$, $3d_{xz}$, $3d_{yz}$ and $3d_{z2}$ orbitals from two copper ions; four sulfur p orbitals; a p_x and p_y orbital from the two sulfur atoms, and two N p_x orbitals (Figure 8). It is easiest to think of the nature of these MOs if one thinks of them as a group comprised of four sets. The highest-lying (energetically) set consists of four orbitals that are primarily Cu/S antibonding in character. The next highest set consists of six orbitals that are primarily nonbonding in character, i.e. the Cu d_{z2}, d_{xz}, and d_{yz} orbitals. The two remaining sets, in order of increasing energy, are four orbitals that are primarily Cu/S bonding and two orbitals that are primarily Cu/N bonding. No observable transitions at wavelengths of >300 nm are expected form any of the remaining, higher energy, orbitals, hence the nature of these orbitals will not be discussed in detail.

The Cu_A HOMO calculated by DFT for the structure with Cu-S-Cu = 65° is a Cu/S antibonding orbital with A_u symmetry that is primarily Cu 3 d_{x2-y2} and S p_x in character, with a smaller contributions due to N p_x orbitals (Figure 9). The character of the HOMO is similar to the $^2B_{3u}$ HOMO calculated by the semiempirical INDO/S method[11] and agrees qualitatively with the σ antibonding HOMO derived from S K-edge XAS data.[12] Contours of the sixteen orbitals shown on the MO diagram are shown in Figure 10.

Figure 8. Molecular orbital diagram calculated for the C_i Cu_A model complex with a Cu-S-Cu angle of 65°. The character of the orbitals is indicated on the right. The predicted symmetry allowed transitions are shown as arrows on the left. The polarizations of the transitions are indicated at the bottom of each arrow.

Molecular Orbital Diagram for $Cu_2(SCH_3)_2(Im)_2$ C_i Symmetry (Cu-S-Cu = 65°)

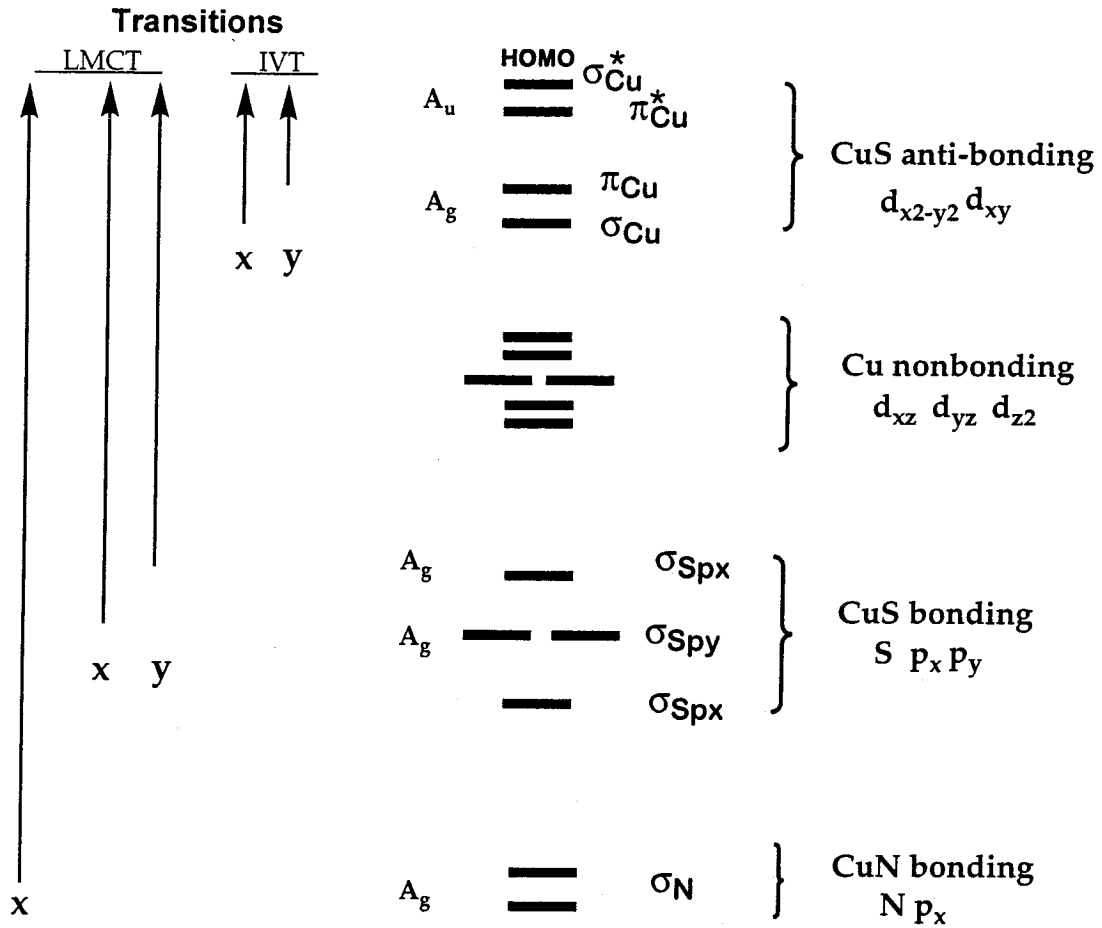

Figure 9. The HOMO calculated by DFT C_i symmetry Cu_A model complex with a Cu-S-Cu angle of 65°. The σ^* HOMO has A_u symmetry and is primarily Cu $3d_{x2-y2}$/S p_x/N p_x in character. The character of this HOMO is similar to the $^2B_{3u}$ HOMO calculated by the semiempirical INDO/S approach.

σ* Cu_A HOMO

(Cu-S-Cu = 65°)

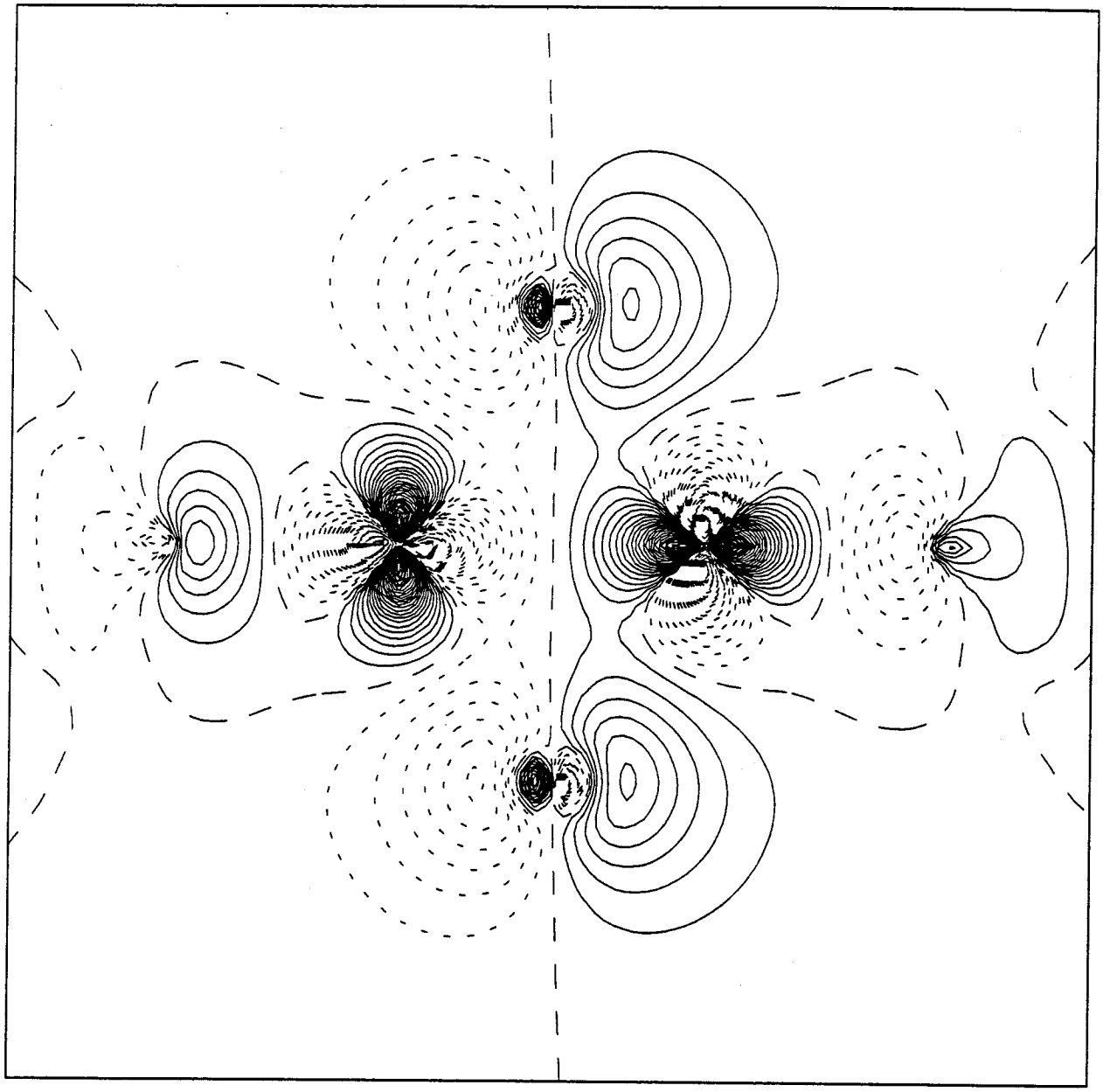

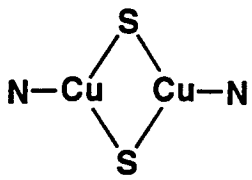

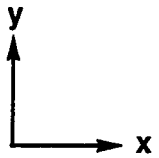

Figure 10. The sixteen highest-lying molecular orbitals of the optimized C_i symmetry Cu_A model complex with a Cu-S-Cu angle of 65°. The orientation is the same as in Figure 9.

σ_{Cu}^{*}

A_u

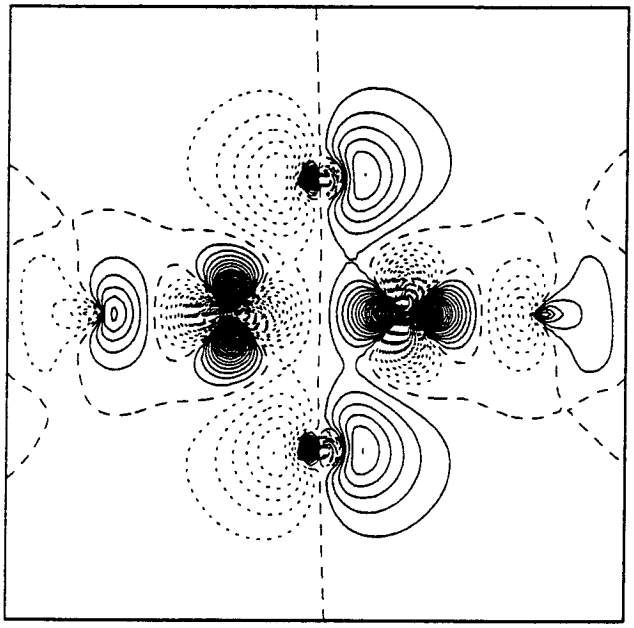

π_{Cu}^{*}

A_u

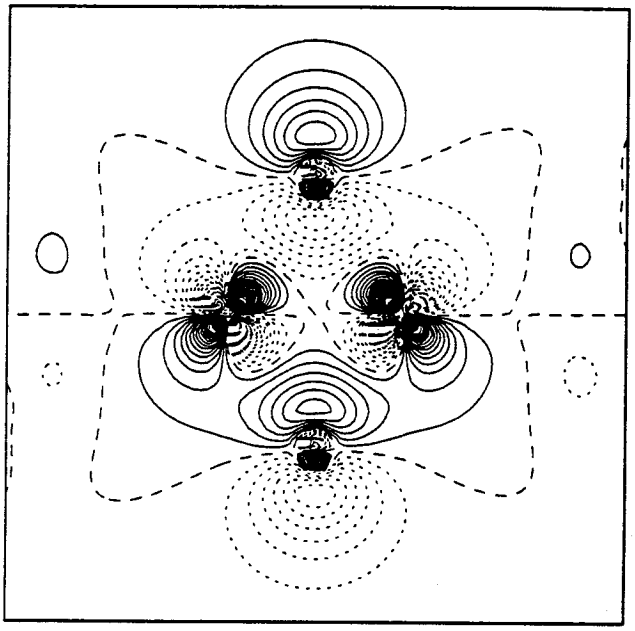

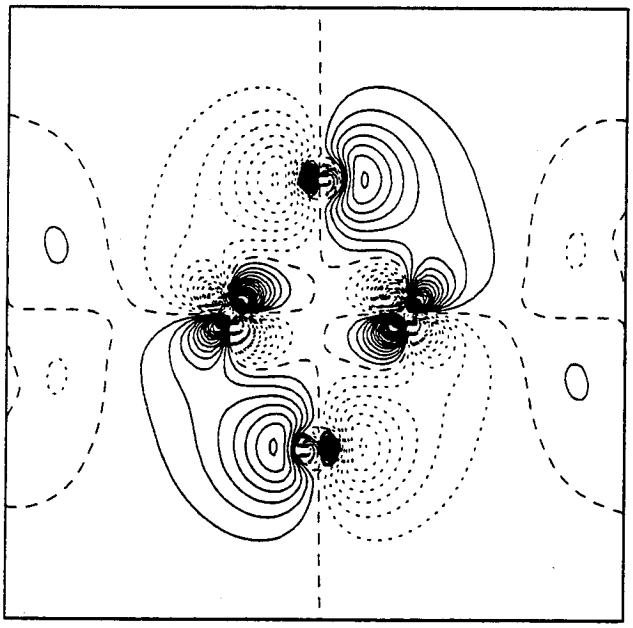

π_{Cu}

A_g

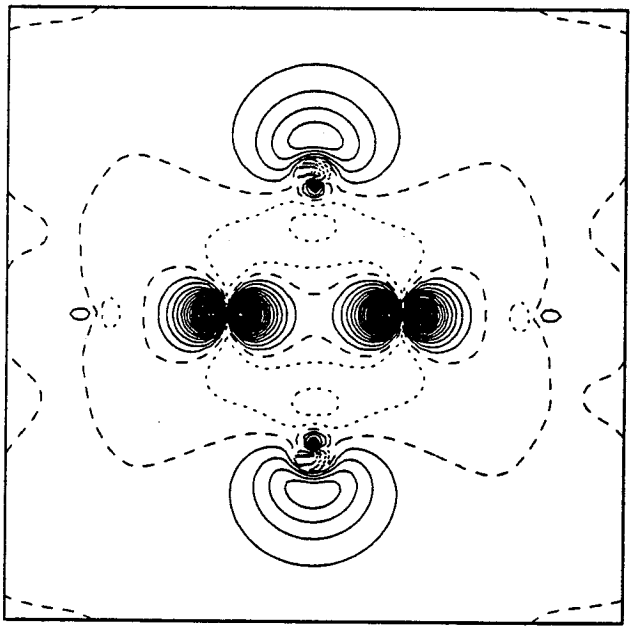

σ_{Cu}

A_g

Cu d_{xz}
A_g

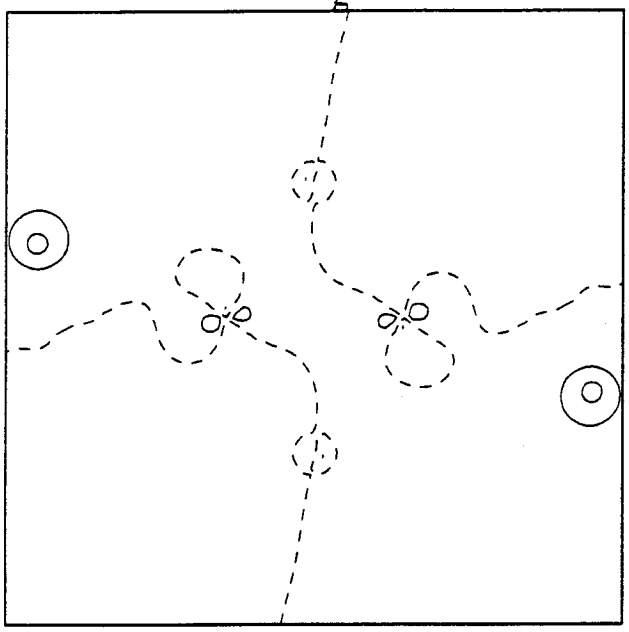

Cu d_{z2}
A_u

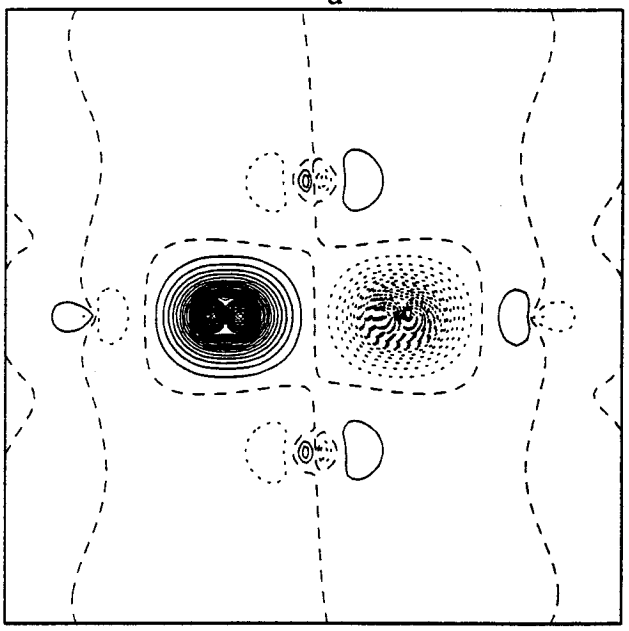

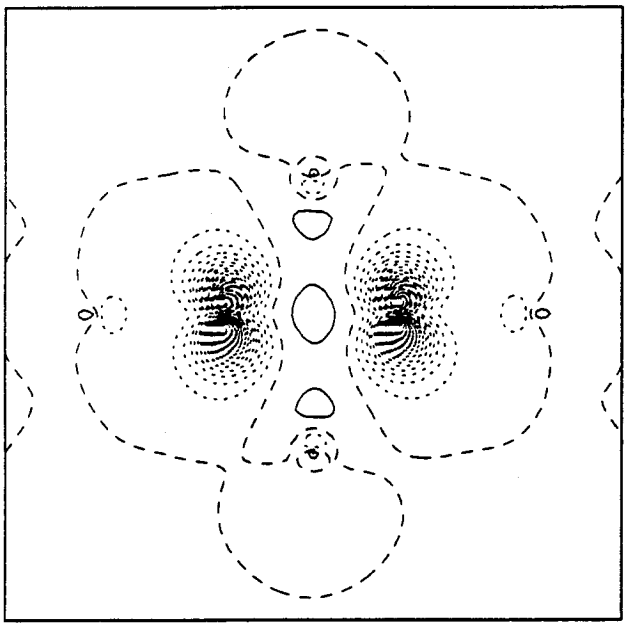

Cu d_{xz}
A_g

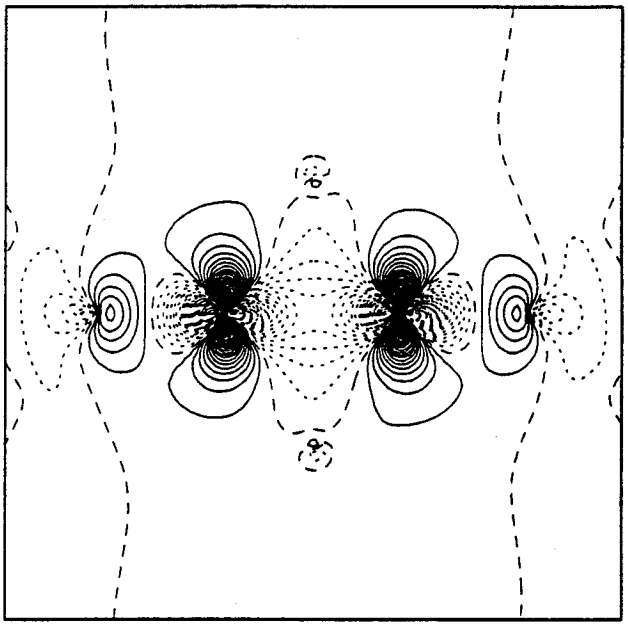

Cu d_{yz}
A_g

Cu d_{yz}
A_u

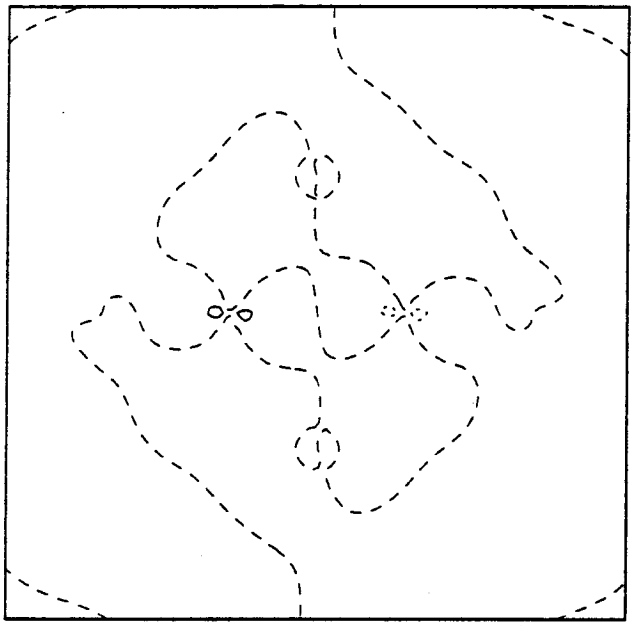

σ_S
A_g

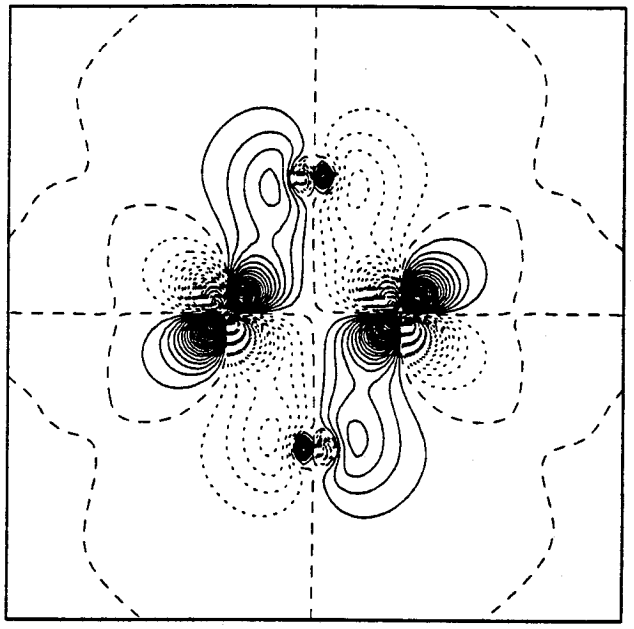

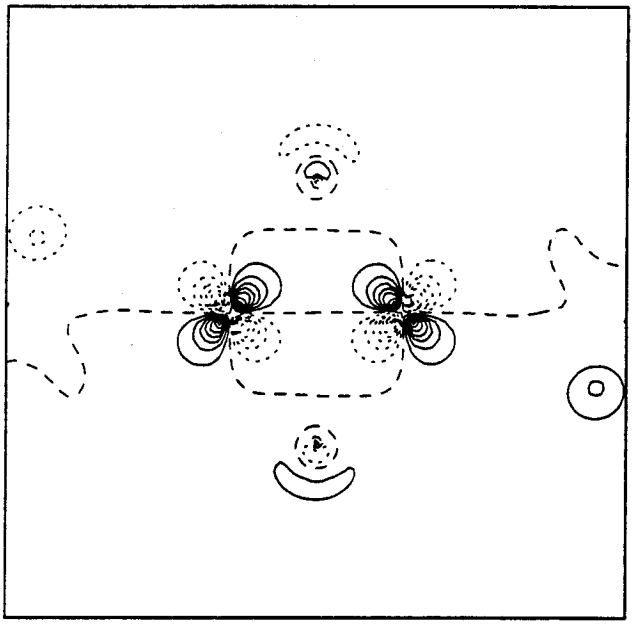

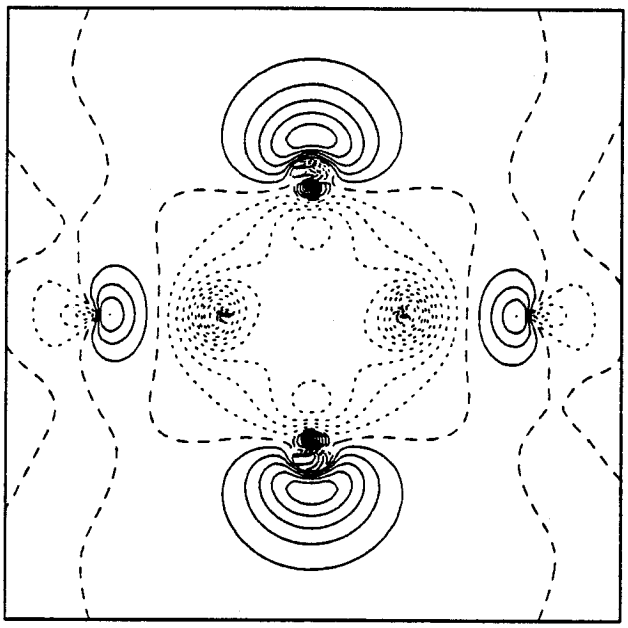

Cu d_{xz}
A_u

σ_S
A_g

σ_S
A_u

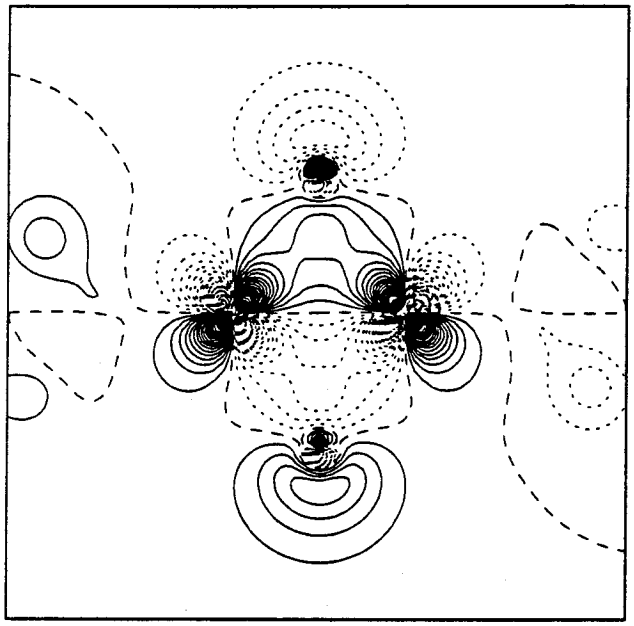

σ_S
A_u

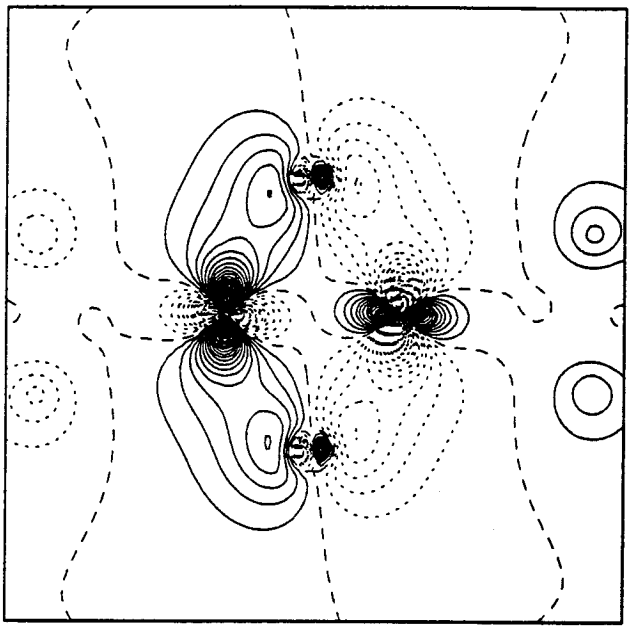

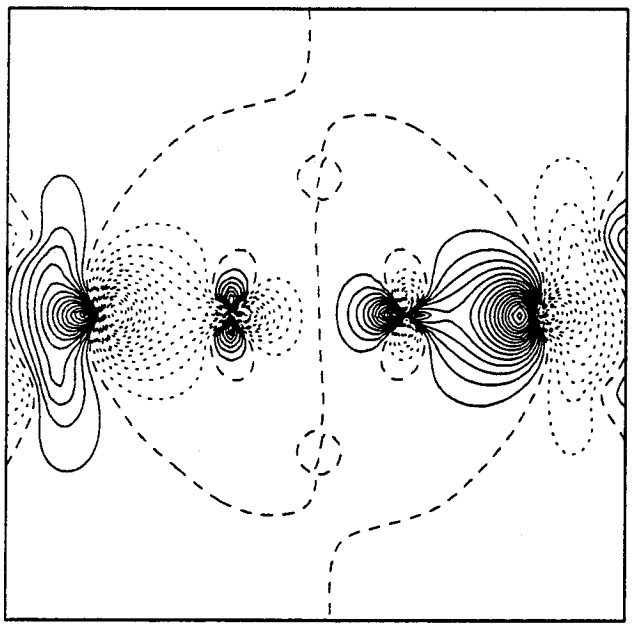

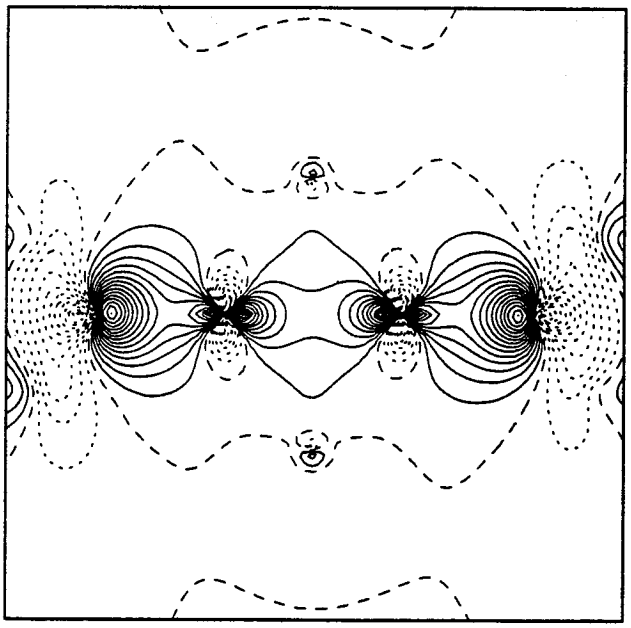

σ_N
A_u

σ_N
A_g

The Cu(I)/Cu(I) form of the protein is colorless, i.e., there are no low-lying excited states. On the other hand, the Cu(I)/Cu(II) form of the protein has a number of visible spectroscopic transitions. Thus, the observed spectroscopic transitions are due to transitions that occur from lower lying molecular orbitals into the singly occupied HOMO (SOMO). As described earlier, all Cu_A centers share three absorption features, two fairly intense transitions at ~480 and ~530 nm, that are oppositely polarized, and a broader less intense feature centered at ~830 nm. In addition, most UV/Vis spectra also show a medium intensity absorption peak, to the blue of the 480 nm absorption peak, at ~360 nm. This peak will prove to be quite critical in confirming the agreement of the observed and predicted polarizations of the optical transitions.

Assignment of absorption spectra

The calculation provides the following interpretation of the Cu_A UV/Vis absorption spectrum: the experimentally observed transitions can be assigned as electronic transitions from the lower-lying fifteen MOs into the A_u Cu d_{x2-y2} /S p_x/N p_x HOMO. The optimized structure is in the C_i symmetry group; hence, of the sixteen high-lying molecular orbitals discussed above, there are eight orbitals that have A_g symmetry and eight that have A_u symmetry. There are, theoretically, eight symmetry allowed transitions. Three of these transitions, those from A_g orbitals that belong to the set of Cu nonbonding orbitals, are not observed experimentally. The five remaining transitions, in order of increasing energy, are: (a) two oppositely polarized transitions arising from two Cu/S antibonding A_g orbitals(Figure 11), (b) two oppositely polarized transitions arising from two Cu/S bonding A_g orbitals (Figure 11), and (c) an x-polarized transition from an Cu/N bonding A_g orbital. The assignment of the Cu_A absorption spectrum is as follows:

Figure 11. The polarizations of the calculated symmetry allowed transitions corresponding to the transitions observed in the Cu_A absorption spectrum.

Polarization of Optical Transitions (Cu-S-Cu > 70°)

σ* HOMO

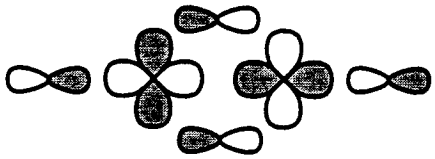

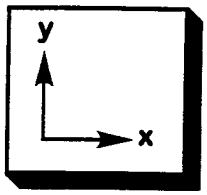

transition

>900 nm

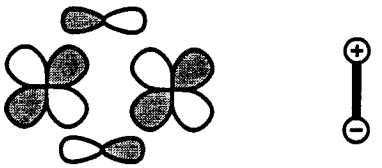

830 nm

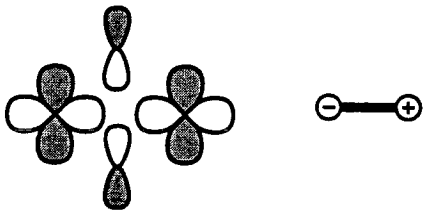

530 nm

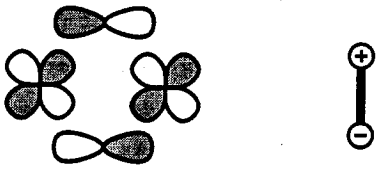

480 nm

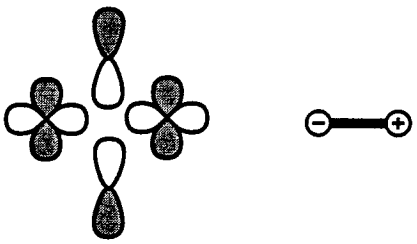

there are two low energy transitions arising from A_g Cu/S antibonding orbital. The lowest energy transition is polarized in the y-direction and occurs at a wavelength 950 nm. The other low energy transition is polarized in the x-direction and is assigned as the experimentally observed 830 nm absorption band. The two transitions from Cu-S bonding A_g orbitals are assigned as the 530 and 480 nm transitions that are polarized in the y-direction and x-direction, respectively. We assign the x-polarized transition from the Cu/N bonding A_g orbital as the transition observed at 360 nm.

Calculated Transition Energies and Intensities

The method of calculating transition energies is based on Koopman's theorem. It states that the ionization energy is equal to the energy of the HOMO. The excitation energy is merely the difference between the HOMO and the orbital from which the transition originates. Although this is a crude approach, it allows one to discuss the physical relevance and meaning of the calculated orbitals.

In doing the Koopman's calculation for the copper active sites studied here, an SCF calculation is done on the reduced form for a particular geometry. The molecular orbitals calculated for the reduced Cu(I)/Cu(I) form include the "excited-state" orbital, i.e., the doubly-occupied A_u HOMO, and the "ground-state"orbital, i.e., the doubly-occupied lower-lying A_g orbital. We calculate the dipole transition matrix elements between these two orbitals.

We calculated energies and intensities for transitions from these five doubly filled orbitals into the SOMO of the optimized Cu(I)/Cu(II) structure with a Cu-S-Cu angle of 65° (Figure 12). This structure was obtained by simply changing the Cu—Cu and S—S distances by the appropriate amount, while maintaining all other bond lengths and angles

Figure 12. Calculated spectrum of the Cu_A model complex with a Cu-S-Cu angle of 65°. Striped bars indicate transitions that are polarized in the y-direction. The other bars indicate transitions that are polarized in the x-direction. As before, the vertical lines with y-coordinates 0.5 and 1.0 along the x-axis represent the relative energy spacing of the highest-lying orbitals.

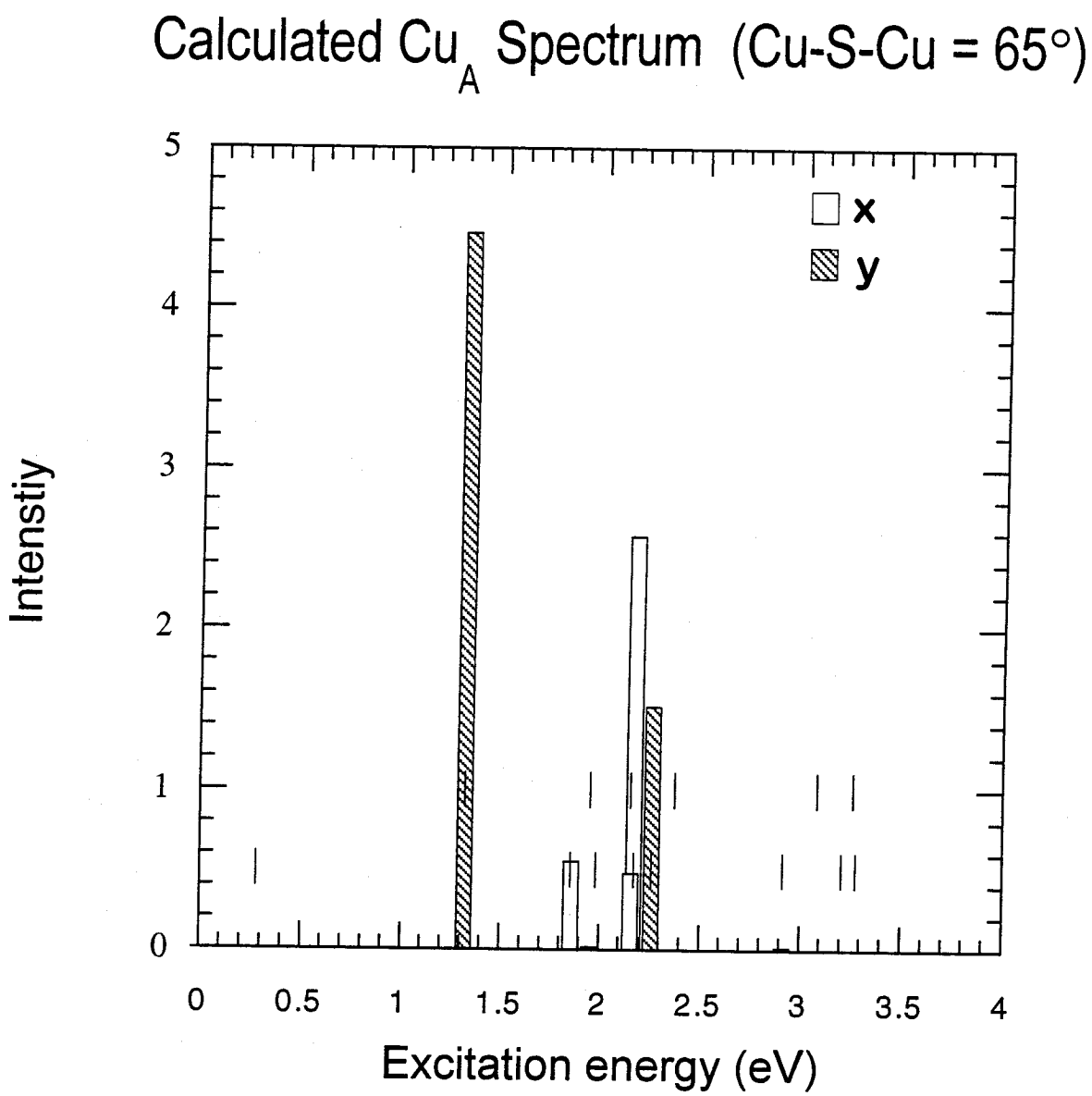
Calculated Cu A Spectrum (Cu-S-Cu = 65°)
Intenstiy
Excitation energy (eV)
x
y
0
1
2
3
4
5
0
0.5
1
1.5
2
2.5
3
3.5
4

fixed. The calculated transition energy of the >950 nm and 530 nm bands are within a reasonable error, but the calculated energy of the 830 nm, 480 nm and 360 nm transitions are calculated to be at significantly higher energies, in some cases up to 20 % higher. As for the intensities, it is observed that of the four major absorption bands, the 830 nm transition has the weakest intensity. Any bands lower in energy than(to the red of) this transition are weaker. The oppositely polarized transitions at 530 and 480 nm are both stronger (and nearly equal) in intensity than the 830 nm band. The 360 nm absorption band is intermediate intensity. The calculated intensities of the 830 nm and 530 nm band are reasonable. However, the lowest energy transition (at ~950 nm) is predicted to be the most intense and the 480 nm transition is predicted to have very little intensity. The calculated and experimental transition energies, intensities and polarizations are summarized in Table V.

Although the calculated transition energies and intensities do not agree well with the experimental values, the calculated polarizations of the Cu_A optical transitions agree with all experimental data that are available. The earliest studies were performed on oriented samples of cytochrome oxidase deposited on mica surfaces. The polarization assignments from these studies are tentative; the most definitive assignment is the polarization of the 480 nm transition in the x-direction. This agrees with the polarization assignment derived from the molecular orbital diagram for the 65° Cu_A structure.

Single crystal polarized absorption spectra were recorded on a sample of the *Thermus thermophilus* soluble Cu_A fragment. The spectra are quite impressive (Chapter 2, Figure X). Since the crystal structure of the *Thermus thermophilus* soluble Cu_A fragment has not been determined, the observed polarized spectra can not be assigned

Table V. Cu_A Spectroscopic Data

	wavelength		intensity		polarization	
	expt	*theory*[a]	*expt*[b]	*theory*	*expt*[c]	*theory*
transition						
2	>950	939	~0.25	4.46	-	y
3	830	670	1	0.55	-	x
9	530	548	~2	1.52	-	y
10	480	424	~2	0.02	x	x
16	360	200	0.5	0.57	-	x

a. All calculated values based on Cu_A structure with Cu-S-Cu = 65°.
b. Relative intensities; intensity of 830 nm band set to 1.
c. Based on MCD studies of oriented cytochrome oxidase samples.

with complete certainty. However, one can deduce which transitions in the optical spectrum are polarized in the same direction. It appears that the absorption bands at >900 nm and 530 nm are polarized in one direction and the 830 nm, 480 nm, and 360 nm bands are polarized in the opposite direction. This grouping of polarizations is also present in our calculations.

Since the calculated transition energies were overestimated up to 20 % in some cases, we searched for factors that may give rise to this disagreement. Structural features that differ between the calculated structure and the structure found in the protein may account for the disagreement between the experimental and calculated transition energies and intensities. Differences in bond lengths, bond angles, and relative conformations of coordinating groups could have a enormous effect on transition energies and intensities. The observed absorption spectrum may be a result of fine-tuning due to the coordination environment imposed by the protein. In discussing the geometry optimized structure and

the experimental structure data, two features that differed significantly are: (1) the angle the methyl group (i.e., the C_β of Cys) makes with the Cu_2S_2 plane; and (2) the tilt of the imidazole rings. We reasoned that these features could affect the energies and intensities of optical transitions. We chose to investigate what effect changing the value of these quantities has on the calculated energies and intensities by doing calculations on two structures. In the first structure, the angle of the methyl group was changed from 107°, the value in the calculated structure, to 120°, the value reported in the cytochrome oxidase crystal structure. In the second structure, the tilt of the imidazole rings, which is calculated to be nearly coplanar with the Cu_2S_2 plane (i.e. Cu—Cu-N angle = ~ 180°), was adjusted to 160°, the value observed in the x-ray structure and the value that was used in the model that agrees best with the resonance Raman data. In both cases, to prepare the specific complex, the respective angle was manually adjusted and the bond lengths and angles of the optimized structure were held fixed. Altering either the angle of the methyl group or the tilt of the imidazole rings had little or no effect on the calculated transition energies and intensities (data not shown). We did observe dramatic changes in the calculated energies and intensities upon changing the value the Cu-S-Cu angle. These calculations are discussed in detail in the following section.

Effect of the Cu-S-Cu angle on the electronic structure of Cu_A

Initially, we believed that our results did not accurately predict the geometry of the oxidized Cu_A structure. In comparing solely the Cu-S-Cu angle of the optimized structure to the experimental data available at the time, the calculation consistently produced a Cu-S-Cu angle of ~63°, whereas, up until this last summer, most experimental data supported a value of 70° for this angle. The smaller Cu-S-Cu angle of 63° supports the notion of a Cu-Cu bond in the Cu_A center, since the Cu-Cu distance lies between 2.43 to 2.47 Å, depending on the length of the Cu-S bond. This past summer (July 1997), results from the most recent EXAFS studies on Cu_A soluble fragments were reported. To our delight and amazement, the EXAFS structure is in remarkable agreement with our calculated structure. Had we known these data beforehand, we probably would have been less apt to pursue the calculations described in this section. However, these calculations make some very interesting predictions concerning excited state energies, intensities and polarizations. At the outset, we wanted to pursue an optimization of Cu_A for a structure where the Cu-S-Cu angle is constrained to 70°. Unfortunately, we were never able to achieve successful convergence of a constrained geometry optimization. As an alternative, we decided to vary the Cu-S-Cu while maintaining the bond lengths, angles, etc. of the optimized structure. This type of distortion is a natural motion for the Cu_A center. This motion corresponds to motions that occur in the lowest energy vibrational modes.

Effect of Cu-S-Cu angle on transition energies and energy of the excited state

It is not unexpected that changing the value of the Cu-S-Cu angle would alter the molecular orbital diagram. What is not known is how sensitive these changes are and

what are the trends in terms of changes in the transition energies and intensities. We find that the electronic structure of the Cu_A center is *extremely* sensitive to the exact value of this angle (Figure 13). At a value of the Cu-S-Cu angle = 65°, the HOMO is entirely Cu d_{x2-y2}/S p_x/N p_x. Over the range of 69°-71°, the two highest-lying orbitals flip-flop, inverting the polarizations of the optical transitions. Near the middle of this range, the two highest energy orbitals appear to be nearly degenerate and have undergone a good deal of mixing, such that the d character is nearly 50 % d_{x2-y2}/50 % d_{xy}. When the Cu-S-Cu angle = 75°, the HOMO is now entirely Cu d_{xy}/S p_y in character. The HOMO of the 65°, 71° and 75° structures are compared in Figure 14. Over this range of angles, the Cu-Cu distance varies from 2.5 to 2.85 Å (Figure 15). The dependences of excitation energies and the excited state energy on the Cu-S-Cu angle are shown in Figures 16 and 17. In general, as the angle is increased from 65° to 75°, most of the transition energies increase, except the calculated energy for the 530 nm transition, which increases slightly. The excited state energy decreases to the point where the Cu-S-Cu = ~ 71°, seemingly headed to zero, and then increases again. Lastly, in varying the value of the Cu-S-Cu angle from 65° to 75° the polarizations of the optical transitions invert, the point of inversion being ~70.75°. At 65° the 530 nm transition is y-polarized and the 480 nm transition is x-polarized. At 75°, it is the opposite, the 530 nm transition is x-polarized and the 480 nm transition is y-polarized. The calculated spectrum for the case where Cu-S-Cu = 65° has already been presented above. Results are presented below on the calculated spectrum for two cases: Cu-S-Cu = 70° and Cu-S-Cu = 75°.

Figure 13. Molecular orbital diagrams of Cu_A model complexes with three different Cu-S-Cu angles but otherwise having equal bond lengths and angles. At 65°, the d character of the HOMO is d_{x2-y2}. At ~71°, the d character of the HOMO is 50 % d_{x2-y2}/50 % d_{xy}. At 75°, the d character of the HOMO is now entirely d_{xy}. With this flip of the HOMO, the polarizations of the transitions in the 75° case are opposite what they are in the 65° case

Molecular Orbital Diagrams for $Cu_2(SCH_3)_2(Im)_2$: HOMO Character Varies with the Cu-S-Cu

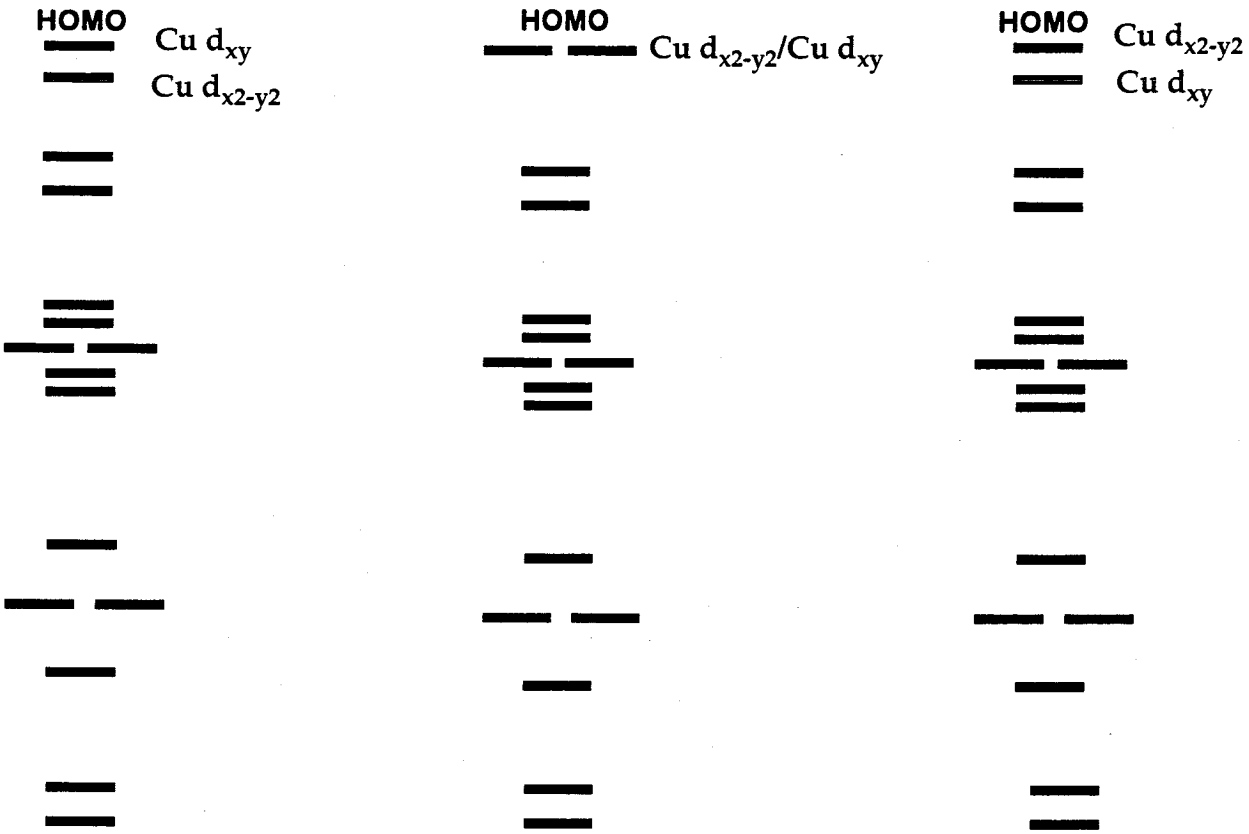

Figure 14. Comparison of the two highest-lying orbitals calculated for the Cu_A model complexes having Cu-S-Cu angles of 65°, ~71°, and 75°. On the left is the HOMO and on the right is the next highest-lying orbital.

HOMO

σ_{Cu}^{*}

A_u

π_{Cu}^{*}

A_u

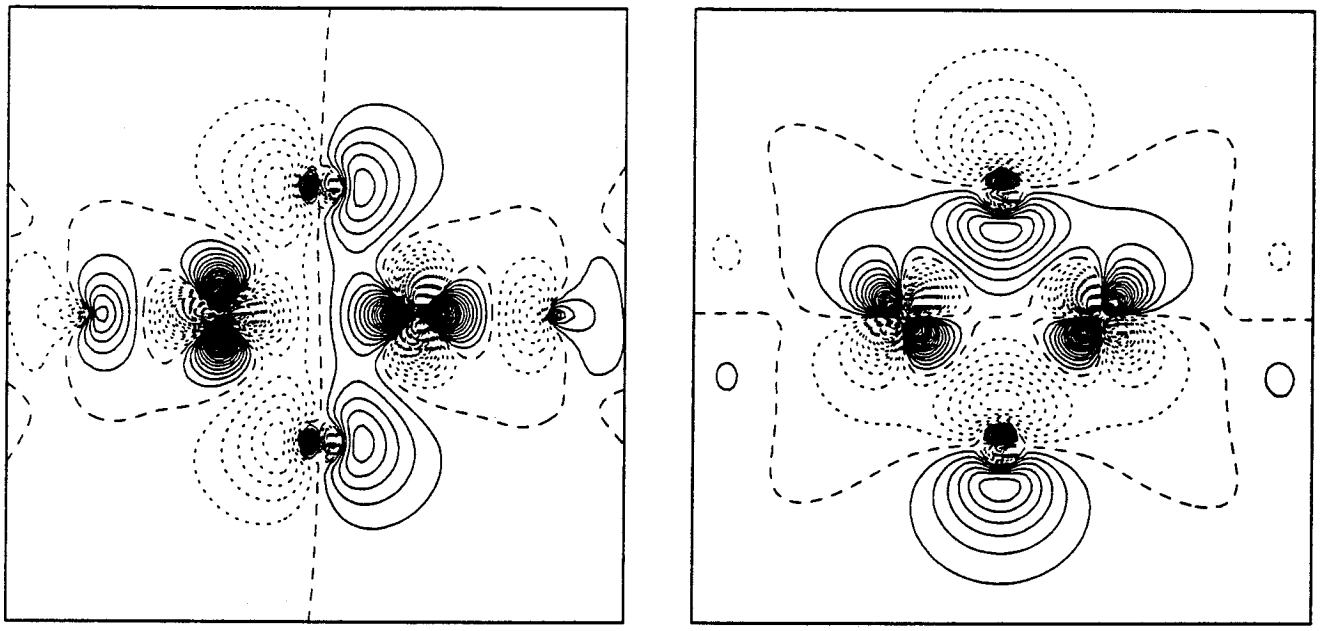

Cu-S-Cu = 65°

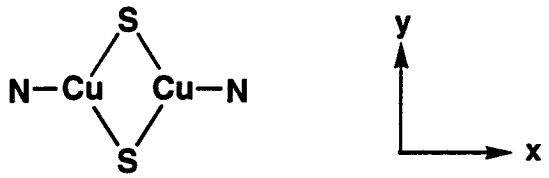

HOMO

A_u A_u

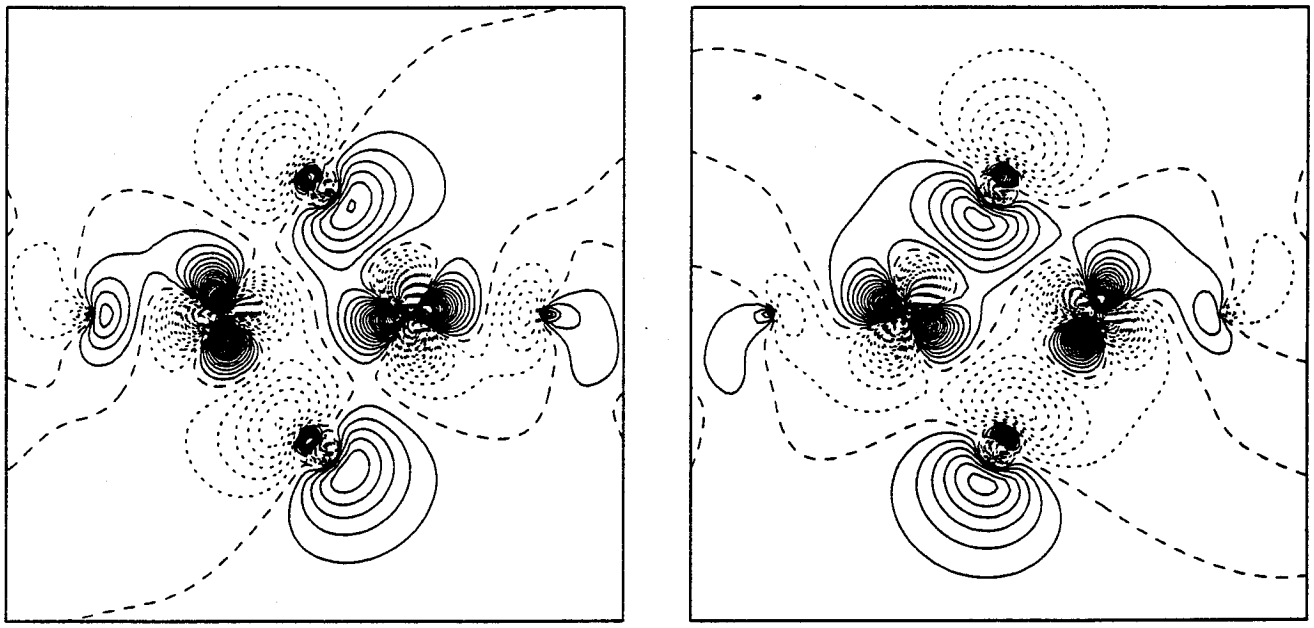

Cu-S-Cu = ~ 71°

HOMO

π_{Cu}^{*}

A_u

σ_{Cu}^{*}

A_u

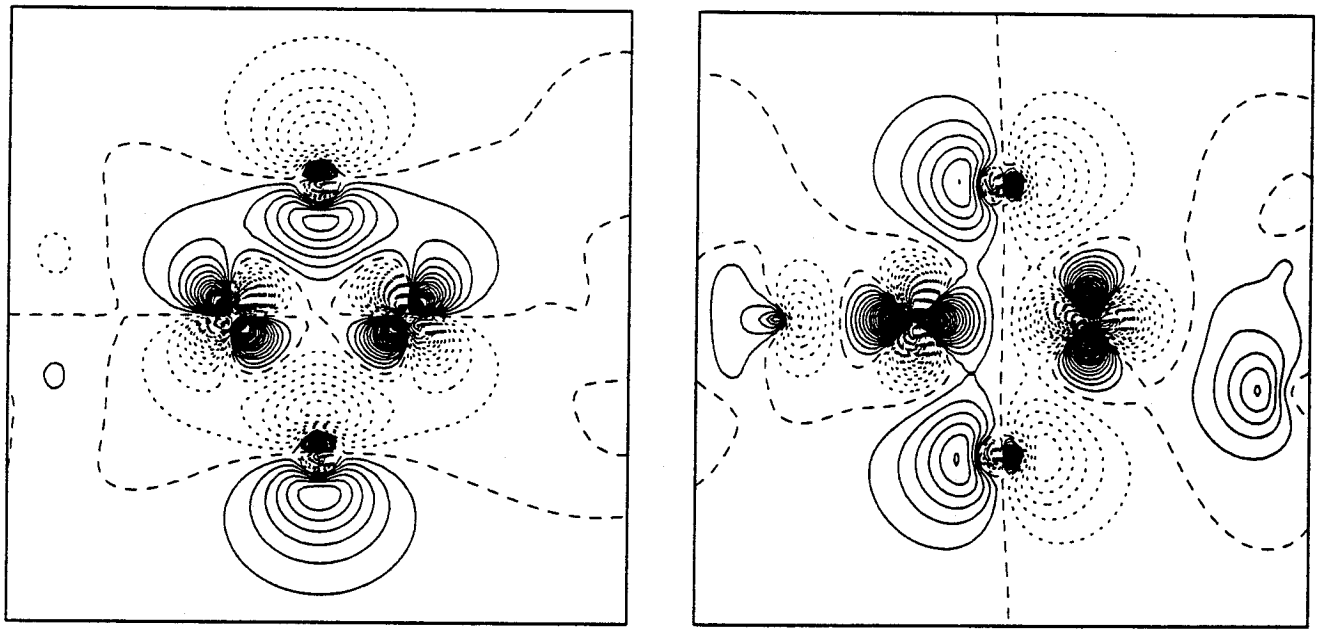

Cu-S-Cu = 75°

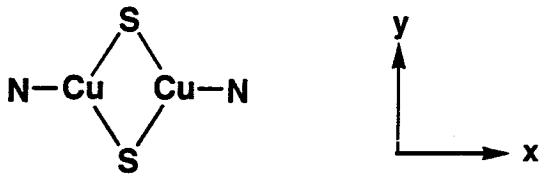

Figure 15. The Cu-Cu distance as a function of the Cu-S-Cu angle in the Cu_A model complex studied herein. At 65°, the Cu-Cu distance is 2.5 Å; at 75°, the Cu-Cu distance is 2.86 Å.

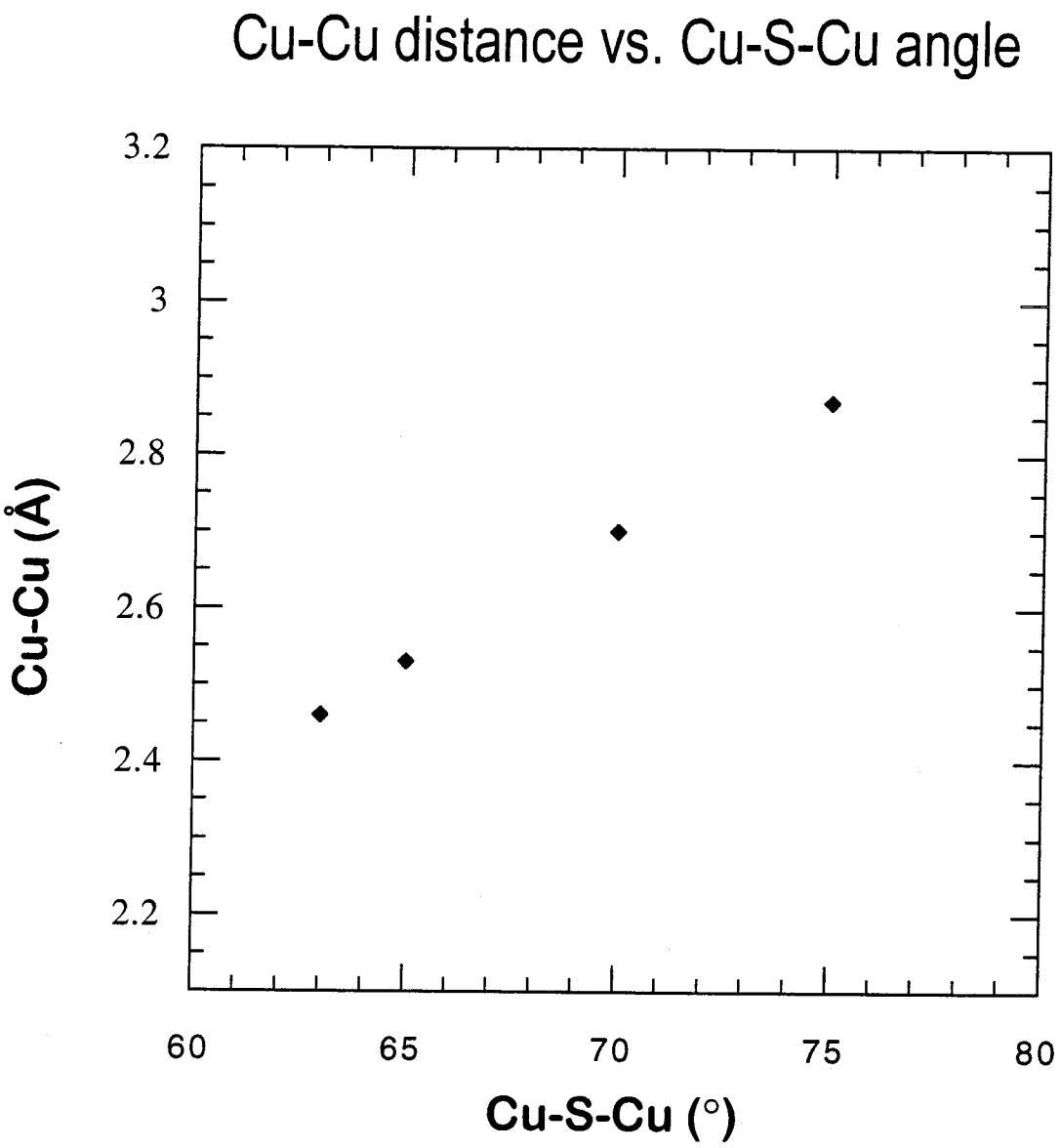
Cu-Cu distance vs. Cu-S-Cu angle
3.2
3
2.8
2.6
2.4
2.2
Cu-Cu (Å)
60
65
70
75
80
Cu-S-Cu (°)

Figure 16. The transition energies as a function of the Cu-S-Cu angle. In general, most of the calculated transitions energies decrease except for the transition that corresponds to the 530 nm band, which increases slightly. The shaded bar represents the FWHM of the experimental bands.

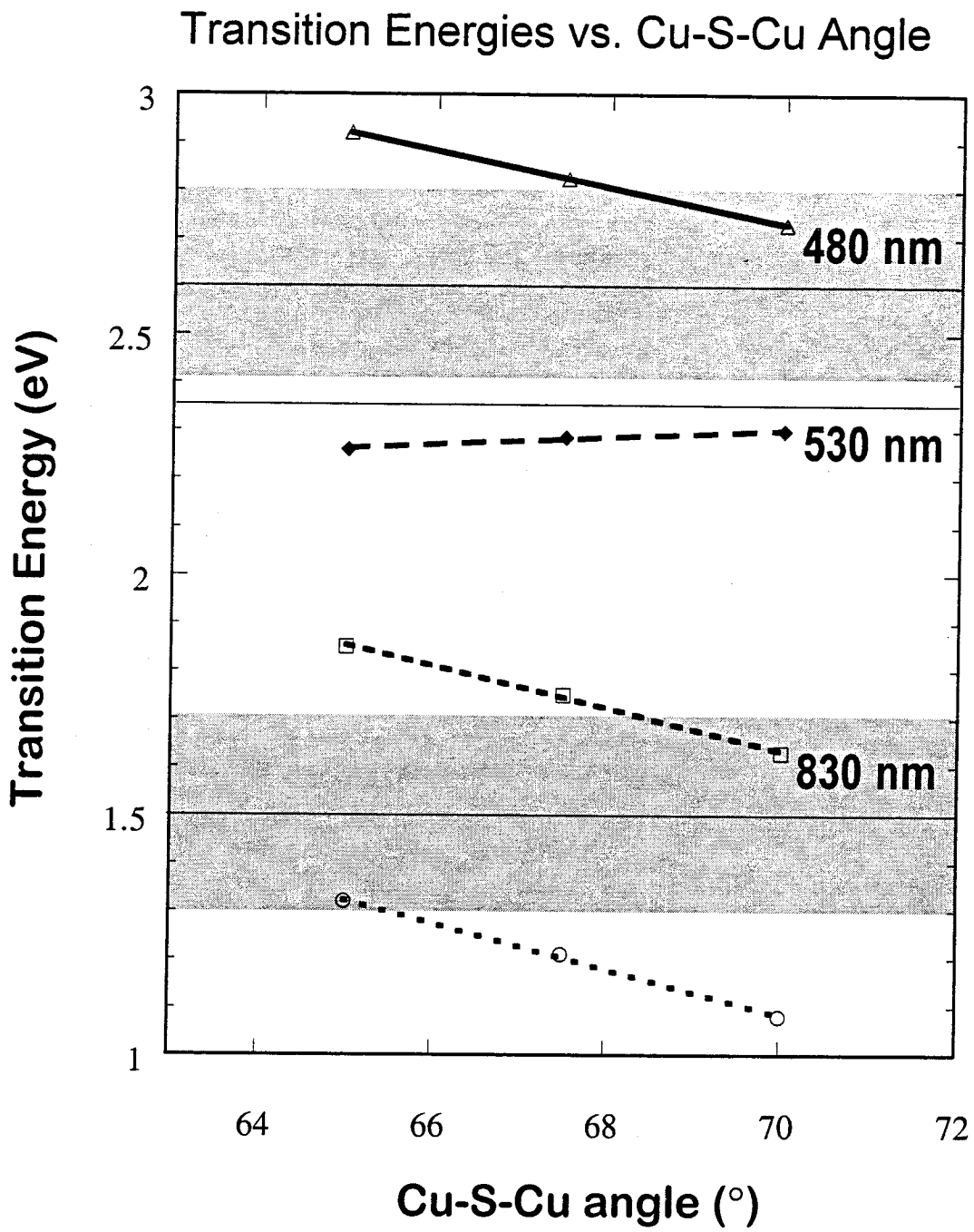
Transition Energies vs. Cu-S-Cu Angle
Transition Energy (eV)
3
2.5
2
1.5
1
480 nm
530 nm
830 nm
64
66
68
70
72
Cu-S-Cu angle (°)

Figure 17. The difference in energy between the HOMO and the next highest-lying doubly occupied orbital as a function of the Cu-S-Cu angle. The energy difference between the two orbitals goes to zero for an angle ~71°, At this point the d character of the orbital flips.

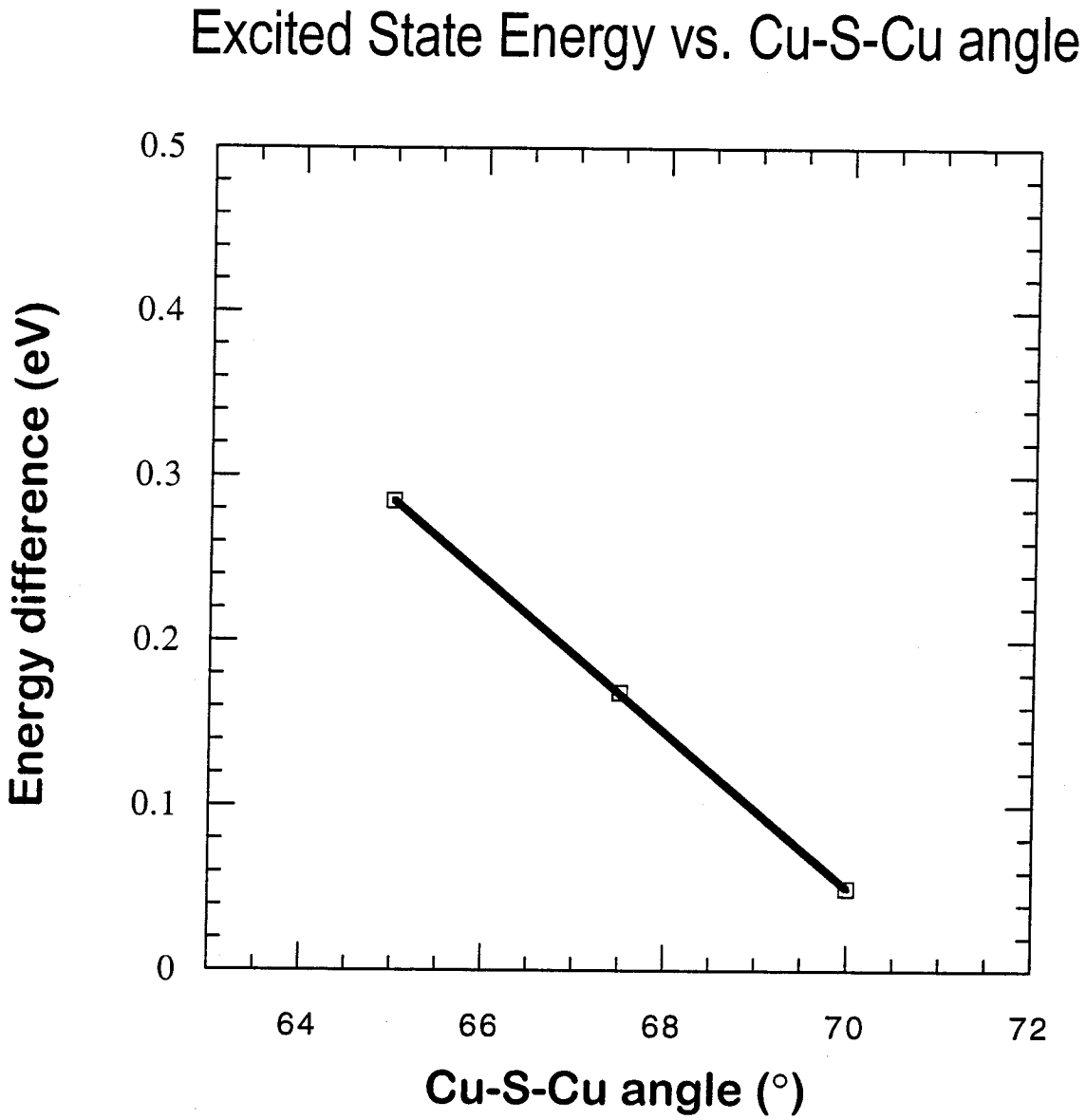
Excited State Energy vs. Cu-S-Cu angle
Energy difference (eV)
0.5
0.4
0.3
0.2
0.1
0
64
66
68
70
72
Cu-S-Cu angle (°)

Calculated MOs and spectrum for 70° and 75° structures

For the case where Cu-S-Cu = 70°, the Cu-Cu distance is ~2.70 Å. The calculated excitation energies as well as intensities are shown in Figure 18. The HOMO has d character that is still primarily d_{x2-y2}, but a tiny amount of d_{xy} character is present. The excited state energy has decreased substantially compared to the case where the Cu-S-Cu = 65°, from 0.3 eV (~2,265 cm^{-1}) to < 0.05eV (~400 cm^{-1}). At this angle, the energies of most of the transitions decrease, except the 530 nm transition. The intensity of the two lowest energy bands decreases and the intensity of the higher energy oppositely polarized transition increases (Figure 14).

The transition point in terms of the change of d character in the HOMO occurs between the values of 70.5° and 71° for the S-Cu-S angle. At an angle of 70.5° (Cu-Cu = 2.718 Å),), the two highest-lying orbitals are nearly degenerate in energy, with an energy difference ~0.01 eV (< 100 cm^{-1}). The HOMO still has primarily d_{x2-y2} character (~50 %), but a small component (< 10 %) from the d_{xy} orbitals is also present. At 71° (Cu-Cu = 2.735 Å), the two highest-lying orbitals are still nearly degenerate in energy. However, this angle is beyond the transition point in terms of the change in d character of the HOMO. The HOMO is now primarily d_{xy} in character (~ 35 %) with a smaller, yet significant, contribution (~12 %) from the d_{x2-y2} orbitals. As the character of the HOMO has changed from primarily d_{x2-y2} to d_{xy}, the polarizations of the optical transitions are inverted.

At a Cu-S-Cu angle of 75° (Cu-Cu = 2.867 Å), the HOMO is entirely d_{xy} in character, the excited state energy has increased to ~ 0.2 eV (1613 cm^{-1}). At this angle, most of the calculated transition energies as well as the intensities agree much better with

the observed values (Figure 19). Although it is tempting to suggest that the structure of the Cu_A center is actually more like the 75° structure as opposed to the 65° structure, the polarizations of the transitions and the Cu-Cu distance of the 75° structure do not agree with experimental data. As mentioned above, there are no definitive experimental data on the polarizations of the Cu_A optical transitions. The results of spectroscopic studies of oriented cytochrome oxidase samples indicate that the 480 nm transition is polarized in the x-direction, in agreement with the calculation of the 65° structure. At 75° the 480 nm transition is polarized in the y-direction. So, while it is good that the calculations provide a very clear measure for judging the agreement with experimental data, we have to await definitive polarized absorption data before we can conclude which structure best describes the actual Cu_A site.

Another aspect of the 75° structure that does agree well with available experimental data is the Cu-Cu distance, which at 2.86 Å is 0.15 Å larger than value deduced from x-ray structure data. At 2.8 Å resolution, the error in the Cu-Cu distance is ±0.2 Å, so it is within the range determined by x-ray crystallography. However, this distance is 0.35 Å larger than the value obtained from the results of EXAFS studies. The reported error of the EXAFS results is ±0.02 Å. If we decide to base our interpretation of the Cu_A spectra on the 75° structure, we will have to reconcile the less favorable agreement of the Cu-Cu distance.

Figure 18. Calculated spectrum of the Cu_A model complex with a Cu-S-Cu angle of 70°. Striped bars indicate transitions that are polarized in the y-direction. The other bars indicate transitions that are polarized in the x-direction. As before, the vertical lines with y-coordinates 0.5 and 1.0 along the x-axis represent the relative energy spacing of the highest-lying orbitals.

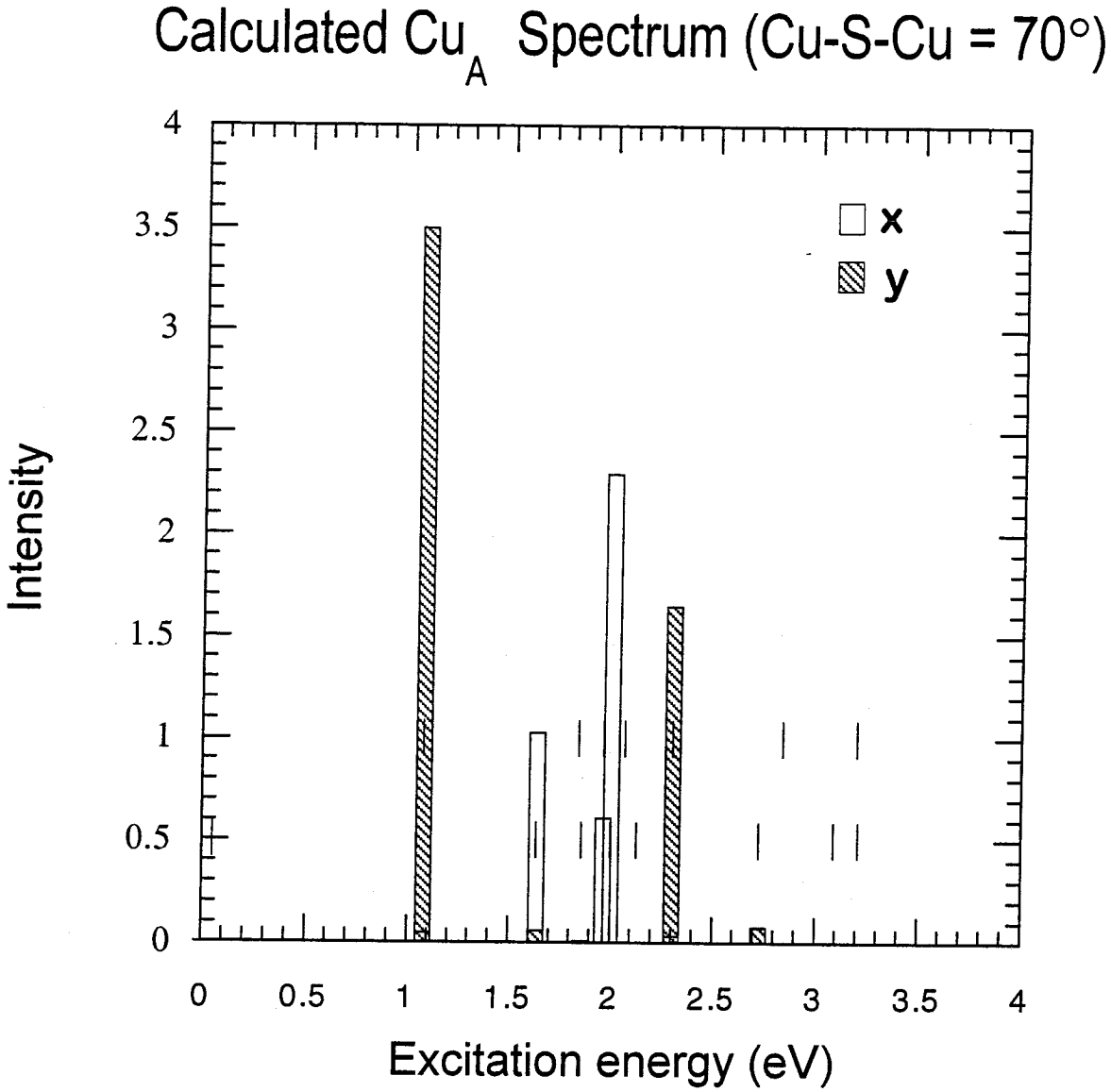
Calculated Cu A Spectrum (Cu-S-Cu = 70°)
Intensity
Excitation energy (eV)
x
y
0
0.5
1
1.5
2
2.5
3
3.5
4

Figure 19. Calculated spectrum of the Cu_A model complex with a Cu-S-Cu angle of 75°. Striped bars indicate transitions that are polarized in the y-direction. The other bars indicate transitions that are polarized in the x-direction. As before, the vertical lines with y-coordinates 0.5 and 1.0 along the x-axis represent the relative energy spacing of the highest-lying orbitals.

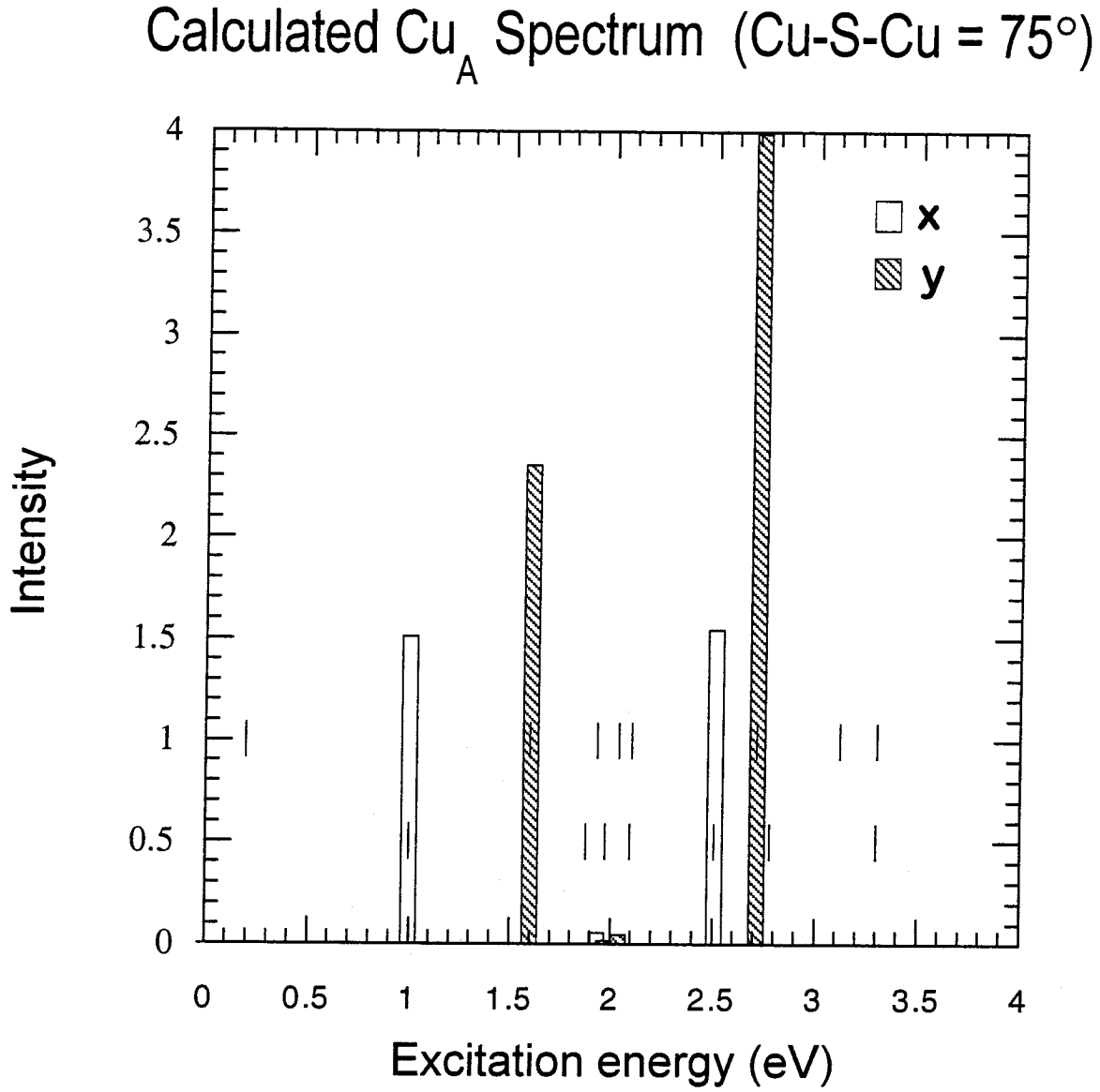
Calculated Cu A Spectrum (Cu-S-Cu = 75°)
Intensity
Excitation energy (eV)
x
y
0
0.5
1
1.5
2
2.5
3
3.5
4

Optimized structure of reduced copper sites and reorganization energies

The Cu_A center transfers electrons from cytochrome c, which floats in the intermitochondrial space, to cytochrome a embedded in subunit I of cytochrome oxidase. The structure of the cytochrome c:cytochrome oxidase complex has not been determined. Based on the crystal structure of cytochrome oxidase, one can estimate that the metal to metal distance between the iron atoms of cytochrome c and cytochrome a to be ~ 40 Å. Cu_A serves to very efficiently "catalyze" the long-range transfer of an electron over 40 Å in under a millisecond. Efficient electron-transfer centers have the property that the magnitude of the reorganization energy (λ) is such that for the driving force (ΔG) of the reaction in which it participates, the rate is at or as near as possible to the top of the Marcus curve. That is, the reorganization energy just about equals the driving force ($\lambda = -\Delta G$). Most physiological ET reactions occur at low driving forces, hence for ET reactions to occur efficiently the reorganization energies of biological redox centers has to be low. The ET reaction between Cu_A and cytochrome a has a driving force of ~ 50 mV. For this reaction to occur at the maximum possible rate, λ would have to be ~ 0.1 eV. This is a very small value. The best studied protein ET reactions have reorganization energies in the range 0.7 to 1.3 eV.[13] For the ET reaction between Cu_A and cytochrome a to occur at a reasonable rate, either one or both of the redox centers should have extremely low reorganization energies.

Biological systems have numerous ways of creating low λ redox centers (centers with low reorganization energies). Some redox centers are completely shielded from water. However, since the redox centers must transfer electrons efficiently, they need to be well coupled to the surface. In many cases, this is achieved by having a portion or

edge of the redox center exposed to the surface allowing it to interact with redox partners. Groups are usually present to exclude water from the site. Minimizing the reorganization cost of the solvent greatly reduces the overall λ. λ can be minimized even further by reducing the inner sphere component of the reorganization energy. Upon accepting or donating an electron, the immediate environment around the ion undergoes distortions. As a result the geometry of the metal center changes; bond lengths can change, angles can open or close, etc. By having the ligands attached to the protein backbone, the protein acts as a framework to prevent the site from distorting to what would be the optimal geometry for a particular oxidation state of the metal ion. When the center participates in ET reactions, very little change in geometry will occur because the coordination environment is ideal for one oxidation state and is imposed upon the other.

To check to see if the geometry observed in the protein is optimal for a particular oxidation of the copper center, we calculated the optimized geometry of the reduced forms of the blue copper and Cu_A model complexes. Since the optimized oxidized structures are not that different from the structures that are observed, we would expect that the optimized reduced structure might be quite different from the observed structures. By calculating the SCF wavefunction of both oxidation states in the reduced and oxidized optimized geometries, we can address to what extent the protein lowers the inner sphere reorganization energy of the copper center. We start first by revisiting the blue copper case and then proceed to the Cu_A center.

The optimized structure of the reduced blue copper site

The blue copper proteins are the most notable example of where it is believed that the protein imposes the coordination environment upon the copper ion. In serving its role in biological electron transfer reactions, the copper ion of blue copper proteins cycles between Cu(I) and Cu(II) oxidation states. It is well known that, generally, Cu(I) prefers a tetrahedral coordination environment and that Cu(II) prefers a tetragonal coordination environment. The rack hypothesis states that the arrangement of the ligands on the protein framework imposes a coordination environment or geometry that is optimal for a particular oxidation state.[14] This would minimize the reorganization energy and facilitate rapid electron transfer at low driving forces. The long held notion in the blue copper field is that the geometry imposed by the protein favors Cu(I) and is *not optimal* for Cu(II). This view is supported by results of Xα-SW electronic structure calculations on blue copper sites. The results of these calculations indicate that the protein rack is manifested in positioning the weak axial Met ligand such that it creates a force that would distort the Cu(II) geometry if the position of the ligands were unrestrained. The protein restrains the movement of the ligands and maintains the position of the Met residue even though it is slightly destabilizing towards Cu(II). However, the results of recent DFT calculations challenge the existence of the protein rack in blue copper proteins. The results of these calculations suggest that the optimized geometry of Cu(I) and Cu(II) blue copper model complexes is not that different than the geometry observed in the protein. The view espoused by the results of these studies is that the protein rack does not impose a particular geometry on either Cu(II) or Cu(I). Also in complete contrast to a long-

Figure 20. Overlap of the optimized oxidized structure (solid color, cylinders) and the optimized reduced structure (half-bond colors, ball and stick) of the blue copper model complex. Note that in the optimized reduced structure one of the imidazoles is no longer bound and that the S-Cu-N angle is nearly 180°.

oxidized

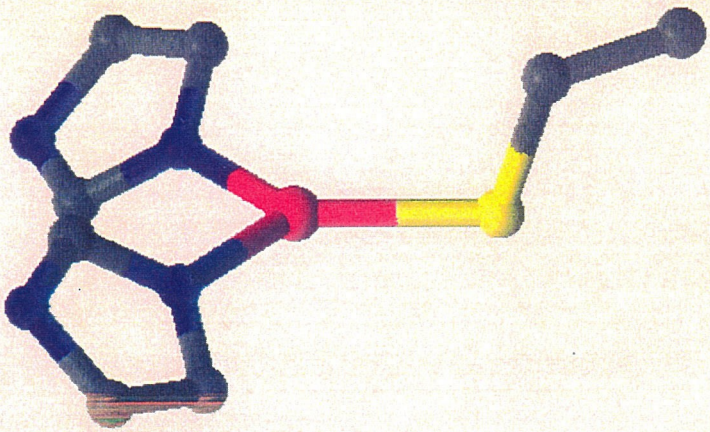

reduced

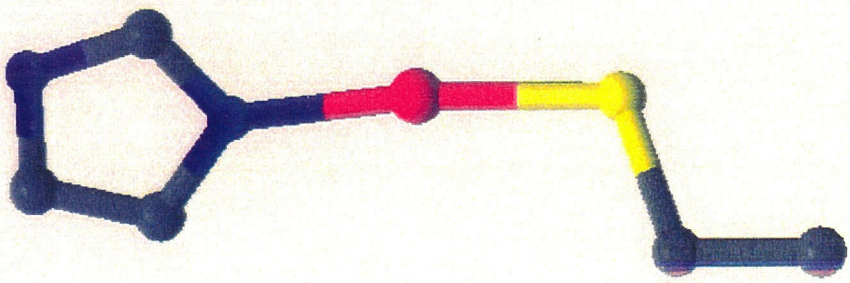

Table VI. Comparison of Oxidized and Reduced Blue Copper Structures

	theory		*experiment*
	oxidized	**reduced**	**oxidized**
distance(Å)			
Cu-S	2.19	2.20	2.12
Cu-N	2.037	2.02	2.06
		2.36	
angle(°)			
S-Cu-N	127	180	120
N-Cu-N	106	-	103

Figure 21. SCF energies of the two oxidized states of the optimized oxidized and reduced structures of the blue copper model complex.

Blue Copper Model

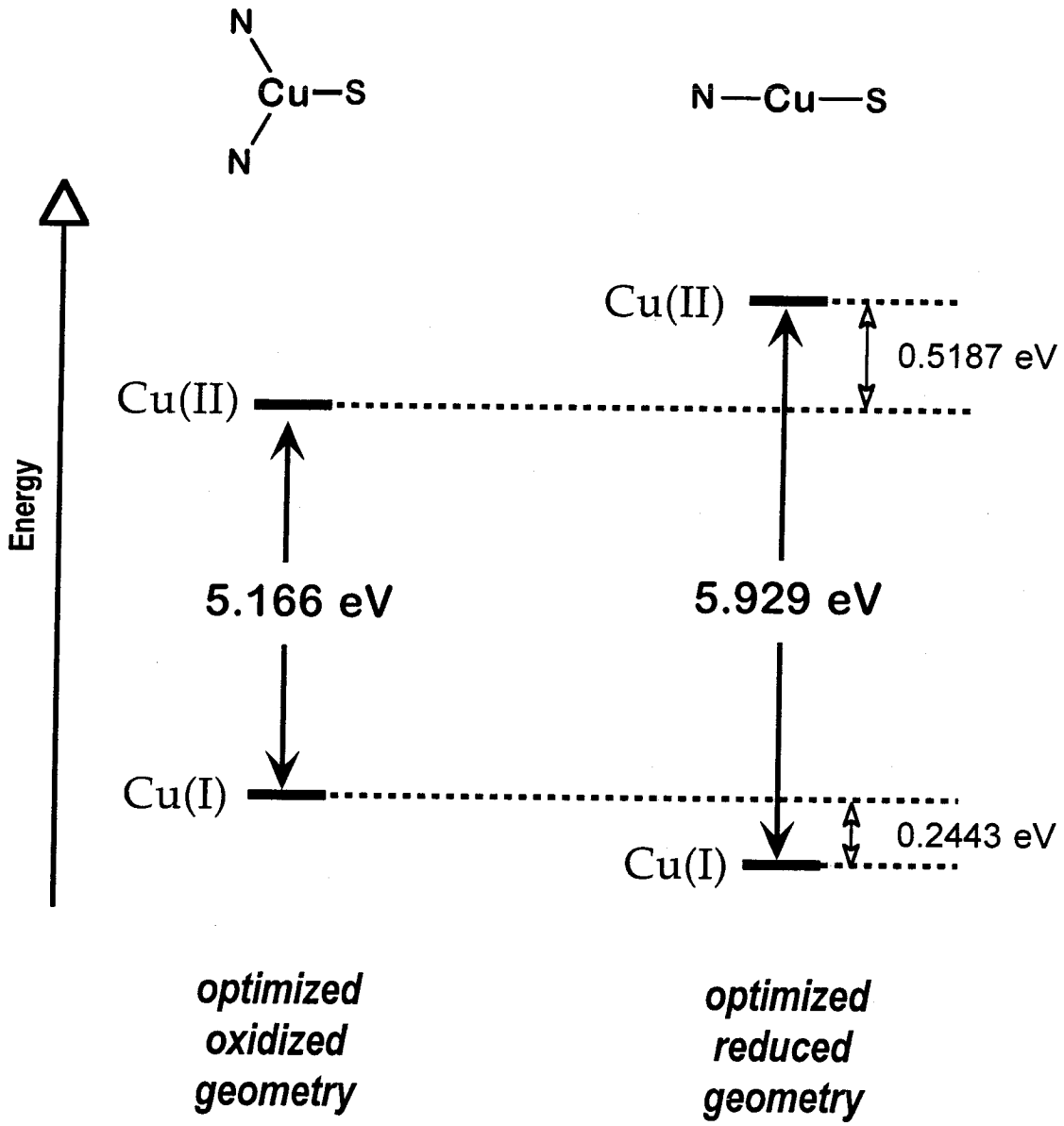

standing notion in the blue copper field, the site in the protein is actually slightly more stable for Cu(II) than Cu(I).

To address this issue, we undertook optimization of the reduced Cu(I) C_1 structure. Our starting point was the reduced optimized Cu(II) structure. In the geometry optimization calculation, the starting trigonal $[Cu(SCH_2CH_3)(Im)_2]$ complex collapsed to a linear $[Cu(SCH_2CH_3)(Im)]$ complex, with one of the imidazole rings dissociated (Figure 19). The Cu-S and Cu-N distances are 2.2 Å and 2.02 Å. The calculated bond lengths and angles of the oxidized and reduced C_1 symmetry structures and the experimental values are compared in Table VI.

The results of our calculations do not support the view that either the protein rack imposes a non-optimal geometry on the Cu(II) ion, or that the rack does not exist at all. Our results indicate that the protein rack has two components. First, for Cu(II), the protein serves to encapsulate or sequester the Cu(II) ion in a low dielectric medium in which a trigonal geometry is optimal. If the protein is unfolded, i.e., if our model complex is solvated, the trigonal Cu(II) center would convert to a tetragonal center. The folding of the protein restricts the set of ligands to three and positions groups to exclude water from the coordinating to the copper ion, creating a site where the optimized geometry of the Cu(II) ion is trigonal. The rack is also present for Cu(I). The Cu(I) ion would prefer to lose a ligand and collapse to a linear geometry. The protein rack prevents the reduced site from collapsing to a linear coordination geometry. This keeps the reorganization energy of the site low, resulting in efficient physiological electron transfer. We calculate that the protein reduces the inner-sphere reorganization energy of the blue

copper site by ~0.25 eV (Figure 21), the energy difference between the reduced form of the optimized, trigonal oxidized structure and the energy of the optimized linear, reduced structure. As a result, the potential of the unfolded reduced state is expected to be large because Cu(II) is very unstable in a linear coordination environment. It will also have a large reorganization energy because of the drastic ligand coordination differences in the optimized structures of the two forms. In summary, if the rack were not present, electron transfer from the blue copper sites would be very inefficient, if not completely inhibited, because of the high potential of the linear Cu(I) site and the significant reorganization that occurs between the optimized structures of the two oxidation states, trigonal for Cu(II) and linear for Cu(I).

The optimized structure of the reduced Cu_A site

Just as for the blue copper case, the starting structure of the reduced Cu_A geometry optimization calculation was the optimized oxidized structure. The calculated structure had fairly good optimization criteria (Table VII). There are obvious differences between the oxidized and reduced Cu_A structures (Figure 22). The Cu-Cu distance in the optimized reduced structure is 2.69 Å. The Cu-S bond lengths are inequivalent; one is a short bond 2.31 Å in length and the other is a long bond 2.55 Å in length. The Cu-N distance is 2.04 Å. The S-Cu-N angles are inequivalent in the reduced structure: the sulfur of the long Cu-S bond has a S-Cu-N = 103°, the sulfur of the short Cu-S bond has a S-Cu-N = 143°. In the reduced Cu_A structure, the two Cu(I) ions are collapsing to a linear geometry, although not to the same extent as in the blue copper Cu(I) case. One can visualize the Cu_A reduced site as two linear Cu(I) blue copper sites fused together.

Figure 22. Overlap of the optimized oxidized structure (solid color, cylinders) and the optimized reduced structure (half-bond colors, ball and stick) of the Cu_A model complex.

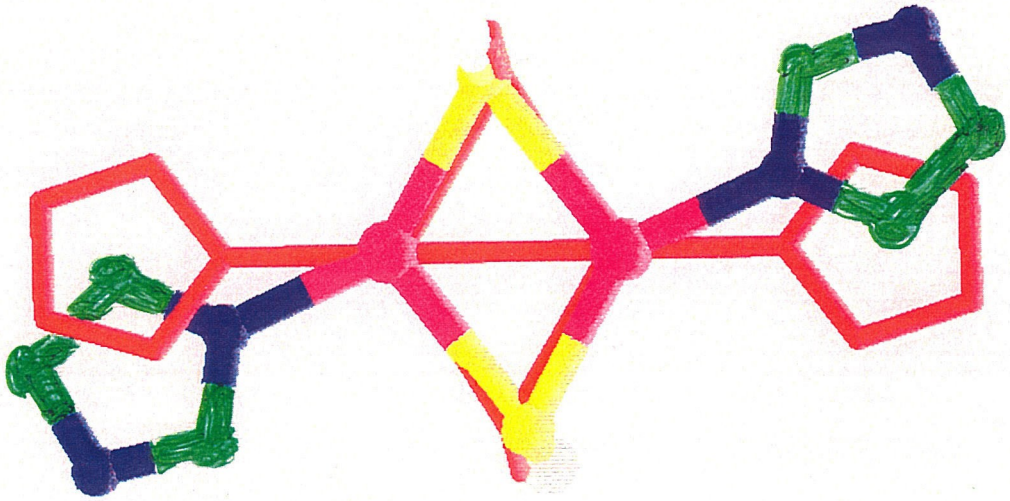

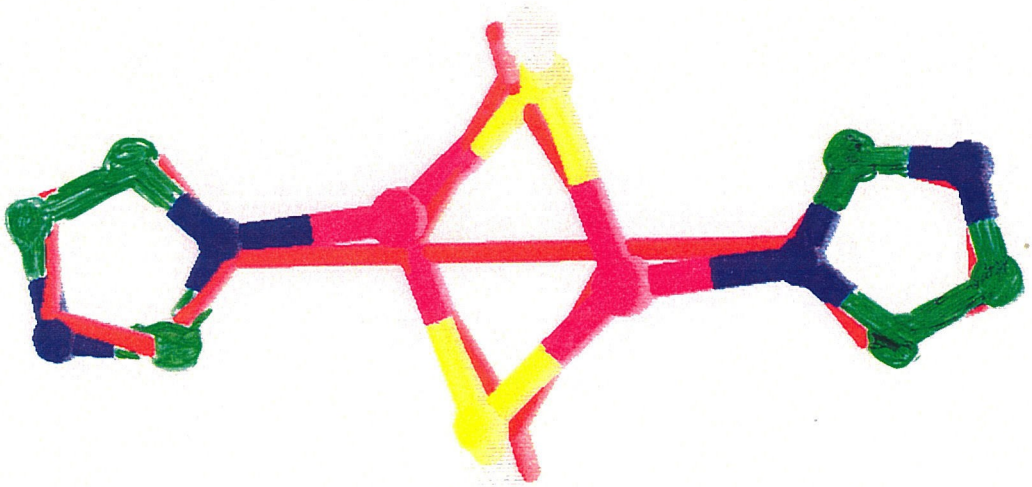

Table VIII. Comparison of Oxidized and Reduced Cu_A Structures

	theory		*experiment*	
	oxidized	reduced	oxidized	reduced
distance(Å)				
Cu-Cu	2.46	2.69	2.43	2.51
Cu-S	2.35	2.55	2.30	2.33
Cu-N	1.98	2.31	1.96	1.96
angle(°)				
Cu-S-Cu	63	67	65	65
C-S–S	107	113	-	-
N-Cu–Cu	180	180	-	-
N-Cu–S	121	143 103	-	-

Figure 23. SCF energies of the oxidized states of the optimized oxidized and reduced structures of the Cu_A model complex.

CuA Model

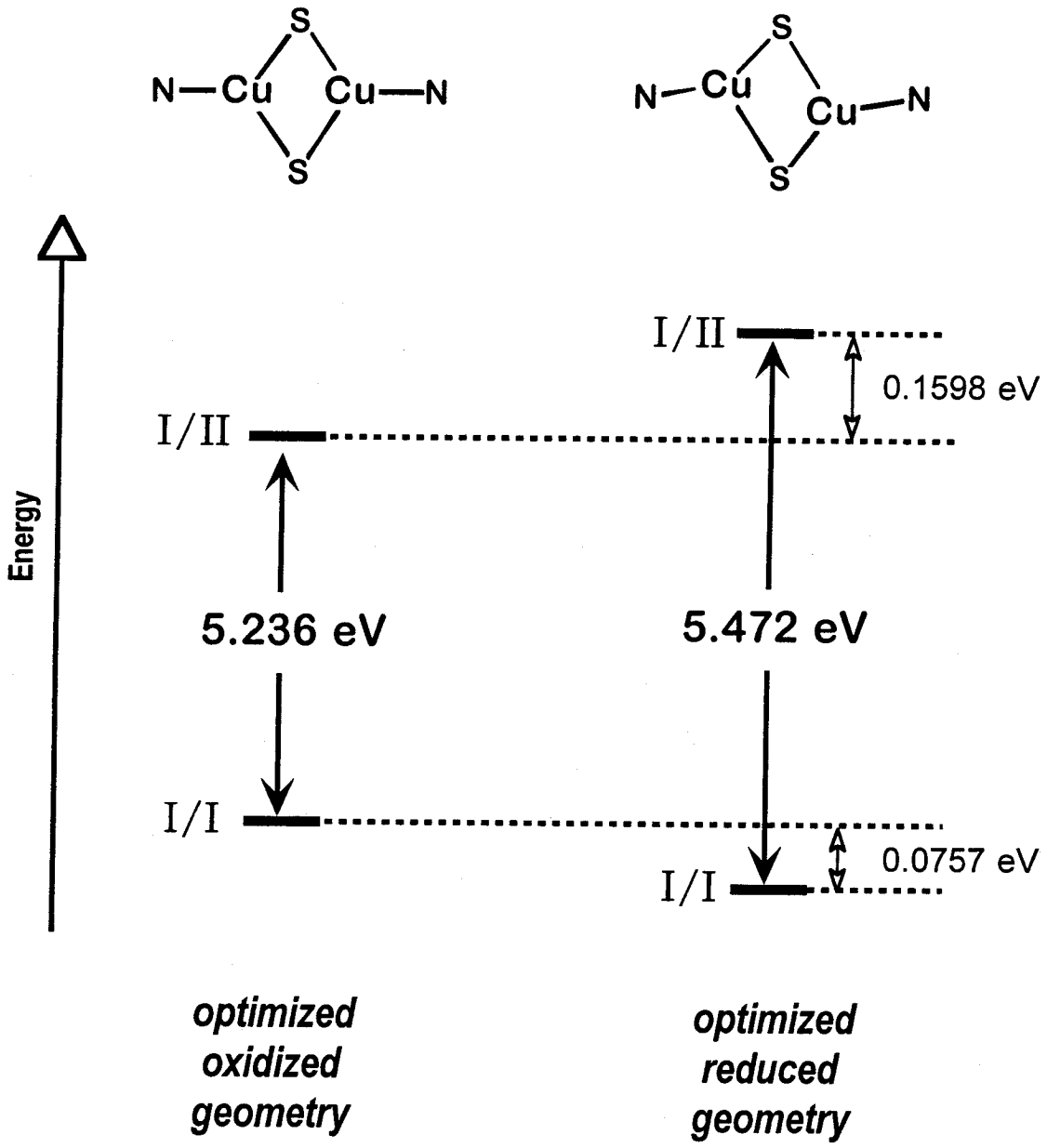
S
N—Cu Cu—N
S
S
N—Cu Cu—N
S
Energy
I/II
I/II
0.1598 eV
5.236 eV
5.472 eV
I/I
I/I
0.0757 eV
optimized oxidized geometry
optimized reduced geometry

Table VII. Geometry Optimization Statistics of Cu(I)/Cu(I) Cu_A Structure

criteria	actual values
Gradient maximum	1.42×10^{-4}
Gradient rms	4.07×10^{-5}
Displacement maximum	1.56×10^{-3}
Displacement rms	3.94×10^{-4}

Quantities are in atomic units (hartrees, bohr, etc.).

The bond distances and angles of the optimized oxidized and reduced structures and structural data on the reduced protein derived from EXAFS data is presented in Table VIII.

Many of the conclusions discussed for the blue copper proteins in the previous sections can be applied to the Cu_A center. In its folded structure, the protein sequesters the Cu_A center in a low dielectric environment, with a restricted ligand set that is optimal for the Cu(II) trigonal coordination geometry. The rack enforces the thiolates to be bridging ligands and prevents the formation of a disulfide cross-link, meanwhile promoting the formation of a Cu-Cu bond. If the protein were to be unfolded, the site would convert to tetragonal. The reduced structure, in the low dielectric medium would like to undergo some significant distortions. The rack prevents the reduced state from distorting to what would be the optimal geometry, thereby keeping the reorganization low. Our calculations indicate that the protein reduces the inner sphere reorganization energy by ~ 0.075 eV (Figure 23). This is only about a third of the value calculated for the blue copper center. This suggests that a binuclear copper center has an inherently smaller inner sphere reorganization energy compared to mononuclear center. It is a very efficient electron transfer center with an extremely low λ.

In summary, the protein rack has two components. First, it creates the environment in which the trigonal Cu(II) geometry is optimal. It does so encapsulation of the copper ion in a low dielectric medium, providing a restricted set of ligands, and positioning groups to exclude water from the site. Second, it maintains a trigonal environment for Cu(I). The Cu(I) would prefer to lose a ligand and collapse to a linear geometry. The protein prevents these structural changes from occurring. The environment created by the protein produces a center with a high reduction potential and a low, and in some cases an extremely low, overall reorganization energy. These properties enable copper centers to function as very efficient ET centers in proteins.

---

[1] Parr, R.G.; Yang, W. *Density-Functional Theory of Atoms and Molecules* Oxford, 1989.

[2] Ringnalda, M.N.; et al. PS-GVB v2.35, Schrodinger, Inc., 1996.

[3] Martin, C.T.; Scholes, C.P.; Chan, S.I. *J. Biol. Chem.* **1988**, *263*, 8420-8429.

[4] Larsson, S.; Kallebring, B.; Wittung, P.W.; Malmstrom, B.G. *Proc. Nat Acad. Sci.* **1995**, *92*, 7167-7171.

[5] Hay, P.J.; Wadt, W.R. *J. Chem. Phys.* **1985**, *82*, 299

[6] Friesner, R.A. *Ann. Rev. Phys. Chem.* **1991**, *42*, 341.

[7] Lappalainen, P.; Saraste, M. *Biochim. Biophys. Acta* **1994**, *1187*, 222-225

[8] Tsukihara, T.; et al. *Science* **1996**, *269*, 1069-1074.

[9] Blackburn N.J.; et al. *J. Am. Chem. Soc.* **1997**, *119*, 6135-6143.

[10] Andrew, C.R.; et al. *J. Am. Chem. Soc.* **1996**, *118*, 10436-10445.

[11] Farrar, J.A.; et al. *J. Am. Chem. Soc.* **1996**, *118*, 11501-11514.

[12] Williams, K.R.; et al. *J. Am. Chem. Soc.* **1997**, 119, 613-614.

[13] Winkler, J. Gray, H.B. *Ann. Rev. Bioch.* **1996**, .

[14] Malmstrom, B.G. *Eur. J. Biochem.* **1995**, *234*, 363-381.

Chapter 4.

Electron-Tunneling Pathways in Cytochrome Oxidase

INTRODUCTION

Cytochrome oxidase serves to transfer four electrons to oxygen from cytochrome c and in the process pump four protons across the lipid bilayer membrane. Thus, the enzyme is referred to as a redox-linked proton pump. The protons pumped across the membrane establish a proton gradient that is used in the synthesis of ATP. Electrons from cytochrome c are delivered to the site where oxygen reduction occurs via two redox centers. The primary acceptor of electrons (the port of entry) from cytochrome c is the Cu_A center. Electrons are transferred from Cu_A to the heme of cytochrome a in subunit I. Heme a transfers electrons to the heme a_3-Cu_B site where oxygen reduction occurs. The reduction of molecular oxygen to water requires electrons and protons. Hence, in addition to the protons pumped across the membrane, protons must be delivered to the catalytic site. Proton and electron currents in cytochrome oxidase must be carefully regulated to effectively couple the free energy of oxygen reduction and to prevent the release of potentially toxic intermediates. In this chapter we examine the elements in cytochrome oxidase that regulate the flow of electrons.

BACKGROUND

The pathway model

Electron transfer in proteins is mediated by the protein medium, the portion of the protein structure between redox centers. This medium can be thought of as being comprised of pathways that consist of covalent bonds, hydrogen bonds and through space jumps between group in van der Waals contact. The decay of electron transfer across a bond is known from studies on model systems. The decay of electron transfer across a

Figure 1. Diagram showing the primary ET pathways between the Cu_A center and heme a and between heme a and heme a_3. The pathways are indicated by the vertical and horizontal thick lines, respectively.

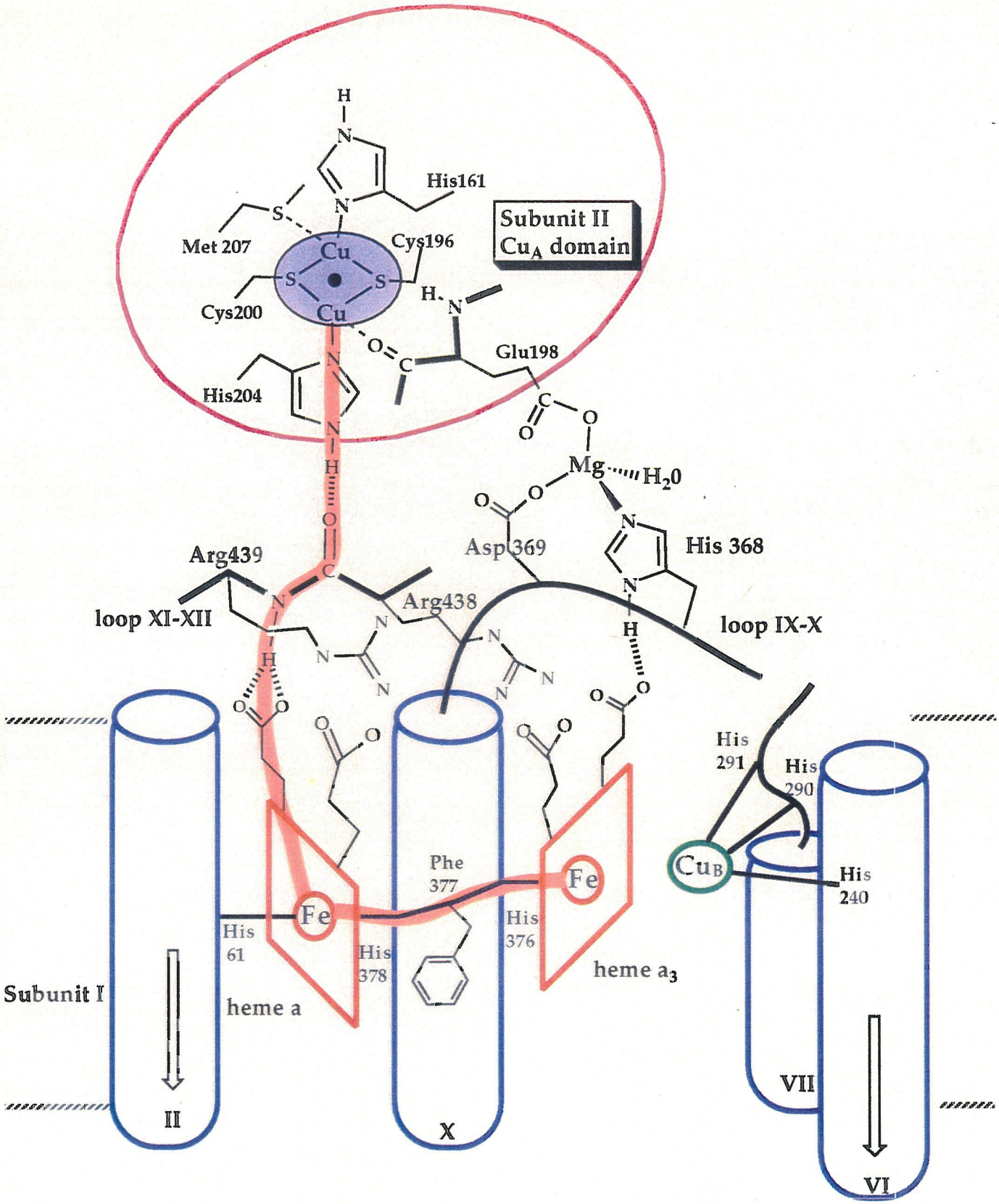
Subunit II
Cu_A domain
His161
Met 207
Cys196
Cys200
Cu
Cu
His204
Glu198
Mg
H_2O
Asp 369
His 368
Arg439
Arg438
loop XI-XII
loop IX-X
Phe
377
Fe
Fe
His
61
His
378
His
376
heme a
heme a_3
Subunit I
II
X
His
291
His
290
Cu_B
His
240
VII
VI

hydrogen bond or the decay due to a through space jump can be estimated as equivalent to the decay across a certain number of covalent bonds. For instance, we might say that the decay across a hydrogen bond is equivalent to the decay across 1-3 covalent bonds, depending on the length of the hydrogen bond, the angle, etc. Similarly , the decay of through space jump can be estimated as the equivalent decay of transferring an electron across 5-10 covalent bonds, depending on the size of the jump. In this manner we have effectively converted an ET pathway comprised of given number of covalent bonds, hydrogen bonds and through space jumps into a effective path consisting of a certain number of covalent bonds.

In describing ET pathways in proteins, we search for pathways that give the best coupling, i.e. possess the least number of *effective* covalent bonds. An automated procedure, such as is implemented in the program PATHWAYS, can be utilized to search for ET paths in a protein structure. Paths are evaluated based on their the "sigma tunneling length", a quantity that is proportional to the number of effective covalent bonds in a pathway. In calculating the sigma tunneling length of a pathway, hydrogen bond lengths and atom-atom distances are taken into account. In general, covalent bonds provide the best coupling and through space jumps the worst. However in certain instances, the transfer of an electron across a hydrogen bond can be as efficient as the transfer of an electron across a covalent bond.

RESULTS AND DISCUSSION

Cu_A-heme a ET pathways

The initial electron transfer step in cytochrome oxidase is the transfer of electrons from the Cu_A center to the heme of cytochrome a. The best ET pathway between Cu_A center and heme a consists of 14 covalent bonds and 2 hydrogen bonds. In this pathway, the electrons exit the Cu_A center via a histidine ligand. One hydrogen bond in the path are formed by the N_ε-H of the imidazole ring with a carbonyl of a peptide unit in a loop connecting transmembrane helices in subunit 1. The other hydrogen bond is between the amide of that same peptide unit and a propionate group of heme a. If we estimate the decay of ET through a hydrogen bond to be equivalent to tunneling across two covalent bonds we calculate a ET pathway between the Cu_A center and heme a consisting of 18 effective covalent bonds with a tunneling length of 24 Å.

Based on analogy to the blue copper centers, it has been proposed that pathways through the Cys residues may be favored over pathways through His residues. Electron transfer in blue copper proteins has been the focus of a great deal of theoretical and experimental work. The conclusions obtained from these studies is that the Cys serves to efficiently couple segments of the protein to the copper center. This is reasonable if we think of the fact that the observed LMCT transition (S^-–Cu(II) $S^{\cdot}$–Cu(I)) mimics a step in the hole transfer picture of electron transfer. Based on this assertion, pathways in blue copper proteins are expected to be dominated by Cys pathways, i.e., pathways that couple donors or acceptors to the copper center via the Cys residue. The best pathway through a Cys residue linking Cu_A and heme a consists of 24 covalent bonds and two hydrogen bonds, or 28 effective covalent bonds. The best ET pathway through Cys is 10 bonds

Figure 2. Structure of the electron-transfer medium between the Cu_A center and heme a. The Cu_A center and heme a are connected via a peptide unit along the His ET pathway. Alternate pathways that do not go through the His ligand are quite circuitous.

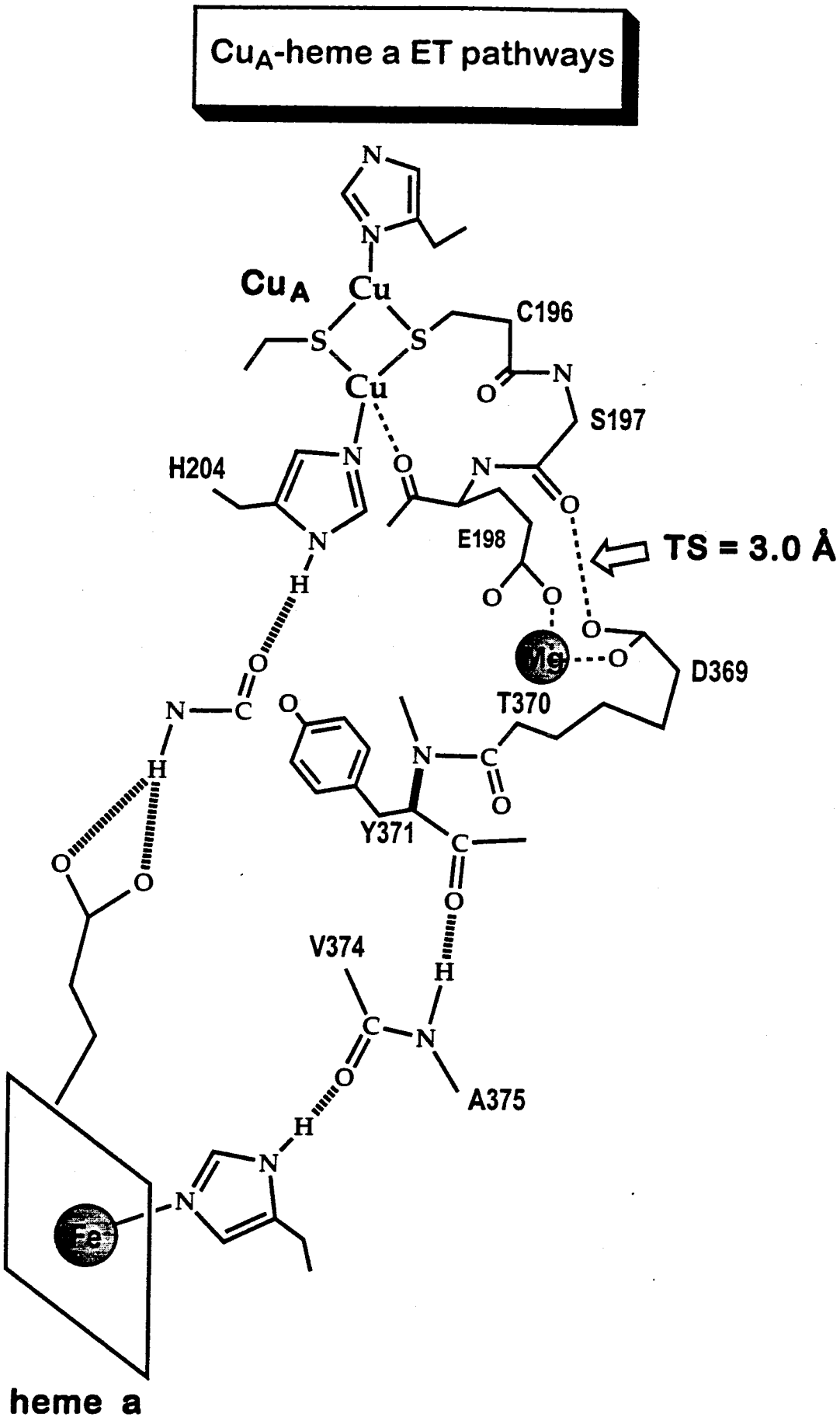
Cu$_A$-heme a ET pathways
Cu$_A$
Cu
Cu
S
S
C196
N
O
S197
H204
N
N
O
E198
TS = 3.0 Å
H
O
O
O
Mg
O
D369
T370
N
C
O
O
Y371
C
O
V374
H
C
N
A375
O
H
N
N
Fe
heme a

longer than the best pathway through a His residue. If we translate this into a difference in rates, we would expect that ET rates through Cys would be ~ 10^3 slower compared to rates through His. Thus, the dominant ET pathway from Cu_A to heme a is through a His residue.

Comparison of the structures of blue copper proteins and Cu_A domains

It is of interest at this point to compare the structures of the blue copper proteins and cytochrome oxidase Cu_A domains. Similarities between these two copper sites had been discussed since the discovery of the Cu_A center. Sequence alignment of Cu_A domains and blue copper proteins showed that the two proteins shared a similar sequence distribution of ligands. Comparing the structures of the Cu_A domain and the blue copper proteins it is evident that the former differ from the latter solely by the insertion of a three amino acids, one of which must be Cys, between the C-terminal Cys and His ligands. The introduction of a single Cys residue changes the capacity or stoichiometry of the site from a single copper ion to two.

A hallmark feature of the blue copper proteins that is altered in the Cu_A domain is the placement of the "northern" histidine. In describing the structures of blue copper proteins, it is common to pick an orientation in which the copper is at the top (or at the northern end) of the protein. This orientation places the C-terminal histidine at the northern most end of the protein. In most blue copper proteins the northern histidine is surrounded by hydrophobic residues, giving rise to a so-called hydrophobic surface patch. This patch has been implicated to function in molecular recognition in the various interprotein ET reactions that involve blue coppers proteins as well as in electron self-

exchange reactions. It is obvious that electron donors or acceptors in contact with the northern histidine would be well-coupled to the blue copper center. Instead of pointing north, the C-terminal histidine of the soluble Cu_A domains faces out on the vertical surface of the protein. This structural rearrangement has a drastic effect on the topological relationship of ET pathways into and out of the copper center via the histidine ligands. Whereas the ET pathways through His in the blue copper proteins are perpendicular, in the case of the Cu_A domain the ET pathways through the His residues are nearly parallel. This arrangement gives rise to very efficient long range ET coupling where the electron enters the Cu_A center through one His and exits out the other. It is as if the Cu_A center of cytochrome oxidase serves as a wire, funneling electrons to heme a. The electronic coupling of the Cu_A center may be anisotropic in the sense the ET is favored in the direction along the histidines. The rearrangement the C-terminal histidine of Cu_A maintains its ability to form an intermolecular hydrogen bond through the N_ε proton. In the crystal structure of cytochrome oxidase the N_ε-H forms a hydrogen bond with a peptide unit of a loop in subunit I. This hydrogen bond forms a crucial link in the ET pathway between Cu_A and heme a. It would appear that if this hydrogen bond were not present life as we know it would be severely impaired. The altered orientation of the His may in part have been driven by the orientation of the Cu_A domain with respect to subunit I of cytochrome oxidase. The Cu_A domain is oriented such that the north-south axis of the blue copper proteins lies roughly parallel to the surface of the membrane. In this arrangement, His ET pathways through a blue copper center would be extremely unproductive for transferring electrons to heme a from cytochrome c, whereas His ET

Figure 3. Overlap of the blue copper and Cu_A centers. This overlap was obtained by minimizing the rms difference between the three beta strands that contain ligands of the copper ion(s). These three beta strands contain ~15 amino acids. The overlap depicts how a blue copper center would be oriented if subunit II of cytochrome oxidase possessed a blue copper enter instead of a Cu_A center. The "northern" histidine of Cu_A points towards the bottom. The blue copper "north-south" axis lies nearly horizontal in this picture. See Figure 4 for how this affects ET pathways into and out of the these centers.

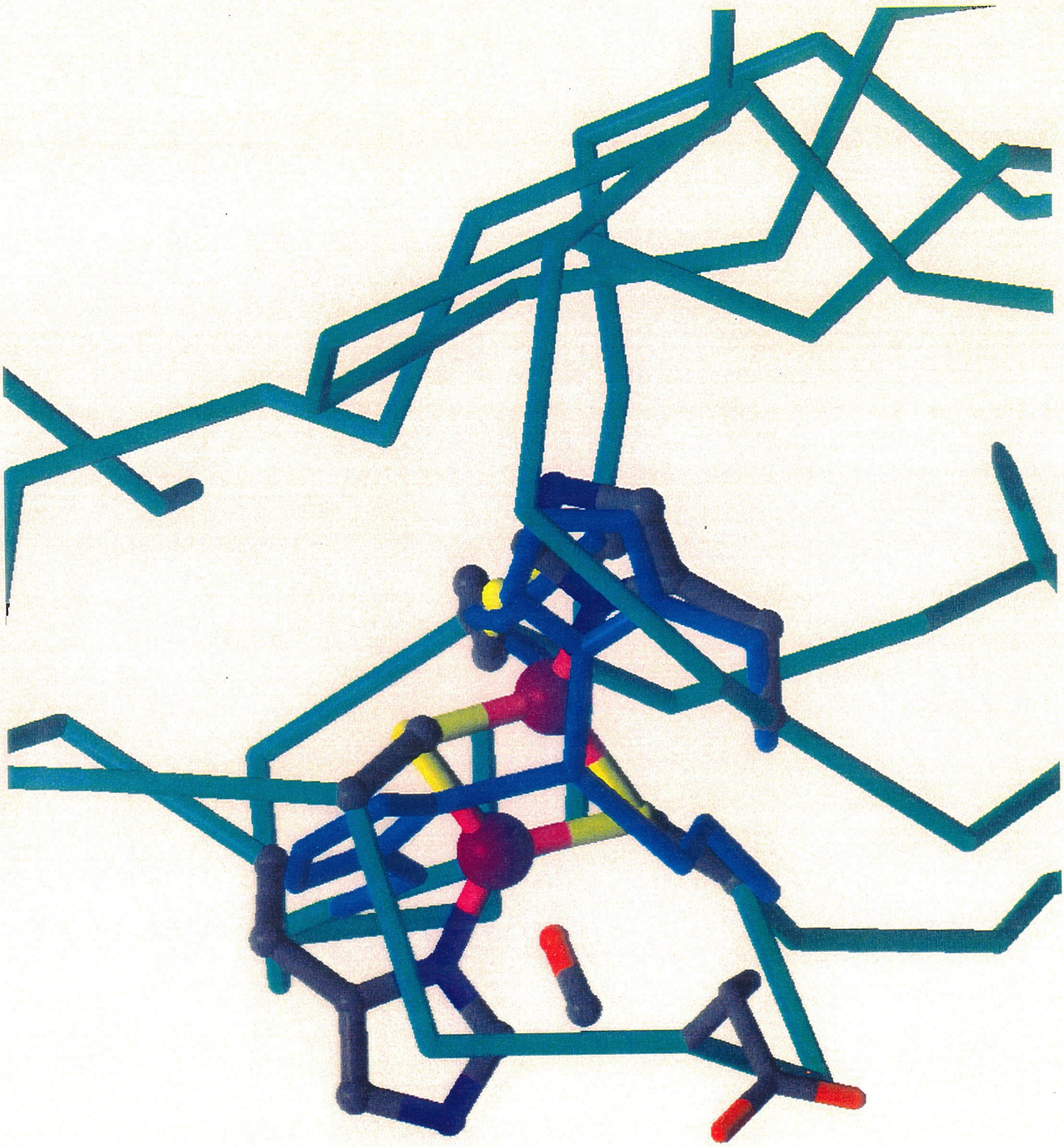

Figure 4. The topology of Histidine ET pathways into and out of the of the blue copper and Cu_A centers. In the case of the "blue copper" subunit II, the orientation of the metal center with respect to subunit I of cytochrome oxidase is determined by the overlap described in Figure 3. In the Cu_A center the His ET pathways are nearly parallel and extend over nearly the maximum amount of space possible. In the case of the "blue copper" subunit II, the His ET pathways are nearly perpendicular. This arrangement is tremendously inefficient for funneling electrons into subunit I.

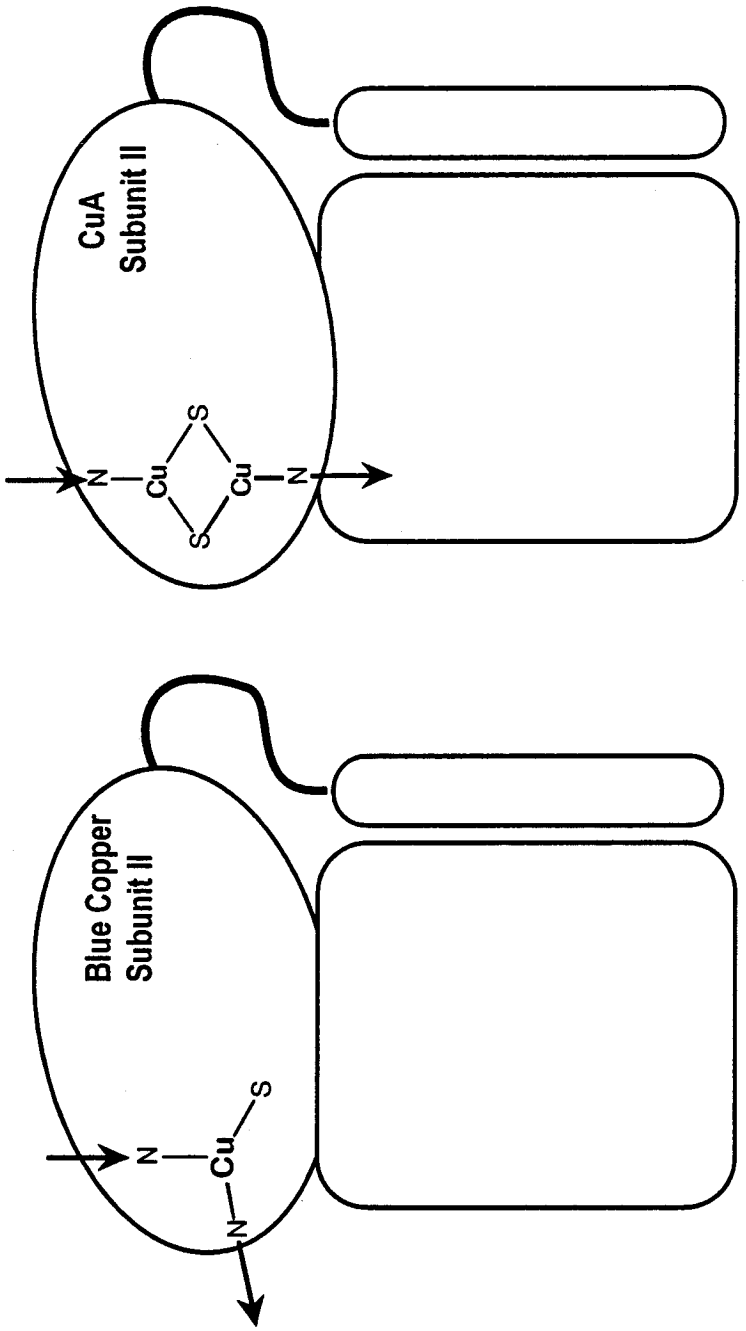
CuA
Subunit II
N
Cu
S
Cu
N
S
Blue Copper
Subunit II
N
Cu
S
N

pathways through Cu_A serve to efficiently transfer an electron over 10 Å through a center with an extremely low reorganization energy.

Cu_A-heme a_3:Cu_B ET pathways

There is no direct experimental evidence indicating that electrons are transferred directly from Cu_A to the heme a_3:Cu_B site. However, there have been some proposals that suggest it may occur based on indirect experimental evidence. Also, since the distance between Cu_A and heme a_3 is only three angstroms longer than the distance between Cu_A and heme a, others have reasoned that direct ET between Cu_A heme a_3 can effectively compete with ET between Cu_A and heme a. The best coupled His pathway from Cu_A to heme a_3 consists of 19 covalent bonds two hydrogen bonds. Cys pathways out of the copper center to heme a_3 are at least 10 bonds longer. We can exclude these paths based solely on their poor electronic coupling. Again, we find a situation in which the His ET pathways are considerably shorter than ET pathways through Cys.

To examine whether ET occurs directly between Cu_A and heme a_3, we need to consider two points: the differences in coupling with competing pathways, namely the Cu_A to heme a His pathway. This is essentially the electronic coupling element, the difference in going via one path compared to another. The other aspect is the nuclear factor, which takes into account the reorganization energy and reaction driving force. If we compare just the coupling aspect, we would predict that ET between Cu_A and heme a_3 does not effectively compete with ET between Cu_A and heme a because the rate is ~70 – 100 times slower due to the five additional bonds. The reorganization energy is expected

Figure 5. Structure of the electron-transfer medium between the Cu_A center and heme a_3. A reasonable ET pathway, through a His residue of the Cu_A center, to heme a_3 via Arg438 is apparent. Again, alternate pathways that do not go through the His ligand are quite circuitous. Pathways through Cys either go through the Mg ion or take the indicated through space jump.

Cu_A-heme a_3 ET pathways

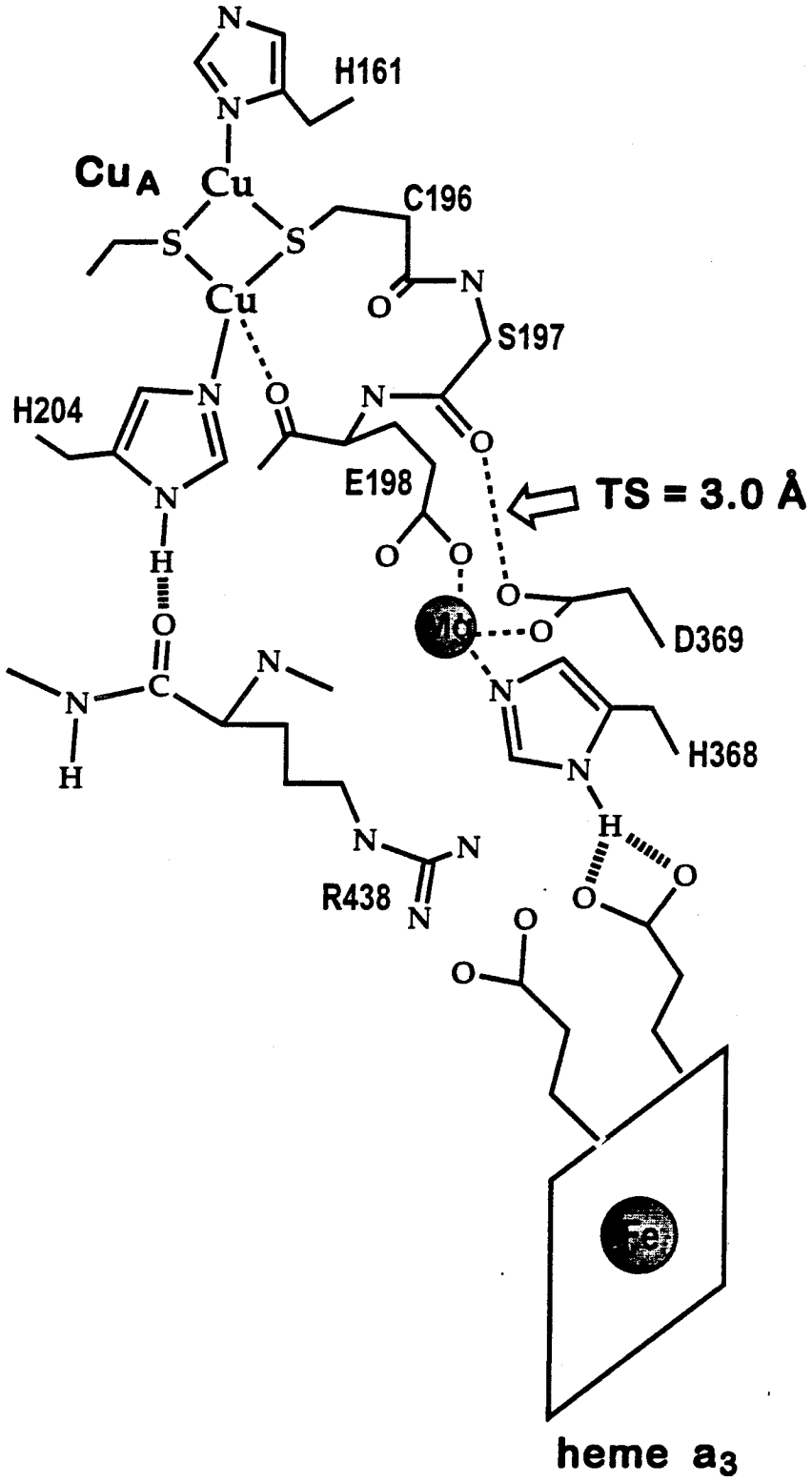

to be substantial for the heme a_3 center. Hence, both the nuclear and electronic factors disfavor the direct transfer of electrons from Cu_A to heme a_3.

Appendix

Cloning and Mutagenesis of Amicyanin for Studies of the Effect of Active Site Protonation on Electron Transfer

INTRODUCTION

The blue copper proteins, such as azurin and plastocyanin, are a class of mononuclear copper proteins of ~10 known members that function in various biological redox processes. In addition, blue copper centers are found in domains of larger multidomain proteins such as ascorbate oxidase and nitrite reductase. Many features are conserved in these proteins despite a large degree of sequence diversity. The blue copper proteins contain a single copper ion coordinated by one Cys residue and two His residues in a nearly trigonal fashion. Most of the blue copper proteins have a weakly coordinated Met residue that is an axial ligand; in the case of azurin, a backbone carbonyl is a weak axial ligand as well. The blue copper proteins all share a common fold comprised of two stacked four-stranded beta sheets. In addition to the conserved metal coordination and fold, all blue copper proteins share unique spectroscopic features. The UV/Vis spectrum is dominated by an intense absorption band ($\varepsilon \approx 5000\ M^{-1}\ cm^{-1}$) centered at ~600 nm. The EPR spectral parameters have low g-values and small hyperfine coupling constants. Furthermore, all these proteins have relatively high redox potentials ranging from 184 mV to 680 mV, the average being ~300 mV. Finally, the blue copper center has a very low reorganization energy, making these proteins very efficient electron transfer (ET) catalysts.

Considering all the conserved features blue copper proteins share it should seem remarkable that not all the members of this family exhibit the same active site protonation behavior. In some blue copper proteins, when the copper site is in the reduced state,

Cu(I), under mildly acidic to neutral conditions, the His ligand nearest the C-terminus of the protein undergoes protonation (Figure 1). The only blue copper proteins in which this is known to occur are plastocyanin, pseudoazurin and amicyanin. The pH at which this occurs varies for these three proteins; for plastocyanin and pseudoazurin the pKa of the His ligand is ~ 4.8, for amicyanin the pKa is ~ 7.0. In the process of active site protonation, the Cu-N_δ bond is broken, the N_δ is protonated and the copper ion coordination is modified such that it is bound in trigonal fashion by a Cys, a His and a Met residue. Active site protonation drastically alters the redox properties of this site, increasing both the redox potential and the reorganization energy. This in effect shuts down the site for further ET to physiological partners. Oxidation of this site is not possible until deprotonation of the His occurs and the Cu- N_δ bond reforms. Complicating the analysis of the kinetics of His rebinding is the rotation of the His side chain. With the Cu- N_δ bond broken, the imidazole ring is free to rotate about the C_β-C_γ bond. The complete description of the process involves equilibria among three states: Cu(I):His bound (A), Cu(I)':HisH+ unbound (B), and Cu(I)';HisH+ unbound and rotated (C) (Figure 1). Possible rate-limiting steps of the His rebinding include deprotonation, ring flipping or movement of the copper ion.

The role of active site protonation in physiological ET reactions is not completely understood. The simplest view is that active site protonation acts as a switch shutting down ET in response to certain environmental conditions. For example, it may be that after having undergone reduction by the cytochrome b_6:f complex, plastocyanin resides in

Figure 1. Equilibrium that results upon protonation of the His ligand in the reduced (Cu(I)) state. The letters beneath each species refer to the description in the text. k_1 is the proton dependent rate of protonation. k_2 is the rate of imidazole ring flipping. k_{-1} and k_{-2} are the respective inverse rate constants

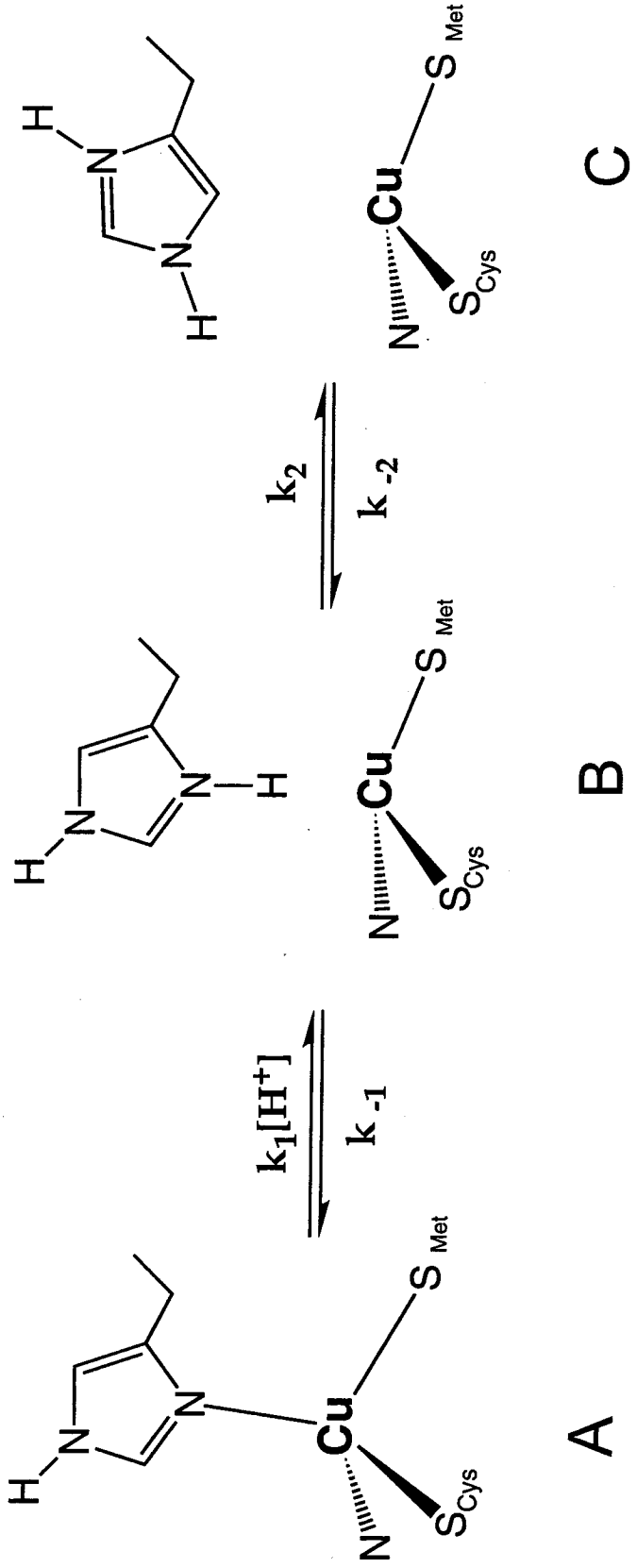
A
B
C
$k_1[H^+]$
k_{-1}
k_2
k_{-2}
Cu
S_{Met}
S_{Cys}
N
H

the relatively acidic environment of the lumen with the His ligand protonated preventing it from losing its electron to any adventitious acceptors. Only upon binding to photosystem I (PS I) does the His ligand rebind, allowing plastocyanin to donate an electron to PS I. If the rate of His rebinding is slower than the rate of ET, the ET reaction is said to be gated. In this scenario, the observed rate of ET is the rate of the rate-determining step of His rebinding. Gated ET reactions may serve to modulate the rate of ET when subsequent reactions are linked to conformational changes, proton translocation or the generation of toxic or highly reactive intermediates. One system in which the latter situation may occur are the multicopper oxidases. In these enzymes, blue copper centers donate electrons to catalytic centers, such as the trinulcear copper center in ascorbate oxidase.

Both of the systems discussed thus far, plastocyanin and the multicopper oxidases, pose many difficulties for studying active site protonation and the role it may serve in physiological ET reactions. These problems include heterologous protein expression, the introduction of alternate and unique surface histidines and the solubility of redox partners. Of all the blue copper proteins that undergo active site protonation, amicyanin is the most attractive to study for a variety of reasons. First, the crystal structures of amicyanin as well as binary and ternary complexes with it redox partners, methylamine dehydrogenase (MADH) and cytochrome c_{551i} are known. Second, both of its redox partners are water soluble. Last, wild-type and mutants of amicyanin can be expressed in appreciable amounts. After a brief section describing the background of the MADH:amicyanin:cyt c_{551i} system, the design of experiments utilizing ruthenium

modified amicyanin constructs to examine the role active site protonation in ET reactions and the expression of wild-type and mutants of amicyanin are discussed.

BACKGROUND

The blue copper protein amicyanin was first isolated from methyltrophic bacteria (bacteria that are able to use methyl containing compounds as there sole source of carbon and electrons) grown on methylamine.[1] Amicyanin has been isolated from a variety of bacterial sources, including *P. dentitrificans, T. versutus* and *M. extorquens* AM1. The gene encoding amicyanin is located in the locus designated *mau* for methylamine utilization.[2] This locus encodes the genes for approximately ten proteins in addition to amicyanin, including the trytophantryptophylquinone (TTQ) containing enzyme methylamine dehydrogenase and proteins believed to be involved in the biosynthesis of the TTQ cofactor. TTQ is a novel quinone cofactor formed by the crosslinking of a tryptophan with a tryptophan that has been post-translationally modified to an o-quinone.[3] The TTQ cofactor catalyzes the conversion of methylamine to formaldehyde and ammonia via an iminoquinone intermediate.

Amicyanin is essential for methylamine metabolism as demonstrated by the fact that bacterial harboring a disrupted amicyanin gene are longer able to grow on methylamine.[4] Reduced MADH readily reduces amicyanin; furthermore, upon binding the redox potential (E^o) of amicyanin shifts from 294 mV to 221 mV.[5] This shift in redox potential favors the subsequent reduction of cytochrome c_{551i} ($E^o \sim 190$ mV). Cytochrome c_{551i} is reduced by amicyanin alone, although to a significantly lower extent

than in the presence of MADH. The structure of the MADH:amicyanin complex was solved by x-ray diffraction.[6] Subsequently, the structure of the ternary complex of MADH:amicyanin:cyt c_{551i} (Figure 2) was also solved by x-ray diffraction.[7] The binding interactions between MADH and amicyanin are not disturbed by the binding of cyt c_{551i}. This has lent support to the hypothesis that the ternary complex occurs *in vivo* and facilitates the physiological ET reactions.

The active site protonation of amicyanin has been examined by NMR, x-ray crystallography, and ET studies with small inorganic redox agents. Both NMR[8] and ET[9] studies determined the pKa of His95 in the reduced state to be ~ 7.0. The crystal structure of the reduced low pH form of amicyanin has been solved[10] and shows structural rearrangements that are very similar to those observed in the analogous plastocyanin structure.

EXPERIMENTAL DESIGN

The fact that the pKa of His95 of amicyanin is ~ 7.0, suggests that it may serve a role in physiological electron transfer reactions. Further detailed ET studies are required to verify this assertion. The use of physiological redox partners in ET experiments is not ideal for many reasons, including the difficulties in changing the driving force, electronic coupling and reaction conditions such as pH or ionic strength. An alternative approach to the using physiological redox partners is to attach photoactivatable ruthenium polypyridyl complexes to histidines located on the surface of a protein. Using ruthenium-modified proteins one can construct a donor-acceptor system having a well-

Figure 2. Schematic diagram of the MADH:amicyanin:cytochrome c_{551i} complex. MADH is heterodimer; the β subunit contains the redox active TTQ cofactor that catalyzes the oxidation of methylamine to ammonia and formaldehyde. Electron transfer proceeds from the TTQ cofactor to the blue copper center of amicyanin to the heme of cyt c_{551i}. However, the relevance of the ternary complex in the physiological ET reactions is not known for certain.

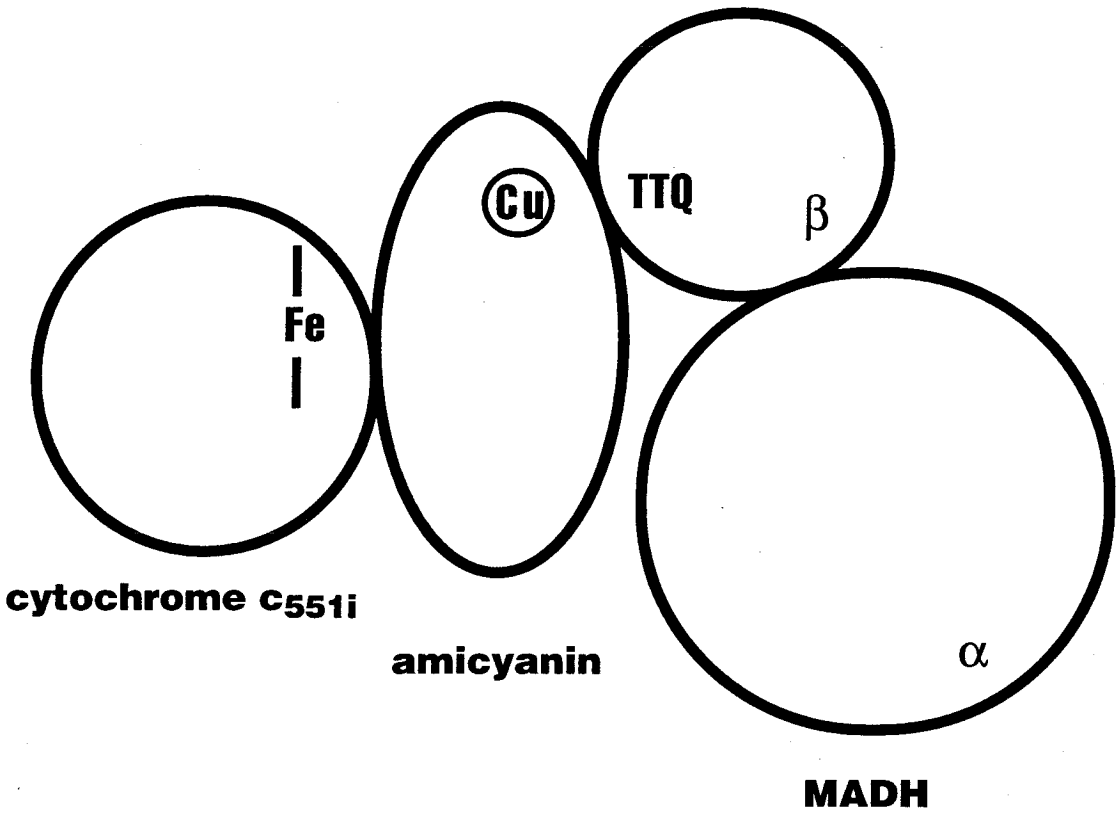
Cu
TTQ
β
Fe
cytochrome c551i
amicyanin
α
MADH

defined, fixed separation distance as well as easily vary things such as the driving force, electronic coupling and pH. Ruthenium-modification does not alter the properties of the native redox center and has virtually no effect on the overall structure of the protein. The one drawback to this approach is the necessity to develop a heterologous expression system and perform site-directed mutagenesis. For proteins such as blue copper proteins, bacteria are suitable hosts for heterologous expression. Thus, in principle it is feasible to pursue ET studies of using ruthenium-modified constructs of amicyanin.

The objectives of electron transfer studies of blue copper protein active-site protonation are measuring the rate of the rate-limiting step (RLS) of reoxidation of the protonated, reduced state and determining the factor that limits the rate. In order for one to be able to measure the rate of the RLS, the rate of ET must be faster than this rate, i.e. ET must not be rate limiting. If ET is not rate limiting, than the observed rate is the rate of the process that is rate-limiting. In this situation, the ET reaction is said to be "gated". Preliminary NMR studies and stopped-flow ET kinetics experiments with small inorganic redox complexes, have estimated the rate of the RLS to be ~10^4 s^{-1}. It is possible to construct ruthenium-modified derivatives of amicyanin that have ET rates approaching 10^9 s^{-1}. By systematically increasing the donor-acceptor distance, usually defined as the metal-to-metal distance (i.e. the distance between the Cu and Ru ions), it is possible to span a range five orders of magnitude from the upper limit of 10^9 s^{-1} to 10^4 s^{-1}. For ruthenium-modified derivatives of amicyanin that have a rate greater than the RLS, the rate of the oxidation by Ru^{3+} of Cu^{+} in the reduced protonated form of amicyanin corresponds to the rate of the RLS (k_{RLS}). (The oxidant in these experiments, Ru^{3+}, is

generated by standard flash-quench techniques.) Varying the donor-acceptor acceptor results in a change in the electronic coupling between the two metals. As the distance is increased, the electronic coupling decreases. By constructing ruthenium-modified derivatives of amicyanin that have different electronic couplings, one can confirm that the observed rate of oxidation of Cu^+ in the reduced protonated form of amicyanin is limited by a process that does not involve ET and that the reaction is indeed gated. The ET rate (k_{ET}) measured at pH > 8 should vary for each mutant, reflecting the differing electronic couplings. However, if the ET rate is measured at pH > 7, for each mutant, one should observe a slow component, with the same rate k_{RLS}, that corresponds to the rate of oxidation of the protonated site. The slow component should have the same rate for any mutant in which $k_{ET} > k_{RLS}$, despite the fact that each mutant has a different electronic coupling, indicating that the ET reaction is gated.

The mutants of amicyanin designed to examine the rate of gated ET reactions in active site protonation are outlined in Figure 3. These mutant proteins correspond to the following mutants of amicyanin: K68H, K73H, D89H, all of which carry the additional mutant H36Q (see below). The K68H mutant is analogous to the native H83 of azurin and the D89H mutant is analogous to the T109H azurin mutant. The K73H mutant is analogous to the native H59 found in *Scenedesmous obliquus* plastocyanin. Analogous refers to the similarity of the electronic coupling as predicted by the PATHWAY model. Based on experimental studies of ET in ruthenium-modified derivatives of these proteins, the K68H, K73H, D89H mutants of amicyanin are predicted to have rates of 10^5 s^{-1}, 10^7 s^{-1} and 10^6 s^{-1}, respectively. Ruthenium modified derivatives of these mutants should be

Figure 3. Location of surface histidines on amicyanin introduced via site-directed mutagenesis. The jagged lines represent β-strands; the dashed lines represent interstrand hydrogen bonds. The S represents the sulfur atom of the Cys ligand.

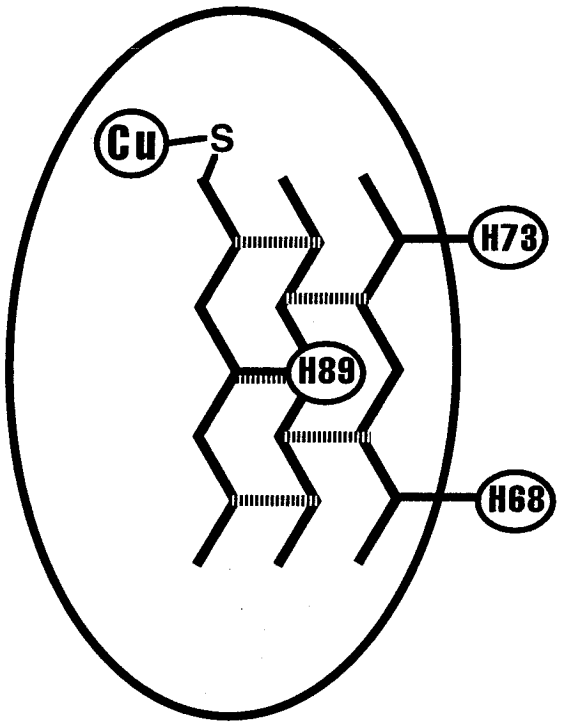
Cu
S
H73
H89
H68

suitable for examining if gating occurs in the oxidation of the protonated blue copper site in amicyanin.

DISCUSSION

Amicyanin is normally expressed in the periplasmic space, hence, the first approach undertaken in cloning and overexpressing the protein was cloning the gene with the native periplasmic leader sequence intact. The DNA segment encoding the periplasmic leader sequence and the mature amicyanin protein was amplified by PCR from a pUC vector containing the *P.denitrificans* amicyanin sequence (kindly provided by G. Boyd, Washington University). The PCR primers were designed so as to incorporate a *Nde I* restriction site at the 5' end of the amplified product and a *Hind III* restriction site at the 3' end in order to faciltate cloning the gene into a pET vector. The pET24a vector was chosen for the following reasons: the multiple cloning site region, the superior transcription control of the T7 lac promoter and because it confers kanamycin resistance.

Expression of amicyanin was reasonable on a 50 ml culture scale (estimated to be ~10 mg/liter of culture). However, none of the mutants yielded viable colonies when transformed into the *E. coli* BL21(DE3) expression strain. Alternate vectors were examined to overcome this problem. The vector pRSET was selected because it combines the cloning and promoter features of pET vectors with the high copy number feature of pUC plasmids. Transformation of BL21(DE3) *E. coli* with native and mutants of amicyanin yielded viable colonies, however, the amount of protein isolated from the periplasm was low (~1-2 mg/L) from pellets obtained from 1 or 2 L cultures. At this

Figure 4. Construction of the DNA constructs encoding the cytoplasmic and periplasmic versions of amicyanin. The segments with the diagonal lines represent the regions incorporated by the primers that contain restriction sites for ligation into the pET24a vector. The criss-cross pattern represents the DNA segment encoding the periplasmic leader sequence.

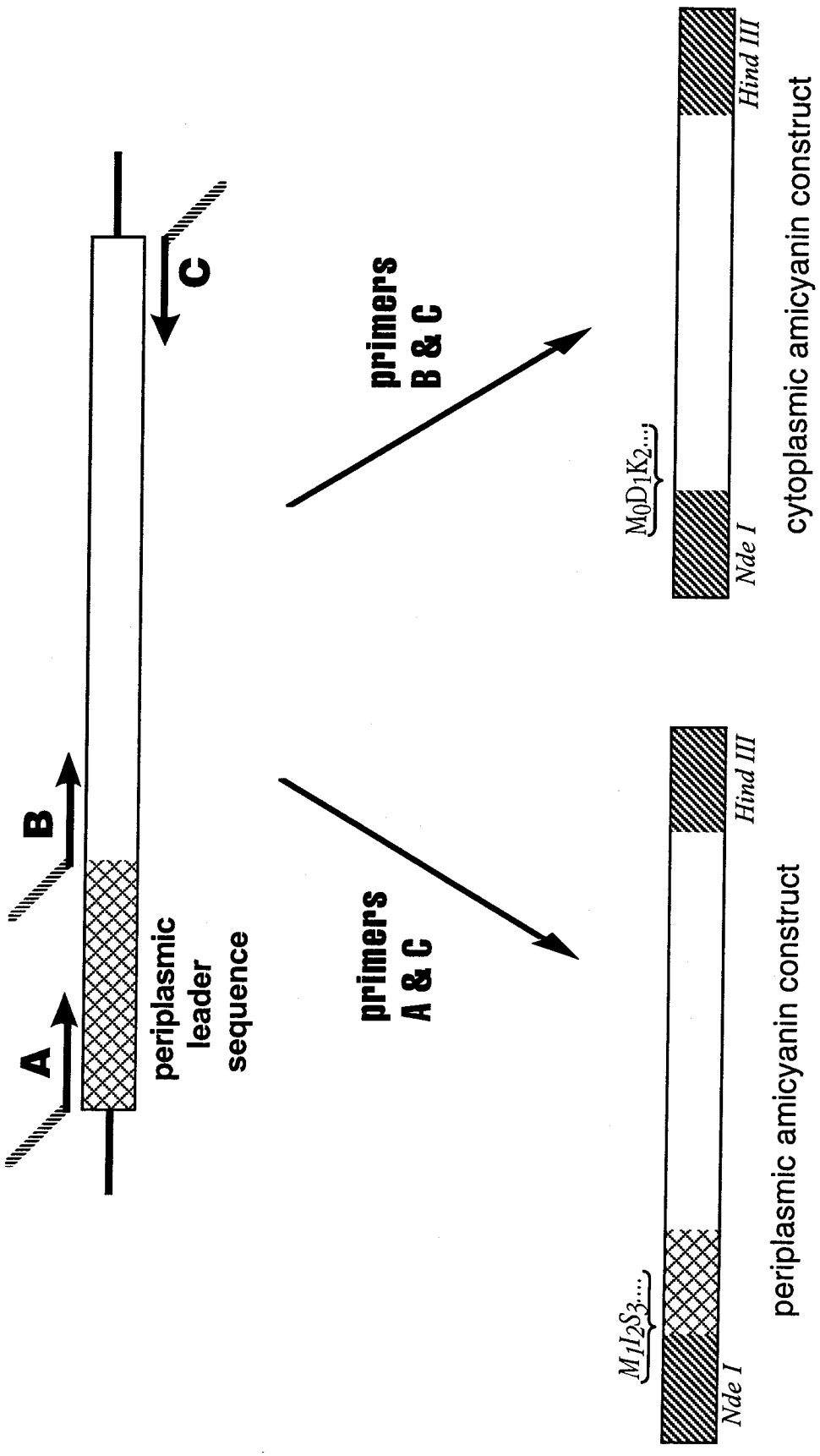
A
B
C
periplasmic
leader
sequence
primers
A & C
primers
B & C
M1I2S3....
Nde I
Hind III
periplasmic amicyanin construct
M0D1K2...
Nde I
Hind III
cytoplasmic amicyanin construct

point, it was decided to pursue cloning and expression of a cytoplasmic version of amicyanin. In this construct, a Met residue is placed before the first amino acid of the mature protein (Figure 4). Consequently, this protein will not be transported to the periplasm and will remain in the cytoplasm. This approach has some drawbacks including the inability to incorporate copper during expression, the additional steps involved in isolating the expressed protein, and the fact that the cytoplasmic version differs from wild-type, albeit only by the addition of a single amino acid (Met) at the N-terminus. The cloning of a cytoplasmic version of amicyanin was similar as described above except that the 5' primer differed so as to add a Met residue to the N-terminus of the protein and only the segment of the mature amicyanin protein was amplified (Figure 4). The amplified gene of the cytoplasmic amicyanin was incorporated into the pET24a vector. The cytoplasmic constructs of wild-type and mutants of amicyanin expressed at reasonable levels (15-20 mg/L) in BL21(DE3) *E. coli*. The addition of Met at the N-terminus has no effect on the spectroscopic features of amicyanin (data not shown).

All of the mutants constructed for examining gated ET in amicyanin possessed the mutation H36Q because ruthenium labeling studies with wild-type amicyanin indicated that ruthenium complexes were readily incorporated at H36. The H36Q mutation abolishes the ability of this side chain to bind ruthenium, preventing competition for the label and possible ambiguity in the characterization of labeled mutants. Cytoplasmic versions of the following three mutants were constructed: K68H, K73H and D89H. All the mutants expressed in good yield.

MATERIALS and METHODS

Cloning and Mutagenesis

Primers were diluted in ddH_2O to a concentration of 100 pmol/λ (1 λ = 1 μl). A typical PCR reaction consisted of the following components: 1 λ of each primer, 1 λ of template, 10 λ of 1 mM dNTPs, 10 λ of PCR reaction buffer, 0.5 λ of Taq polymerase (Boehringer Mannheim) and the required amount of ddH_2O to achieve a final reaction volume of 100 λ. A typical PCR reaction profile consisted of the following steps: 2 minutes at 95° C, 30 cycles of 95 °C for 30 seconds, 30 seconds at the annealing temperature, and 1 minute at 72 °C, followed by 5 minutes at 72 °C and then cooled down to 4 °C. The annealing temperature was optimized to be as high as possible in order to maximize the stringency of amplification. Typical annealing temperatures were in the range of 50 -60 °C. The optimal temperature was based on the amount of the desired product obtained (judged by the intensity of the band stained with ethidium bromide on an agarose gel) from PCR reactions run at 50 °C, 55 °C and 60 °C. To analyze PCR reactions by gel electrophoresis, 10 λ aliquots of a given reaction were loaded onto a 1.3 % agarose/TAE gel. To improve the yield of amplified product, PCR reactions were further optimized by varying the pH and Mg^{2+} concentration as described in the Invitrogen PCR optimization kit.

For all PCR reactions that utilized a vector for the template, the PCR products were gel purified as follows. Aliquots of the reaction were loaded onto a 1.3 % low-melt

agarose gel, the desired band was excised from the gel, and the amplified product was isolated form the agarose slice using the QIAquick DNA purification kit. If a vector was not used in the PCR reaction, as in the case of the second PCR reaction in the mutagenesis reaction (see below), the PCR products were isolated directly from the reaction mixture using the QIAquick DNA purification kit. In all instances, the purified DNA was eluted into 30 λ ddH_2O in preparation for restriction digest.

Mutants of amicyanin were constructed by the PCR overlap-extension method (Figure 5). PCR reactions were as described above. The template for the first PCR reaction was either the vector encoding the wild-type protein, or for constructs containing multiple mutants, the vector containing the insert encoding the appropriate mutant protein. The annealing temperature and reaction buffers of the PCR reaction of the first mutagenesis step were optimized as described above. Purification was as described above, except that amplified DNA fragments < 100 basepairs in length were purified using the QIAEX II DNA purification kit. In the second PCR reaction of the mutagenesis process, 3 λ of the purified products of the first PCR reactions were combined with the outside primers and the other necessary components (dNTPs, buffer, and Taq). The PCR products were purified using the QIAquick purification kit in preparation for restriction digest.

Restriction Digest and Ligation

Figure 5. PCR overlap extension method of site-directed mutagenesis. The mutagenic primers X_1 & X_2 contain the mutated DNA sequences. The first PCR reaction produces the oligonucleotide fragments containing the mutated DNA sequences. In the second PCR reaction, the complementary segments of the two oligonucleotide fragments overlap and extension produces the full-length mutant DNA construct. The "outside" primers B & C amplify the full-length mutant construct.

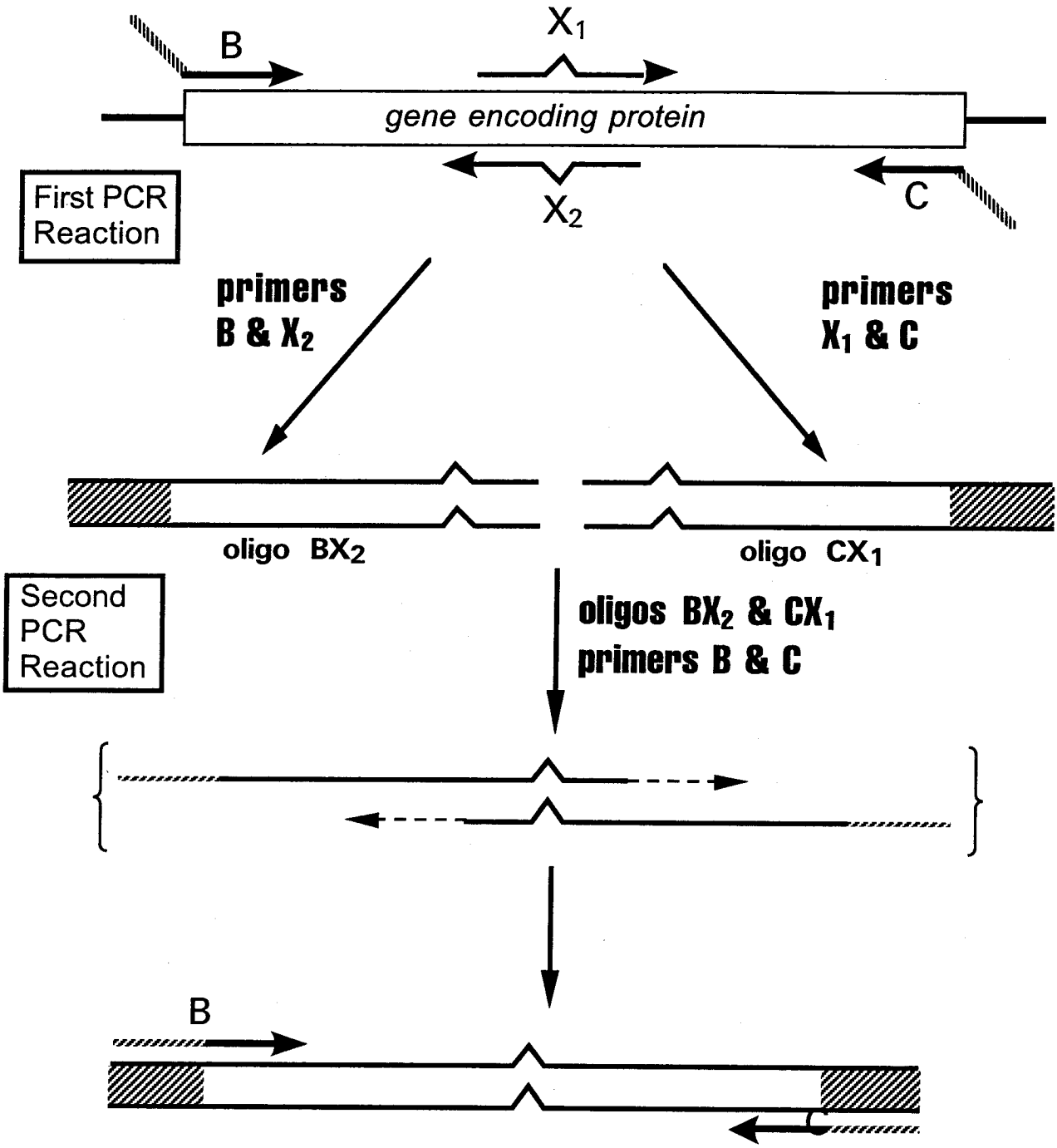
B
X1
gene encoding protein
X2
C
First PCR Reaction
primers B & X2
primers X1 & C
oligo BX2
oligo CX1
Second PCR Reaction
oligos BX2 & CX1
primers B & C
B
C

Typically all amplified DNA products were double-digested. The buffer of the least robust restriction enzyme was used as the buffer in the double digest reaction. All restriction enzymes were purchased from New England Biolabs. The usual volume of the digest reaction was 30 λ. The reaction contained 20 λ of substrate DNA, 3 λ of reaction buffer, 5 λ of ddH_2O and 1 λ of each restriction enzyme. The reaction mixture was incubated at 37 °C for 2 - 4 hours, (often prolonged incubation, i.e. overnight, resulted in better yield of transformed bacteria). The restriction digest mixture was purified using the QIAEX II DNA purification kit. The final eluted volume was 30 λ. 3 λ of the digested vector (~50 ng/ λ) and 10 λ of the purified digested DNA were combined with 4 λ of ddH20, 2 λ of ligase buffer and 1 λ of T4 DNA ligase (Gibco BRL) and incubated overnight at 16 °C. Control ligation reactions contained all the above components except the digested DNA insert; ddH_2O was added in place of the insert. In preparation for electroporation, the ligation reaction mixture was desalted using the QIAEX II DNA purification kit. The final eluted volume was 30 λ.

Transfection

The cloning strain was transfected with the vector containing the desired DNA insert by the electroporation method. 10 λ of purified ligated vector was added to 40 λ of freshly thawed electroporation competent bacterial cells (either HB101 or HMS174) and incubated on ice for 3-5 minutes. Electroporation was performed using the Gene Pulser

unit (Bio-Rad). Immediately following electroporation, 800 λ of LB media was added to the transfection mixture and the cells were cultured for 1 hour at 37 °C. After 1 hour, 100 λ of the culture was plated out on LB/agar containing kanamycin (30 μg/ml). The agar plates were incubated overnight at 37 °C. The total incubation period typically lasted from 12-16 hours.

Screening and Sequencing

Colonies were screened directly for vector containing insert by PCR. A given colony was stabbed with sterile toothpick and the toothpick was dipped into a 0.8 ml eppendorf tube containing 70 λ of ddH_20. To facilitate the preparation of the numerous PCR reactions, a reaction cocktail was made that contained primers, dNTPs, buffer and Taq. The temperature profile was used as described above, however the amplification was performed for 45 cycles. Products were examined on a 1.3 % TAE/agarose gel. A false positive did not exhibit a band corresponding to the amicyanin insert. A sample of the vector from a positive transformants was prepared for sequencing using the QIAGEN Maxiprep Purification Kit in order to achieve maximum yield and purity. Samples were submitted for automated DNA sequencing which was performed by the DNA Sequencing Core Facility. Sequencing of both strands was typically performed.

Protein Expression and Isolation

The first step involved transforming a clone with the correct desired sequence into into the BL21(DE3) *E. coli* expression strain. Chemically competent cell stocks purchased from Novagen were used as in-house prepared stocks never matched the transformation efficiency of the commercial cells. For a typical transformation, 5 λ of 1:100 diluted purified vector was incubated with 20 λ of freshly thawed cells on ice for 10 minutes. Then the mixture was placed at 42 °C for 40 seconds, after which 80 λ of LB media was added to the mixture. After the 2 minutes on ice, the cells were cultured in eppendorf tubes for 1 hour at 37 °C with shaking. After shaking, the culture was diluted 10-fold and 50-100 λ of each culture was plated out onto LB/agar plates containing kanamycin. Plates were incubated overnight at 37 °C for 12 - 16 hours.

A starter culture of 25 or 50 ml (depending on the scale of the preparation) was prepared as follows: the starter culture was inoculated with a freshly-grown colony that was transferred from an agar plate using a sterile toothpick. The culture was grown for only 3-6 hours, to the point that the culture was just turning turbid, so as to minimize saturation of the culture, consumption of all the antibiotic and the possibility of the bacteria losing the vector. After the required growth period, the starter culture was stored in the refrigerator until it was used, which was typically the next day. The following day, generally as early in the morning as possible, 10 or 20 ml of the starter culture was used to inoculate 1 or 2 liter cultures, respectively, to which kanamycin had been added (30 μg/ml). The culture was incubated at 37 °C with shaking until it reached an OD_{600} of

~0.8, at which point protein expression was induced by the addition of IPTG (for the T7lac promoter, the suggested concentration of IPTG is 1 mM). The cells were incubated for another 3 hours at 37 °C with shaking. Aliquots were taken at 0, 1, 2, and 3 hours after addition of IPTG for analysis of protein expression by PAGE. After three hours at 37 °C, the cells were harvested by centrifugation at 5000 rpm for 10 minutes. Bacterial pellets were stored at -80 ° C.

The isolation of protein expressed in the cytoplasm followed the freeze-thaw protocol. The pellet was allowed to thaw on ice and then 10 ml of 10 mM Tris (pH 8.0) was added to the pellet. The pellet was resuspended and then $Cu(SO_4)$ (from a stock solution) was added to a final concentration of 0.5 - 1 mM, followed by thorough mixing. The suspension was frozen using a EtOH/dry ice bath. Once frozen, the suspension was thawed again, completeley resuspeded, and then freeze/thaw cycle repeated once more. After the final thaw, an additional 10 ml of 10 mM Tris(pH 8.0) was added to the suspension and the cells were repelleted by centrifugation at 5000 rpm for 10 min. The filtrate was carefully decanted from the pelleted bacterial cells. The pellet was stored at -80°C. The solution, containing the expressed protein was concentrated to 1/10 the volume using an Amicon ultrafiltration system. After concentration, the samples were refrigerated overnight. The following morning, a noticeable color change could be easily observed due to the absorbance of copper that was now incorporated in the protein. The sample was further concentrated using Centricon ultrafiltration units and the buffer was exchanged in preparation for purification by FPLC using a metal affinity columns

(IMAC). After this single purification step, the protein was sufficiently pure to be used in a ruthenium labeling reaction.

REFERENCES

1. Tobari, J.; Horada, Y. *Biochem. Biophys. Res. Comm.* **1981**, *101*, 502-508.

2. Lindstrom, M.E.; Chistoserdov, A.Y. in *Microbrial Growth on C-1 Compounds* Intercept, Andover: **1993**, 381-413.

3. McIntire, W.S.; Wemmer, D.E.; Chistoserdov, A.Y.; Lindstrom, M.E. *Science* **1991**, *252*, 817-824.

4. van Spanning, R.J.M.; Wansell, C.W.; Reijinders, W.N.M.; Oltmann, F.; Stouthamer, A.H. *FEBS Letters* **1990**, *275*, 217-220.

5. Gray, K.A.; Davidson, V.L.; Knaff, D.B. *J. Biol. Chem.* **1988**, *263*, 13987-13990.

6. Chen, L.Y.; Durley, R.; Poliks, B.J.; et al. *Biochemistry* **1992**, *31*, 4959-4964.

7. Chen, L.Y.; Durley, R.C.E.; Matthews, F.S.; Davidson, V.L. *Science* **1994**, *264*, 86-90.

8. Lommen, A.; Canters, G.W. *J. Biol. Chem.* **1990**, *265*, 2768-2774.

9. Kyritsis, P.; Dennison, C.; Kalverda, A.P.; Canters, G.W.; Sykes, A.G. *J. Chem. Soc.-Dalton Trans.* **1994**, *20*, 3017-3023.

10. F.S. Matthews, personal communication.